2009

Storm surge dynamics over wide continental shelves: numerical experiments using the Finite-Volume Coastal Ocean Model

Joao Lima Rego
Louisiana State University and Agricultural and Mechanical College

STORM SURGE DYNAMICS OVER WIDE CONTINENTAL SHELVES: NUMERICAL EXPERIMENTS USING THE FINITE-VOLUME COASTAL OCEAN MODEL

A Dissertation

Submitted to the Graduate Faculty of the
Louisiana State University and
Agricultural and Mechanical College
in partial fulfillment of the
requirements for the degree of
Doctor of Philosophy

in

The Department of Oceanography and Coastal Sciences

by
João Lima Rego
Licenciado, University of Lisbon, 2004
M.S., University of Louisiana at Lafayette, 2006
August 2009

ACKNOWLEDGEMENTS

I begin by thanking my adviser, Dr. Chunyan Li, whose teaching skills and hard work set an example that will be hard to forget. His patience and guidance were very much appreciated during my years at LSU. I am also grateful to the other committee members, Drs. Jaye Cable, James Catallo, Dimitris Nikitopoulos and Clinton Willson, for suggestions which improved this dissertation substantially. Dr. Masamichi Inoue, who initially also served on my committee, provided noteworthy contribution as well.

I thank Dr. Changsheng Chen (University of Massachusetts-Dartmouth) for kindly sharing the FVCOM code, Dr. Lianyuan Zheng (University of South Florida) for initial discussions about the code, and Mr. Imtiaz Hossain (LSU's Shell Coastal Environmental Modeling Laboratory) for help with the cluster.

A special appreciation is due to LSU's Troy H. Middleton Library, whose abundant resources and kind and helpful librarians were a powerful tool in my research.

I have to acknowledge some of the people I became friends with, while in Louisiana: Dr. Ikhlas Ajbar, Ms. Lisa Gardner, Ms. Amy Scaroni and Ms. Amy Spaziani; also Mr. João Abecasis, Dr. Claes Eskilsson, Mr. Zhixuan Feng, Mr. Gustavo Ferreira, Dr. Felix Jose, Mr. João Pereira and Dr. Gabriel Retana. They also provided frank and useful comments about my research. Lastly, the seemingly endless patience and support of my family back in Portugal must also be recognized.

This work was made possible by the financial support from the Portuguese "Fundação para a Ciência e a Tecnologia", Doctoral Fellowship 28815/2006, which is greatly appreciated.

TABLE OF CONTENTS

ABSTRACT

Storm surge is an abnormal rise of the sea surface caused by atmospheric forcing, including the wind stress and atmospheric pressure associated with extra-tropical and tropical cyclones. Hurricanes and typhoons have a great impact on coastal regions, and can cause severe loss of lives and great damages. A systematic investigation of storm surge impact to the coasts of Louisiana and Texas, where the continental shelf reaches up to 200 km in width, is conducted here using the hydrodynamics Finite-Volume Coastal Ocean Model, FVCOM (Chen et al., 2003). The model is applied to the northern Gulf of Mexico to simulate the storm surges caused by Hurricanes Rita (September 2005) and Ike (September 2008), and allows the resolution of the flooding along the Louisiana and Texas coasts. Observations of inland flooding from USGS are used to validate the model with satisfactory results. Various idealized scenarios are also simulated using FVCOM, to gain insight into specific surge mechanisms. This study focuses on the following topics: 1) The roles of shelf geometry and tides in a hurricane surge are explored in a set of experiments where the nonlinear interaction between tide and surge is investigated and found to be important, relative to the tidal amplitude; 2) The receding flow of Hurricane Rita's surge waters back to the Gulf of Mexico and the different dynamics that produce the remarkably different flooding (~0.5 days) and return (>7 days) periods are explained; 3) The effect of the often overlooked forward speed of a hurricane, which was found to have an unexpected and significant impact on coastal surges, in that faster storms produce higher coastal peak surges but smaller overall inland flooding (vice-versa for slower storms); and 4) The importance of Galveston Bay's barrier islands on the propagation of Hurricane Ike's surge, where results suggested that under a realistic erosion scenario for Bolivar Peninsula's, the bay is exposed to

dangerously high water levels almost as much as if the Peninsula was leveled to about Mean Sea Level, underlining the non-linear nature of this bay-barrier system.

CHAPTER 1

GENERAL INTRODUCTION

1.1. Motivation

A storm surge is an abnormal rise of sea surface height caused by atmospheric forcing, including the wind stress and atmospheric pressure at sea surface associated with extra-tropical cyclones or tropical cyclones such as hurricanes and typhoons (Flather, 2001). Since tropical cyclones have lower interior pressures and higher wind speeds, they typically produce significantly higher surges than extratropical cyclones do (Resio and Westerink, 2008).

The deadliest natural disaster ever to strike the USA was the Galveston Hurricane of 1900, which flooded Galveston, Texas on September 8 and caused 8,000-12,000 lives to be lost (Rappaport and Fernandez-Partagas, 1995). Hurricane Katrina was the costliest hurricane to ever strike the USA, and caused an estimated $125 billion in damage (Graumann et al., 2006). Katrina's storm surge in August 2005 exceeded 9 m in several locations along the Mississippi coast, resulting in the death of over 1000 people in Louisiana and 200 in Mississippi (Blake et al., 2006).

The greatest loss of life caused by storm surges has occurred in the northern Bay of Bengal. Due to dense population, a wide and shallow continental shelf and inefficient warning and evacuating systems, Indian and Bangladeshi coasts have suffered enormous storm-related casualties. The most severe cyclone-related event in recorded History, with respect to inundation and loss of life, occurred in Bangladesh in November 1970. The cyclone produced a maximum surge height of 10 m and the loss of life was estimated to be 300,000-500,000 (Madsen and Jakobsen, 2004). Another storm in April 1991 caused the death of about 140,000 people in Bangladesh (Flather, 2001), and the October 1999 cyclone that hit the Orissa coast of India

produced a 7.5 m surge causing 11,000 deaths (Dube et al., 2000). More recently, in May 2008, the "very severe tropical cyclone" Nargis crossed over southern Myanmar (formerly known as Burma) with winds of 65 m/s, causing coastal surges of about 4 m that inundated some areas 40 km from the coast. The passage of cyclone Nargis resulted in the loss of over 130,000 lives, and had devastating consequences to the Irrawaddy delta region (Webster, 2008).

The consequences of a major tropical storm making landfall are so significant that some researchers have tried to find a way to stop hurricanes altogether. Brier and Simpson (1967) designed large-scale experiments to evaluate the effect of silver iodide seeding upon individual tropical oceanic cumulus clouds. This was the U.S. Navy's "Project Stormfury", in which clouds were seeded by Navy aircraft. Simpson (1979) later admitted that this "may be more difficult to achieve than landing a man on the moon." In another project, and because covering water with a surfactant can reduce evaporation by an order of magnitude, it was proposed that large quantities of surfactant should be distributed by aircraft along the storm's predicted path (Simpson and Simpson; 1966). Recently, Emanuel (2007) maintained that "given the stakes, this idea is surely worth deeper exploration."

Historically, 90% of all hurricane related-deaths are attributable to coastal storm surge drowning (Zhang et al, 2008). But from 1970 through 2002, coastal surge-related deaths accounted for only about 6% of all hurricane deaths – inland flooding, winds and tornadoes account for the majority of hurricane-related deaths (National Oceanic and Atmospheric Administration, 2005). "Post-Camille" developments of NOAA's storm surge models have led to better hurricane forecasts and coastal evacuations and have helped in the planning of coastal development and hurricane evacuation routes. These developments are also credited for having greatly increased storm surge awareness among coastal residents (National Oceanic and

Atmospheric Administration, 2005). But hurricane induced storm surge is still the primary reason for coastal evacuations.

The importance of preparedness is demonstrated by the manner in which Bangladesh has learned to deal with the threat of tropical cyclones. In November 2007, cyclone Sidr made an almost identical landfall (both in terms of intensity and location) in Bangladesh as the 1970 storm, which had killed hundreds of thousands of people. Although Sidr cost over 3,500 lives, this death toll was far less than the previous storm (Webster, 2008). This was achieved through the establishment of a national emergency network and the construction of storm shelters as well as dikes along the coast. In addition to the Indian Meteorology Department's forecasts of cyclone Sidr's intensity and track, storm surge forecasts from the USA were communicated to the Bangladesh Meteorological Department. Hence there was ample and timely warning for the Bangladeshi disaster management authorities to take precautionary actions and over two million people were evacuated (Webster, 2008).

Given the increase of global sea-surface temperature, both the total number and proportion of intense tropical cyclones have increased notably since 1970 (Webster et al., 2005; Emanuel, 2005). Therefore, more intense hurricanes may hit bays and estuaries and generate storm surges as those described above. This problem can be aggravated by the prospect of accelerated sea-level rise in the 21st century (Church et al., 2001), and compounded by continuing subsidence of low-lying lands surrounding these estuaries.

The improvement of present understanding of surge dynamics over wide and shallow shelves is vital for the improvement of our ability to forecast storm surge impacts to coastal regions, particularly the low-lying land areas that are more vulnerable to hurricane flooding. In combination with improving meteorological observation and modeling, accuracy of bathymetric

information, computational capabilities and enhanced national disaster planning and hurricane warning systems, this is a research field that may help save lives and resources.

1.2. Historical Overview of Storm Surge Forecasting

"Surge modeling is an art" (Jelesnianski et al., 1992). Numerical modeling of storm surge is still improving in the 21st century and has become a global activity: surge generation by extra-tropical storms is studied in Europe (e.g. Kliem et al., 2006; Zampato et al., 2006), while that by hurricanes in the Gulf of Mexico and Eastern USA is studied in North America (e.g. Weisberg and Zheng, 2008; Peng et al., 2006a,b; Shen and Gong, 2009), and that by typhoons in Asia and Oceania (e.g. Kohno, 2007; McInnes et al., 2002; Jain et al., 2007). In the first half of the 20th century, scientists had studied storm surge with the tools available at the time: either simple empirical methods based on sparse observations (e.g., Conner et al., 1957; Harris, 1959), or highly complex analytical derivations which only covered very simple basins and storms with very limited practical value (e.g. Proudman, 1954; Doodson, 1956; Heaps, 1965).

In the U.S.A., Congress directed the Army Corps of Engineers and the Weather Bureau to conduct an intensified study of the causes and behavior of hurricanes and the methods of hurricane forecast after the tremendous losses in the eastern seaboard in 1954. This is considered the beginning of systematic studies on storm surges in North America (Murty, 1984). Before numerical models were developed and readily available, operational nomograms were designed to forecast the surge whenever a tropical storm threatened to strike a coast. Conner et al. (1957) designed a simple empirical model to approximate peak coastal surges, plotting observed maximum water levels against lowest observed central pressures and determined the best fit line.

Harris (1959) found systematic variations of the surge with two parameters: minimum central pressure and the distance of the 50-fathom (91.44 m) line from shore, but concluded that the slope of the continental shelf has only a minor effect on storm surge (Harris, 1959; Harris,

1963). Harris and Jelesnianski (1964) put forth a set of 2-D hydrodynamic volume-transport equations in linearized form, valid for tidal hydraulics computations for a homogenous fluid, with pressure given by hydrostatic equation, neglecting surface waves. Jelesnianski (1966) used these linearized transport equations without bottom friction to show that the wind is about 4 times more important than the pressure forcing; that the greatest coastal peak surge occurred for a storm speed of about 37 mph and for a shoreline angular crossing of about 65º.

Jelesnianski (1967) included Platzman's (1963) eddy viscosity coefficient to control the amplitude of edge waves and developed his "practical forecasting system for storm surge." Coastal surge profiles were given by $h_c = h_s (V_R/100)^2 F_D$ where h_s is the standard coastal surge profile, V_R the maximum winds (in mph), and F_D the depth profile correction factor, respectively. Depth correction factors were 0.46-1.25 in the Eastern Atlantic US coast and 0.52-1.72 in the Gulf States. This was the systematic attempt to quantify the effect of bottom bathymetry on storm surge generation.

Jelesnianski (1972) also included storm size as a factor in his nomograms, using observations and results from (numerical model) SPLASH, and concluded that the continental shelf slope has truly a major impact on surge levels. He attributed Harris' (1959) erroneous conclusion to the crudeness of the "distance of the 50-fathom line from shore" parameter, since this factor cannot resolve the changes in the coastal bathymetry. In turn, Jelesnianski (1972) erroneously concluded (like most researchers from the 1950's through 1970's) that the influence of storm size on surge was relatively small. At that time, data were taken solely from high-water marks, which contain considerable scatter, making it difficult to distinguish possible storm size-related effects. Indeed, analysis of observed recent and historical storm data along with model simulations demonstrate that storm size plays a key role in hurricane surge generation in coastal areas, particularly for the case of intense storms on very shallow slopes (Irish et al., 2008).

Storm surge calculations in the 1950's through 1960's were intended for use along straight coastlines with only slightly varying bathymetry. They were the basis for much of the storm surge protection infrastructure designed until the 1970's, and many are still in use today (e.g., Russo, 1998; Hsu et al., 2006). Beginning in the late-1960s, high-speed computers allowed the development of numerical approximations to the governing equations using structured computational grids (often squares), first in two spatial dimensions (vertically integrated) and subsequently in three dimensions. This capability eliminated the need to assume a steady state force balance (which is not appropriate for the rapidly changing winds in hurricanes), allowed inclusion of mass redistribution (the balance between the net water flux into an area and the change in water level), and the representation of more realistic shorelines and bathymetries (AGU, 2006). A primary example of such models was developed in the 1980's: NOAA's SLOSH (Sea, Lake and Overland Surges from Hurricanes; described in Jelesnianski et al., 1992) model has been used to compute FEMA's Flood Insurance Rate Maps and is still used by the National Weather Service to forecast storm surge. SLOSH is generally accurate within 20%. For example, if the model calculates a peak 5 m storm surge for an event, the observed peak is expected to range from 4 to 6 m (National Hurricane Center, 2007).

Numerical experiments also helped gain insight of surge mechanisms which in turn contributed to improving storm surge theory. Some important books on storm surge, including theoretical analysis, observed data and numerical results were produced in the 1980's (e.g., Simpson, 1981; Murty, 1984; Pugh, 1987). Recently, many advances have been made in areas relevant to storm surge modeling. Unstructured, finite element numerical techniques were developed for storm surge models that allow the use of computational grids composed of triangles. These grids are easily configured to represent complex topographic and bathymetric features (e.g. irregular coastlines, rivers, inlets, barrier islands), and can therefore provide very

high resolution in areas of interest. With accurate wind fields, these models have demonstrated accuracy of a few feet when running past hurricanes. Combined storm surge and tidal models are now able to account fully for the effect of the astronomical tide on the total water level and therefore the potential flooding during a storm. Research is also under way to include the influence of different land covers on the air-water drag and bottom friction. The latter effects are particularly important in areas of inundation or coastal wetlands (AGU, 2006).

Numerical modeling of coastal hydrodynamics is an important field that keeps growing in many fronts and cannot be completely summarized in a few pages. Current ocean models can be extremely sophisticated with hundreds of person-years invested in all aspects of their development (see Haidvogel and Beckmann, 1999). They have typically evolved to a high degree of sophistication with a range of methods for parameterising the various unresolved physical processes, as well as the use of hybrid meshes in the vertical. Pain et al. (2005) gives a good summary of present-day advances in ocean modeling, including sub-grid scale modeling, mesh adaptivity, wetting and drying methods, and parallel computing using unstructured meshes. The advantages of unstructured mesh ocean models are many: the ability to accurately represent coastlines and bathymetry, the ability to apply appropriate boundary conditions and the ability to arbitrarily choose mesh resolutions (regardless of the vertical coordinate used) so that emphasis can be made in the coastal areas where coastlines and bathymetries can be quite complex and where most severe storm surges tend to occur. The coastal ocean model used in our work is described in detail next.

1.3. The Numerical Model, FVCOM

After the Boussinesq, hydrostatic and shallow-water approximations the primitive equations of momentum and (water) mass conservation can be written in Cartesian coordinates as (e.g., Kowalik and Murty, 1993):

$$\frac{\partial u}{\partial t}+u\frac{\partial u}{\partial x}+v\frac{\partial u}{\partial y}-fv=-\frac{1}{\rho_0}\frac{\partial p_a}{\partial x}-g\frac{\partial \eta}{\partial x}+\frac{\partial}{\partial x}\left(N_h\frac{\partial u}{\partial x}\right)+\frac{\partial}{\partial y}\left(N_h\frac{\partial u}{\partial y}\right)+\frac{\tau_{sx}-\tau_{bx}}{\rho_0(h+\eta)} \quad (1.1)$$

$$\frac{\partial v}{\partial t}+u\frac{\partial v}{\partial x}+v\frac{\partial v}{\partial y}+fu=-\frac{1}{\rho_0}\frac{\partial p_a}{\partial y}-g\frac{\partial \eta}{\partial y}+\frac{\partial}{\partial x}\left(N_h\frac{\partial v}{\partial x}\right)+\frac{\partial}{\partial y}\left(N_h\frac{\partial v}{\partial y}\right)+\frac{\tau_{sy}-\tau_{by}}{\rho_0(h+\eta)} \quad (1.2)$$

$$\frac{\partial \eta}{\partial t}+\frac{\partial}{\partial x}(uh)+\frac{\partial}{\partial y}(vh)+\frac{\partial}{\partial x}(u\eta)+\frac{\partial}{\partial y}(v\eta)=0 \quad (1.3)$$

where u and v are the depth-averaged currents in the x and y directions, respectively, η is the sea surface elevation, h is the undisturbed depth, f is the Coriolis parameter, g is the acceleration due to gravity, p_a is the atmospheric pressure at sea level, ρ_0 is the water density, N_h is the horizontal eddy viscosity coefficient, and τ_{sx} and τ_{sy} are the surface wind stress and τ_{bx} and τ_{by} the bottom friction stress in the x and y directions, respectively. The three unknowns being (u, v, η), nonlinearity in this set of equations comes from the advective terms (2nd and 3rd on the left-hand side of Equations 1.1, 1.2), the surface and bottom friction terms (last term on the right-hand side of Equations 1.1, 1.2), and the shallow-water terms (4th and 5th terms of Equation 1.3).

We use the time-dependent, finite-volume coastal ocean model (FVCOM), a 3-D free surface primitive equation model (Chen et al., 2003), to simulate tide and storm surge. FVCOM has been tested against other well-established models and is being widely used in studies of coastal ocean circulation (e.g., Chen et al., 2007; Li et al., 2008; Huang et al., 2008; Xue et al., 2009) as well as storm surge (Aoki and Isobe, 2007; Weisberg and Zheng, 2006a,b and 2008). FVCOM uses a “terrain following” sigma coordinate transformation in the vertical to accommodate irregular bathymetry, and a non-overlapping unstructured triangular grid in the horizontal to resolve dynamics in regions with complex shorelines. FVCOM uses the modified

Mellor and Yamada “level 2.5” turbulent closure scheme for vertical mixing (Mellor and Yamada, 1982; Galperin et al., 1988) and Smagorinsky eddy parameterization for horizontal dissipation and diffusion (Smagorinsky, 1963). Equations 1.1-1.3 are shown here in 2-D form and Cartesian coordinates because they are easier to interpret; their 3-D, sigma coordinates counterparts (the ones FVCOM solves for) are Appendix A.

FVCOM solves the primitive equations by using a flux calculation integrated over each model grid control volume, which ensures mass, momentum, energy, salt, and heat conservation in individual control volumes and over the entire computational domain. Similar to the Princeton Ocean Model of Blumberg and Mellor (1987), a mode-splitting method is used with external and internal mode time steps to accommodate the faster and slower barotropic and baroclinic responses, respectively, for computational efficiency. The finite-volume method used in FVCOM not only takes advantage of finite element methods in geometric flexibility and that of finite difference methods in computational efficiency, but also ensures volume and mass conservation in individual control volumes.

A detailed description of FVCOM discrete equations can be found in Chen et al. (2003, 2006). Following the convention, the bottom stress is computed using the quadratic law

$$\left(\tau_{bx},\tau_{by}\right)=C_{db}\rho_0\sqrt{u^2+v^2}\left(u,v\right) \tag{1.4}$$

where the bottom drag coefficient, C_{db}, is determined by matching a logarithmic bottom layer to the model at a height z_{ab} above the bottom, i.e.

$$C_{db}=\max\left[\frac{k^2}{\ln\left(z_{ab}/z_0\right)^2},BFRIC\right] \tag{1.5}$$

where $k = 0.4$ is the von Kármán constant, z_0 is the bottom roughness parameter, and *BFRIC* is the minimum value for C_{db}, which typically varies between 0.002 and 0.004. The surface wind stress is computed from

$$\left(\tau_{sx}, \tau_{sy}\right) = C_{ds}\rho_a \sqrt{w_x{}^2 + w_y{}^2}\left(w_x, w_y\right) \tag{1.6}$$

where (w_x, w_y) are the x and y components of the wind velocity, respectively, ρ_a is the air density. The drag coefficient, C_{ds}, is dependent on wind speed, originally assumed constant when $\vec{V}_W > 25m/s$, following Large and Pond (1981):

$$C_d^{srf} \times 10^3 = \begin{cases} 1.2 & \left|\overrightarrow{V_w}\right| \le 11.0 m/s \\ 0.49 + 0.065\left|\overrightarrow{V_w}\right| & 11.0 \le \left|\overrightarrow{V_w}\right| \le 25.0 m/s \\ 0.49 + 0.065 \times 25 & \left|\overrightarrow{V_w}\right| \ge 25.0 m/s \end{cases} \tag{1.7}$$

The flooding/drying process in FVCOM is simulated using an unstructured wet/dry point treatment technique (Chen et al., 2008). A viscous boundary layer (D_{min}) is added to the model at the bottom to avoid singularities when the local water depth approaches zero. The wet/dry criterion for node points is redefined using a sum of D_{min} and the total depth, D:

$$\begin{cases} wet, & if\ D = H + \varsigma + h_B > D_{\min} \\ dry, & if\ D = H + \varsigma + h_B \le D_{\min} \end{cases} \tag{1.8}$$

and that for triangular cells is

$$\begin{cases} wet, & if\ D = \min\left(h_{B,i}, h_{B,j}, h_{B,k}\right) + \max\left(\varsigma_i, \varsigma_j, \varsigma_k\right) > D_{\min} \\ dry, & if\ D = \min\left(h_{B,i}, h_{B,j}, h_{B,k}\right) + \max\left(\varsigma_i, \varsigma_j, \varsigma_k\right) \le D_{\min} \end{cases} \tag{1.9}$$

where h_B is the bathymetric height; i, j and k are integers to identify the three nodes of a triangular cell; H is the still water depth; and ζ is the surface elevation. When a triangular cell is treated as dry, the velocity at the centroid of this triangle is set to zero and no flux is allowed through the three side boundaries. This cell is removed from the flux calculation in the tracer control elements. For a detailed discussion of the wet/dry treatment code, see Chen et al. (2008).

Although the air-sea momentum flux is a key surface forcing in storm surge modeling and a crucial factor determining model performance, most traditional bulk type formulas (based on field measurements in moderate wind regimes below 25 m/s) assume that the wind stress magnitude is independent of sea-state and predict a monotonic increase of the C_d with wind speed (Moon et al., 2007). However, there is a growing consensus that this coefficient "saturates" for wind speeds greater than about 20-30 m/s, representing the fact that under extreme hurricane forcing the wind is dragging the foam and spray in addition to the physical sea surface (Hsu, 2006). As a result, a number of different wind stress parameterizations has been proposed recently, in which C_d either remains constant (e.g., Madsen and Jakobsen, 2004; Hsu, 2006; Zedler et al., 2009; Moon et al., 2009) or decreases (Powell et al., 2003; Jarosz et al., 2007) after a certain threshold speed. However, there is still an open debate on which wind stress scheme is the most appropriate. A correction for strong winds was used in the simulations of Chapter 5, as it slightly improved surge values near Hurricane Ike's track. Here, C_d is decreased by 15% for $\vec{V}_W > 40 m/s$ as suggested independently by Powell et al. (2003) and Jarosz et al. (2007). It should be noted that these studies recommended conflicting C_d values for wind speeds of $20 < \vec{V}_W < 40 m/s$ (Figure 1.1). Sensitivity analyses using this correction showed no improvement for Hurricane Rita's simulations (Chapters 2-4) and therefore the original Large and Pond (1981) formulation was used.

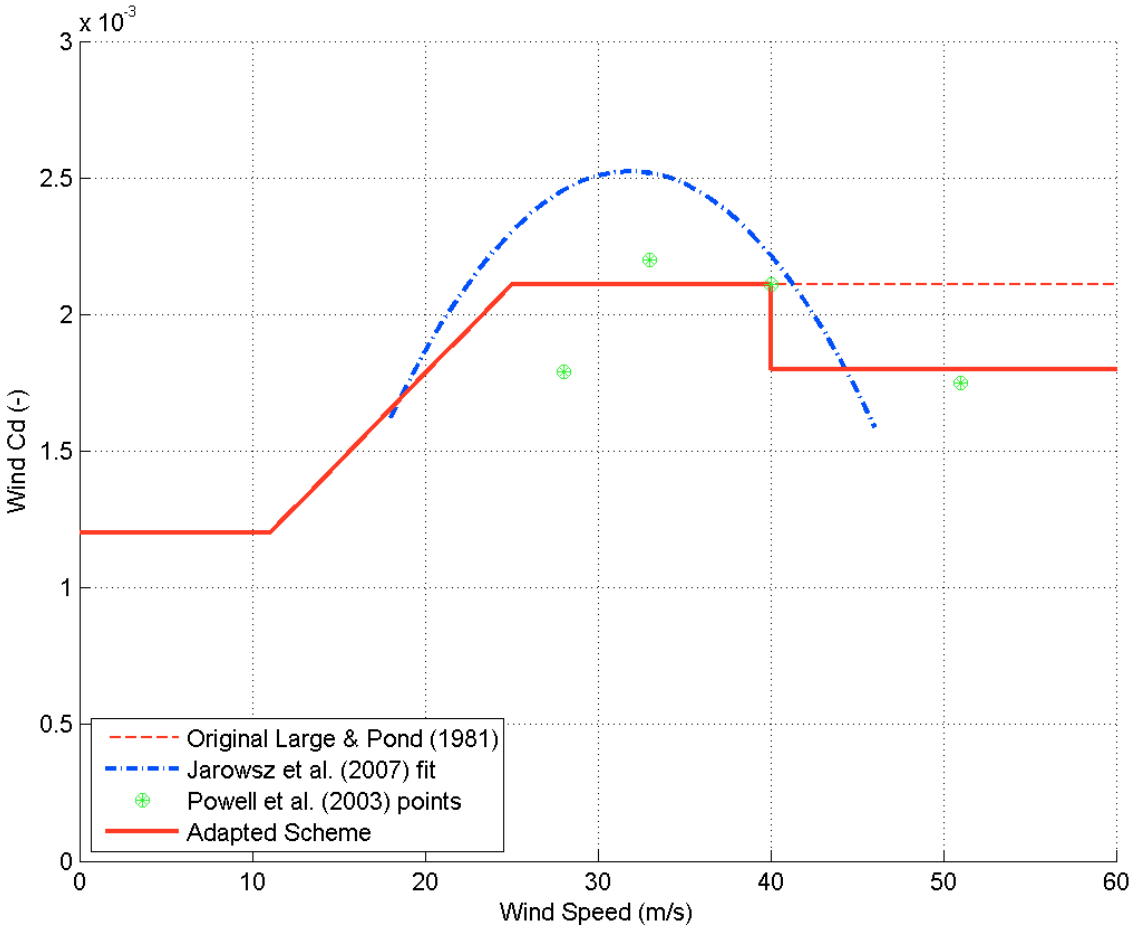

Figure 1.1: Original, recently suggested and "adapted scheme" formulations for wind stress coefficient (C_d) as a function of wind velocity. The latter was used in Chapter 5 (Hurricane Ike), while the "original" scheme was used in Chapters 2-4 (Hurricane Rita).

1.4. Surge Generation Mechanisms

A storm surge is a long gravity wave with a length scale similar to the size of the generating tropical cyclone, which lasts for several hours depending on the size of the cyclone and speed of movement. The surge usually consists of a single passing wave that elevates or depresses the sea surface height (Flather, 2001).

Since it is the wind stress that generates most of the total hurricane-induced storm surge in coastal seas (e.g. Jelesnianski, 1966; Prandle, 1975; Flather, 1994; Blain et al., 1994; Kohno et al., 2007), many numerical studies do not include the atmospheric pressure term (e.g. Johns et al., 1985; Signorini et al., 1992; Verboom et al., 1992; Chu et al., 2000; Jones and Davies, 2004; Dube et al., 2005; Morey et al., 2006). In addition, we are only investigating the effects of the conventional long wave storm surge, and do not include short surface waves. Whereas faster surface flows reduce the air-sea momentum transfer rate (thereby reducing surge), bottom-layer return currents produce a shoreward bottom stress that adds to the wind stress (enhancing surge). These complex opposing effects due to waves depend strongly on local bathymetry (Resio and Westerink, 2008). Furthermore, their effect is partially accounted for by the use of the sea-state strong winds correction (see Section 1.3). With regard to coastal wave setup, this term is relatively less important in wide continental shelves (McInnes et al., 2002, 2009).

Major destructive storm surges are known to occur when extreme storm winds act over extensive regions of shallow water (Simpson and Riehl, 1981; Gornitz, 2005). Since in the governing equations the wind stress term is divided by the total depth whereas the surface pressure gradient force is not, it follows that wind forcing increases in importance in shallower water (Flather, 2001). Coastal peak surges created by a given hurricane over wide continental shelves can be up to three times greater than those created by the same hurricane over narrower shelves (Jelesnianski, 1972). The extensive shallow portion of Louisiana's upper continental

shelf was blamed with Hurricane Rita's storm surge of "historical proportions" over significant portions of the state (URS Group, 2006).

Under ideal and steady-state conditions in deep water, the net transport of water by the wind occurs at a 90° angle to the right of the wind vector (northern hemisphere), and the alongshore component of wind stress causes a storm surge if the coast is to the right of the wind: the "bathystrophic storm tides" (Gill, 1982) or "Ekman setup" (Shen and Gong, 2009). The across-shore component of wind stress becomes more important as the water depth decreases, since the bottom stress diminishes the Coriolis tendency for transport to be to the right of the wind. Winds blowing onshore over shallow water will pile water up along the coast (Weisberg and Zheng, 2006b).

The importance of shelf bathymetry to coastal surges can be illustrated with a simple linear, steady-state expression for the sea surface slope in equilibrium with a constant wind field (Pugh, 1987):

$$\eta \propto \frac{LCW^2}{H} \tag{1.10}$$

where η is the surge height at the coast, L is the shelf width, H is the total (average) water depth, W is the wind speed and C is a constant combining gravity, density and empirical drag. Wind fields are rarely constant and such equilibrium is unlikely, but this expression is used by many authors (e.g., As-Salek, 1997; Resio and Westerink, 2008) to make the important point that wind stress is more effective at raising the sea surface in shallow waters. Hence broad, shallow continental shelves are more prone to large surges than narrow, deep continental shelves. Also, one would expect wind-generated surge to be larger at low tide than at high tide, and this has been observed (Horsburgh and Wilson, 2007). One-dimensional considerations such as this can

be applied with some success when the scale of the storm is large compared to the scale of the shallow sea, but when the scale of the storm is smaller, two-dimensional features will come into play (Welander, 1961). The surge will be smaller than predicted by the one-dimensional approximation, due to the horizontal adjustments that take place.

Hurricane storm surges are not freely propagating waves, but respond very strongly to meteorological reinforcement. In regions outside of intense wind forcing, coastally trapped waves arise that progress along the shoreline, with crests normal to the coastline. The wave height decreases exponentially from the coast with an e-folding length scale equal to the Rossby radius of deformation c/f, in which f is the Coriolis parameter and c is the phase speed of the wave in the alongshore direction. This is relevant in the relaxation phase of a storm surge after a hurricane makes landfall, or for the case of a hurricane traveling parallel to the coast in the areas upstream or downstream of the storm's center (Tang et al., 1997). McInnes and Hubbert (2003) review the propagating dynamics of wind-forced coastally trapped waves off of Australia.

The coastally-trapped wave spectrum generally consists of super-inertial edge waves, Kelvin waves, and sub-inertial shelf waves. The time and space scales of tropical cyclones are usually such that the continental shelf wave portion of the spectrum is preferentially excited. Since continental shelf waves are vorticity waves with predominantly kinetic energy (compared to potential energy), they are more readily identified from current meter observations than sea-level observations (Allen, 1980).

Edge waves are quite common, but they have amplitudes of just 0.10-0.50 m (e.g., Munk et al., 1956; Constantin, 2001). Hurricane-induced shelf waves can have larger amplitudes (of about 1 m) but they are relevant only for fast hurricanes traveling parallel to the coast, which typically happens on the US Atlantic coast rather than on the Gulf of Mexico (GoM) coast (e.g., Mercer et al., 2002; Morey et al., 2006).

Because of the lack of observed current velocity data, its small surface elevation amplitudes compared to maximum surge, and its irrelevancy with hurricanes traveling perpendicular to the coast, we will not discuss shelf wave effects in this study.

1.5. Nonlinear Interaction of Tide and Surge

The effect of tide-surge interaction on extra-tropical surges affecting Europe due to nonlinear processes in shallow water regions has been known for some time (see reviews by Heaps, 1983; Wolf, 2008). Recently, Jones and Davies (2007, 2008) showed that tide-surge interaction, besides influencing the surge, also significantly modifies tidal elevations and currents at the time of the surge in the shallow regions of the Irish Sea.

A tendency for extra-tropical storm surge maxima in the Thames River to occur most frequently on the rising tide has been long recognized, and theoretical solutions for the propagation of an externally forced tide and surge into an estuary of uniform section were developed by Proudman (1955, 1957). However, the analysis was not sufficiently general to explore the underlying dynamics and the results did not agree with observations except in the immediate vicinity of the open boundary. Rossiter's (1961) numerical model results, assuming idealized surges with diurnal periodicity, suggested that a key mechanism of interaction between tide and surge is one of mutual phase alteration: a negative surge would retard tidal propagation whereas a positive surge would increase the speed of tidal propagation and thus advance the high water. In this case, elevations were not predominantly increased by a surge-generating mechanism; instead the residual (or surge) was generated through the change of phase alone.

Wolf (1978) considered the analytical solution of the equations of motion of two plane progressive waves traveling together along a semi-infinite channel. This simplified model reproduced the main features of interaction between tide and surge in the English Channel. Her model indicates that interaction caused by quadratic friction is generally about twice the size of

shallow-water interaction, which is itself about twice the size of advective interaction. Quadratic bottom friction interaction develops where both tidal and surge velocities are largest; the magnitude of interaction increases with decreasing water depth and is proportional to the product of surge and tide amplitudes. She concluded that surge height increases at rising tide and decreases at high tide due to this interaction.

Prandle and Wolf (1978) used numerical models to conclude that the tendency for surge peaks to occur most often on the rising tide arises irrespective of the phase relationship between tide and surge in the northern North Sea. The models made it possible to separate the contribution to interaction from shallow water and bottom friction, and showed that shallow-water interaction is generally restricted to the modification of the tidal propagation by the surge. Wolf (1981) used a 1-D analytical model to show that the shallow water effect became dominant over quadratic friction for tidal amplitudes in excess of 3 m and in depths of 10 m or less. Wolf (2008) explained that in the southern North Sea the surge peak tended to avoid predicted tidal high water due to the speeding up of the tidal wave propagation in the presence of the deeper water caused by the surge; other subtle changes were caused by bottom friction.

Horsburgh and Wilson (2007) studied tide data along the eastern coastline of Great Britain for 1950-2005. Their models suggest that for physically realistic arrival times of any external surge component, the residual peak always avoids high water (and low water) for any finite tidal phase shift. Their analysis of large, long duration surge events confirmed that surge generation is reduced at high water, and that increasing the tidal range reduces the risk of residual peaks near high water. But surges are not freely propagating Kelvin waves, and respond very strongly to the change of meteorological conditions. Relaxing the meteorological forcing demonstrated that a significant enhancement of the surge occurs between Immingham and Sheerness, and that decay scales are of the order 3 hours or 100 km. These scales are likely to be

highly dependent on location and the level of equilibrium between surface elevation and meteorological forcing. Horsburgh and Wilson (2007) contradicted Pugh and Vassie (1980), who stated that there is little tide-surge interaction outside of estuaries.

Although the results summarized above provide considerable insight into tide and surge propagating together, they are limited in that they are obtained under 1-D (e.g. along the Thames estuary) and other simplifications (e.g. some numerical experiments exclude advection terms). But above all, the main limitation is the neglect of traveling wind reinforcement, because in hurricane-induced surge dynamics wind forcing is much more important than wave propagation (e.g., Morey et al., 2006). Studies over the North Sea, where shelf and storm sizes have comparable scales (e.g., Horsburgh and Wilson, 2007), may to some extent ignore 2-D effects (see also Welander, 1961). North Sea and GoM surges have very different surge-to-tide period ratios, i.e. $(T_S/T_T)^{North} = 4$ and $(T_S/T_T)^{GoM} \sim 0.5$, respectively (Wolf, 1978; Rego and Li, 2009b). However, hurricanes are smaller and travel much faster than extra-tropical storms, and 2- or even 3-D effects become important. Thus, investigations of tide-surge interaction during tropical storms will unavoidably draw somewhat different conclusions.

Johns et al. (1985) studied tide-surge interaction for two severe cyclone surge events in the Bay of Bengal, which impacted the Orissa and Andhra coasts. His numerical results showed that this interaction leads to a substantial effect only off the Orissa coast where the shallow water strengthened the contribution of nonlinearity. Maximum elevation was 0.45 m below the expected value (21% of the predicted height).

Zhang et al. (1993)'s simulations using a surge-tide coupled model indicate that the greatest wind piling up occurs during the low and flood tides, when coupling effects strengthen the current component towards the coast. During the high and ebb tides, however, coupling effects reduce this piling up. Comparisons with observations showed that a simple linear

superposition of astronomical tide with a separately computed surge may lead to errors of 1-2 m in surge prediction. Qin et al. (1994) used a 2-D numerical model to compute storm surges and tides dependently and produce total water levels for 16 tropical cyclones hitting the Shanghai region during 1949-1990. They concluded that including nonlinear tide-surge interactions in simulations considerably improved predictions of the total water level for Shanghai, especially in the vicinity of the highest total water level. Average root-mean-square-errors for the highest storm tides given by this method were about 70% of the "traditional method."

Tang et al. (1996) investigated the origin of nonlinear interaction along the Queensland coast of Australia, by running surge and tide simulations without advection on the momentum equations and replacing D (total depth) by H (undisturbed depth) on the pressure gradient and quadratic bottom friction terms. Having obtained surge residuals very similar to those using the complete equations, they concluded that the surge-tide interaction is mainly due to the bottom friction law. When they used a linear friction law and repeated the simulations, the response to a combination of tidal and hurricane forcing was just the linear sum of each separate response. They stated that the effect of this nonlinear interaction was to always reduce the coastal sea level below that obtained by linearly adding the tide to the storm surge (which does not appear to be consistent with other findings, e.g. Wolf, 1981; Johns et al., 1985).

As-Salek (1998) and As-Salek and Yasuda (2001) studied cyclone-generated storm surges off the coast of Bangladesh, where the nonlinear interaction between tide and storm surge was important in the shallow Meghna estuary. For a cyclone striking during flood, the surge spread along the coast whereas for a cyclone striking during ebb nonlinear tide-surge interaction also produced surges in the Khepupara region. Cyclones making landfall before the arrival of the tidal peak produce a higher and shorter-duration surge than cyclones making landfall after the tidal peak.

Kim et al.'s (2008) numerical results for Typhoon Ewiniar of 2006 in South Korea showed that the coupled scheme improved the accuracy by up to 10% for water levels. Performing idealized simulations, they also concluded that the locally generated surge and wave characteristics were strongly related to the tidal amplitude and phase: during high water both surge and wave setup decreased while wave heights increased (vice-versa at low water). This tendency increased with increasing tidal range.

The reason why numerical studies of tide-surge interaction for hurricanes have focused on Asian seas rather than in the GoM is likely twofold: 1) computing capabilities are plentiful in Western countries, allowing for the straightforward simulation of tide and surge simultaneously (implicitly including nonlinear interaction), and thus a "correction" method is not required, and 2) tidal ranges in the coasts of Bangladesh or China are of order 3 m whereas in the GoM they are <1 m, and interaction effects were assumed negligible. While (1) may mean operational success only to some degree as potentially interesting physics are not investigated, (2) is shown here not to be entirely correct, as nonlinear interaction accounts for up to 80% of the tidal effect over shallow shelves.

1.6. Storm Surge in Coastal Bays

Most storm surge studies focus on the coastal distribution of peak surges (e.g. Xie et al., 2006; Irish et al., 2008; Westerink et al., 2008) and only a few investigate surge dynamics within bays. Valle-Levinson et al. (2002) described the response of the lower Chesapeake Bay to Hurricane Floyd (September 1999). Using observed data, they focused on water exchange processes through the estuary's wide entrance. They reported a westward pileup of water within the lower bay when winds were northeasterly, and a seaward barotropic pressure gradient force caused by the change of winds to northwesterly that resulted in a net outflow.

Xie et al. (2004) discussed inundation algorithms and flooding velocities using the Princeton Ocean Model (by Blumberg and Mellor, 1987). They simulated a Category-3 hurricane (on the Saffir-Simpson scale) moving northward 50 km off the eastern border of a synthetic bowl-shaped waterbody with a 60 km diameter. They compared inundation patterns with and without forcing mass conservation, with threshold depths of 0.5-0.8 m, and with inundation speeds given by surface vs. vertically-averaged currents. They briefly mentioned a similar "in-bay" pileup of water, a SW-NE surface elevation difference of about 5 m when the hurricane was due east of the model domain.

Weisberg and Zheng (2006a) used FVCOM to investigate the impact of hurricane storm surges in the vicinity of Tampa Bay (Florida) and the sensitivity to points of landfall and direction of approach of the hurricane. They concluded that a hurricane traveling up the axis of the bay was the best of the worst cases with regard to storm surge, while acknowledging that it was difficult to define an overall worst case direction. Their results, however, were not compared against observed surges. They also did not quantify the oscillating westward and eastward sea level slopes over about 8 hours. Weisberg and Zheng (2006b) studied surge induced by Hurricane Charley (August 2004) and found that its translation up Charlotte Harbor's (Florida) bay axis explained the relatively small storm surge inside the bay, despite its Cat-4 status. The opening of a 450 m wide new inlet in North Captiva Island is explained based on a very large horizontal pressure gradient force across a narrow strip of the island (a 1.25 m surge on the gulf side and 0.9 m depression on the sound side). Data from 4 stations were used for validation.

Shen et al. (2006) used UnTRIM (by Casulli and Walters, 2000) to simulate Hurricane Floyd's storm tide of September 1999 in Chesapeake Bay, with a substantial dataset for validation. They concluded that water levels inside the bay can be explained by the superposition of two distinct mechanisms: offshore surge propagation into the bay (remote wind forcing;

Garvine, 1985) and local wind forcing. Their results indicate that water levels in the lower bay are more influenced by the incoming surge wave caused by remote effects, while at the upper bay they are mainly caused by local wind.

Li et al. (2006) used observations and numerical model predictions to describe a "slab-like sloshing" in Chesapeake Bay caused by Hurricane Isabel (which passed about 70 km to its west) in September 2003. Water in Chesapeake Bay was sloshed forth by the storm's southeasterly winds but subsequently sloshed back due to the presence of a seaward pressure gradient generated by the sloping sea surface. The strong landward winds erased stratification and caused a strong intrusion of high salinity shelf water into the Bay. After Isabel's passage, the longitudinal salinity gradient again produced re-stratification and a two-layer circulation in the Bay.

Shen and Gong (2009) investigated the effect of the Ekman setup along the coast and the influence of model domain size, using Hurricane Ernesto's storm tide of September 2006 in Chesapeake Bay as a case study. They concluded that the Ekman effect ranges from 0.1 to 0.5 m and that a "large domain model" yielded more reliable results, as it captured remote influences. Given the geometry of the region, both studies focused on variations along the bay, but they do show southwestward followed by southeastward surface gradients (elevation differences of about 0.8 m, from coast to coast) separated by about 6 hours (Shen et al., 2006).

1.7. Objectives

Our ability to forecast storm surge impacts to those coastal regions severely affected by hurricane flooding can be greatly improved by a better understanding of surge dynamics over wide and shallow continental shelves. In this dissertation we use a barotropic tide and surge hydrodynamic model with the following Objectives: 1) being able to predict the effect of tidal speed and timing of landfall on peak coastal surges, 2) estimating the relation between

continental shelf geometry and surge propagation, 3) clarifying the difference between surge flooding and receding stages, 4) understanding the consequences on coastal surges of varying a storm's characteristics, such as forward speed, size or intensity, 5) quantifying the shielding importance of a barrier island to a semi-enclosed coastal bay, 6) proposing and testing an improved hurricane wind field description and wind stress formulation for more precise storm surge simulations. This effort will improve the forecaster's knowledge of how to determine where to invest his time when designing surge applications.

1.8. Organization of Dissertation

This dissertation includes six chapters, which summarize the different aspects of my storm surge studies at LSU. Chapter 1 presented the motivation for this work and discussed the existing literature, putting the remaining chapters in context with the present knowledge. Chapter 2 describes the application of the Finite-Volume Coastal Ocean Model (Chen et al., 2003) to Hurricane Rita's surge of September 2005 in Louisiana. By performing dozens of additional idealized simulations, we address the effect of tide-surge nonlinear interaction and the role of continental shelf geometry on coastal surges.

In Chapter 3 the validated Hurricane Rita application is used to study the receding stage of surge floodwaters, over Louisiana's famously low-lying coastal areas. This is a crucial phase in hurricane-induced flooding, very important ecologically, but often overlooked by coastal engineers. Chapter 4 compares the effect on storm surge of different hurricane parameters, taking into account both coastal peak surge heights and total inland flooded volumes to determine their relative importance. Here it is shown how a storm's forward speed significantly affects maximum storm surge heights and inundation volume in opposite ways.

In Chapter 5 an entirely different application is described, focused on the storm surge caused by Hurricane Ike of September 2008 in Texas. The propagation of storm surge into

Galveston Bay is thoroughly analyzed, and the dynamics of the surge within this major coastal bay also described. Upon simulating an extra set of synthetic scenarios, we draw important conclusions regarding the protective effect of this system's barrier islands. Chapter 6 contains a summary of all the work and suggestions for future studies.

CHAPTER 2

THE EFFECT OF TIDES AND SHELF GEOMETRY ON STORM SURGE: NUMERICAL MODEL EXPERIMENTS FOR HURRICANE RITA[1]

2.1. Introduction

In this chapter we describe an application of the finite-volume coastal ocean model FVCOM (Chen et al., 2003) to Hurricane Rita's storm tide in September 2005 and describe the inland flooding along the Louisiana-Texas coast. The model was calibrated for tides and validated against USGS and NOAA water level observations. We seek to explain why peak surges were lower than expected by examining the nonlinear terms. In addition, we conduct numerical experiments with a standard hurricane defined over idealized shelf geometries, using simple tides and by varying the time of landfall in a new set of simulations.

Although there are many storm surge studies in the published literature, most authors do not consider the effect tides have on storm surge, and tend to fall into one of these categories: (a) disregard tide altogether and simulate storm surge only (e.g., Peng et al., 2004; Weisberg and Zheng, 2006a); (b) run storm surge simulations and linearly add pre-computed tidal elevations (e.g., Graber et al., 2006); (c) do as a) or b) while acknowledging that the nonlinearity of surge and tide may be significant (e.g., Dube et al., 2005; URS Group, 2006); (d) run tide and surge simultaneously, without looking at the details of nonlinear interaction (e.g., Peng et al., 2006b; Westerink et al., 2008). Our results provide new insight into how tidal speed and timing of landfall affect tropical storm surges for different shelf geometries.

2.2. Hurricane Rita

In coastal Louisiana the return period for major hurricanes (Category 3 or higher on the Saffir-Simpson scale) is 26 years (Keim et al., 2007). The 2005 Atlantic Hurricane Season was

[1] Submitted to the Journal of Geophysical Research

exceptionally intense and Hurricane Rita made landfall near the Louisiana-Texas state border only three weeks after Hurricane Katrina had devastated the southeast Louisiana and Mississippi coastal regions. Rita intensified quickly upon entering the GoM, and attained Category 5 status and a peak sustained wind of 280 km/h within only 24 hrs. The recorded barometric pressure reached 897 mbar, the third-lowest ever recorded for a tropical system in the Atlantic Basin at that time (Knabb et al., 2006). Hurricane Rita weakened as it approached the north-central coast of the GoM on September 23, and became a Cat-3 hurricane approaching landfall. It veered northward and moved ashore between Sabine Pass and Johnson's Bayou, Louisiana (Figure 2.1) at about 8am UTC, September 24 with sustained winds of 195 km/h. Rita generated a substantial storm surge east of its landfall that reached 5-6 m, then weakened rapidly as it continued northward through east Texas (Guidroz et al., 2006).

Hurricane Rita's landfall placed the western and central Louisiana coast within the right front quadrant of the storm, where maximum winds occur. The highest High Water Marks measured by the Federal Emergency Management Agency (FEMA), ranging from 3.9-5.4 m, were along State Highway 82 in the area between Cameron and Grand Chenier (URS Group, 2006). This road, however, is more than 1.5 km inland so higher values may have occurred along the open coast. Storm surge along the open Gulf was measured above 3 m from Johnson's Bayou to Marsh Island, a distance of about 160 km (URS Group, 2006). To the east, as far as Vermillion Bay, storm surges remained significant and high water marks of up to 3.7 m were measured (Guidroz et al., 2006).

2.3 Mesh for Hurricane Rita Simulations

Our model domain extends from the Mexico-U.S.A. border to Apalachicola Bay in Florida, with a 1300 km long open boundary arching in between, covering water depths of 1000-3000 m in the most part (Figure 2.2a).

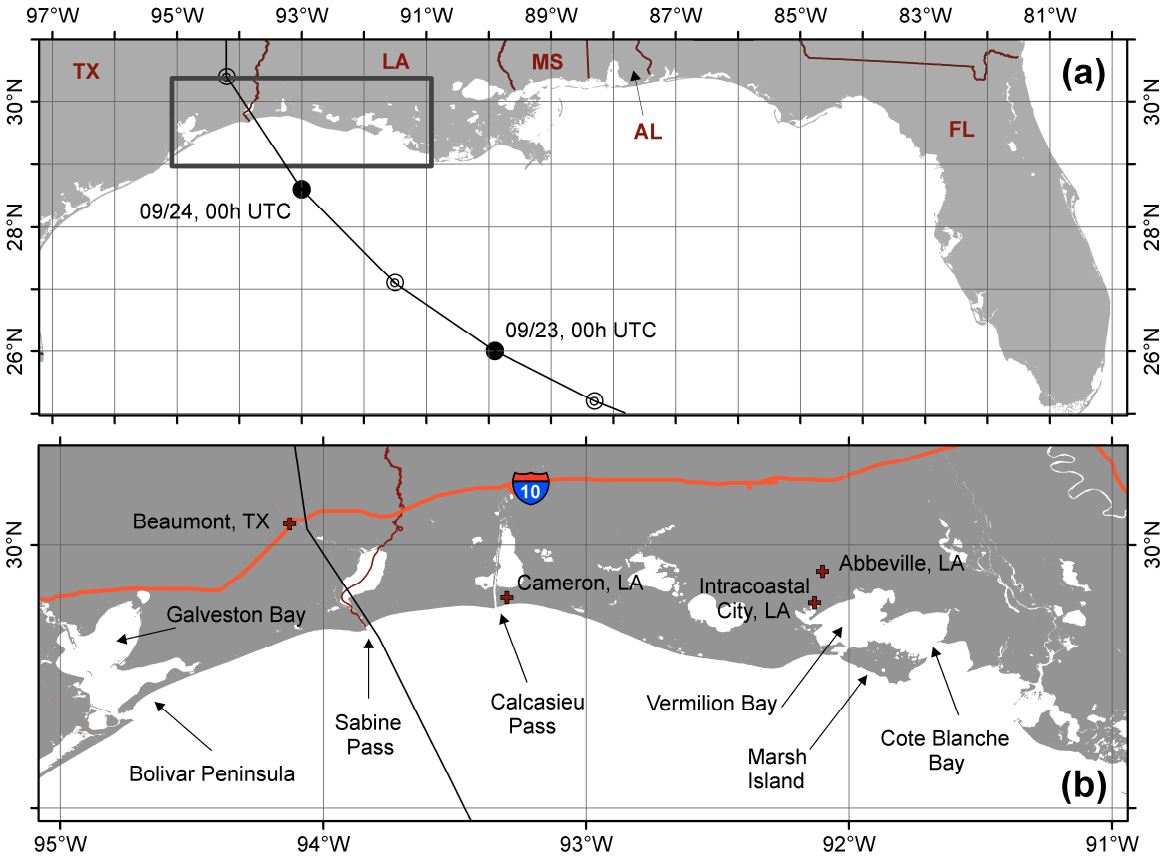

Figure 2.1: (a) Map of the northern Gulf of Mexico, including Hurricane Rita's track. The box indicates the zoom shown below. (b) Map of the Louisiana-Texas region most affected by Hurricane Rita, showing names of coastal features mentioned in the text.

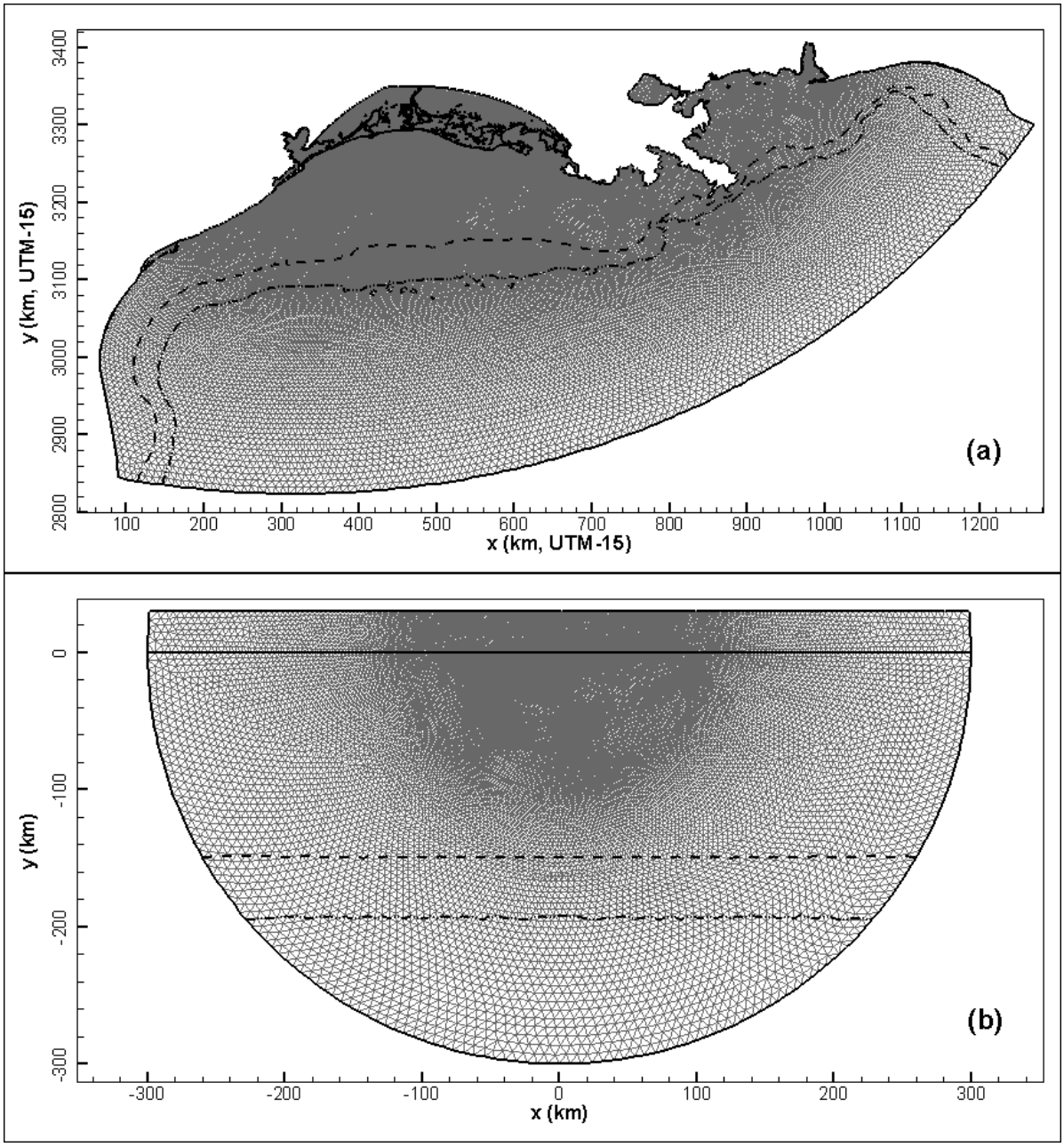

Figure 2.2: Meshes used to simulate tide and storm surge: (a) Hurricane Rita simulations, with the Louisiana-Texas bathymetry; (b) Idealized simulations, with our representative Louisiana shelf geometry. The 0 m, 50 m, and 100 m depth contours are shown.

A total of 178675 triangular cells with 90099 nodes comprise the horizontal; 2 sigma layers comprise the vertical. The mesh resolution increases from 9 km on the open boundary toward the region of Rita's impact. Mesh resolution on the upper continental shelf between Bolivar Peninsula, TX and Marsh Island, LA (Figure 2.1) is about 500 m. The finest resolution (200 m) is located on Sabine Pass and Calcasieu Pass. The model domain extends across the land-sea interface just on the West Louisiana coastal region, to the 6 m elevation contour, or more than 60 km inland (allowing us to include FVCOM's flooding-drying algorithm). Thus, although our mesh captures the entire Northwestern GoM (submarine) bathymetry, it only includes the (subaerial) topography for the area near Hurricane Rita's landfall. This limits our mesh to studies of Hurricane Rita. In our applications, land cells have a 500-2000 m resolution and the flooding threshold depth, D_{min}, was set to 0.1 m. Including inland flooding areas has been demonstrated to significantly improve modeled storm surges over the shelf (e.g., Hubbert and McInnes, 1999; Dietsche et al., 2007). Bathymetry data is a combination of the NGDC's US Coastal Relief Model, the ETOPO-2 Global Relief model and Louisiana State University's (LSU) LIDAR Atlas. In hurricane simulations, time steps of 0.6 and 6 s were used for the external and internal modes, respectively. The model was forced by wind stress and tides, as described in the next sections. The effects of surface air pressure, wave run up, river discharge and density change effects were not modeled. Running on 64 processors of the Shell Coastal Environmental Modeling Lab, FVCOM completes a 5-day simulation in approximately 15 hours.

2.4 Hurricane Wind Fields

In a storm surge model, a common practice for creating hurricane wind fields (Tang et al., 1996; Peng et al., 2004, 2006a; Weisberg and Zheng, 2006a, 2006b) is to reconstruct the wind field by fitting the analytical cyclone model from Holland (1980). The radial distribution of wind relative to the storm center and the maximum wind speed are:

$$V_w = \sqrt{\frac{B(P_{amb} - MCP)}{\rho_a}\left(\frac{RMW}{r}\right)^B \exp\left(-\frac{RMW}{r}\right)^B} \tag{2.8}$$

$$V_{\max} = \sqrt{\frac{B(P_{amb} - MCP)}{\rho_a e}} \tag{2.9}$$

where r is the radial distance from the hurricane center, V_w is the wind speed as a function of r, ρ_a is the air density (=1.15 kg/m^3), p_{amb} and MCP are the ambient and minimum central atmospheric pressures, respectively, e is the natural logarithm base (=2.718…), RMW is the Radius of Maximum Winds, V_{max} is the maximum sustained wind speed, and B is the "peakedness" storm scale parameter, $1.0 < B < 2.5$.

In applying this wind model, we used the gridded wind speed data from NOAA's Hurricane Research Division, the H*WIND dataset (Powell et al., 1996). Our comparisons to H*WIND showed that using the modified Rankine vortex model (Hughes, 1952) consistently underpredicted wind speeds, while the SLOSH wind profile (Jelesnianski, 1992), which is smoother near the RMW than the modified Rankine vortex model, tended to overestimate wind speeds. Powell et al. (1999) showed that SLOSH wind speeds were on average 14% greater than H*WIND's, which would translate into an even bigger difference in terms of wind stress.

Many past studies only used a constant B without comparing against observed data (e.g., Peng et al., 2006a; Weisberg and Zheng, 2006a). Here we used a linear regression for B as a function of the RMW, based on results from 4 major hurricanes that have had landfalls in the region and for which there is H*WIND data available (Table 2.1). Terms (p_{amb} – MCP) and B were determined iteratively, using Equations 2.8, 2.9. We select the combination of these terms that produces a wind profile with the smallest Root Mean Square Error as compared to H*WIND's profile (Figures 2.3a,b).

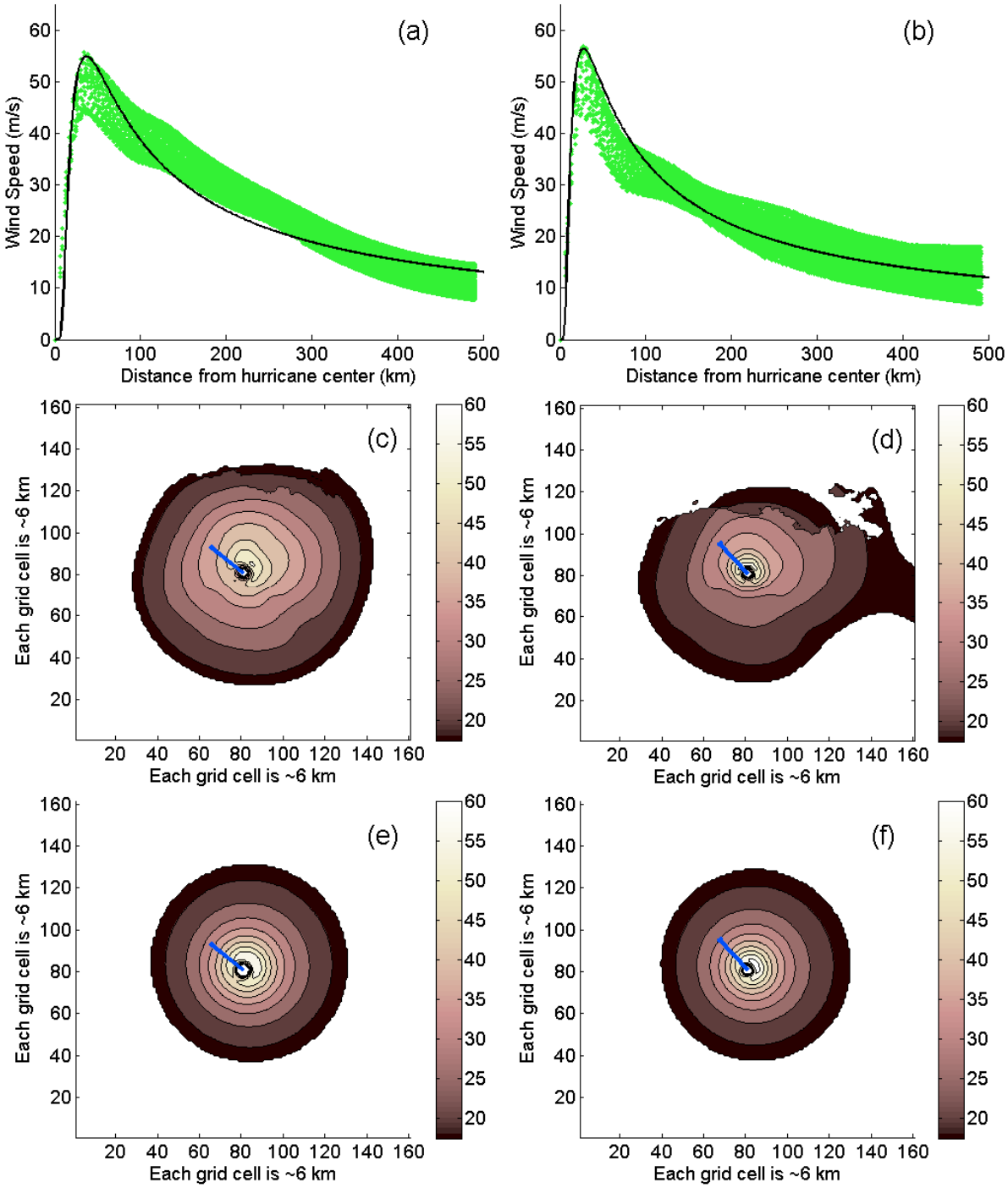

Figure 2.3: Wind field comparison, for two instants on 09/23/2005. Profile of H*WIND points and fitted curves: (a) 13h30 and (b) 19h30. Map of H*WIND speeds: (c) 13h30 and (d) 19h30. Map view of our prototypical wind speeds: (e) 13h30 and (f) 19h30. Color scale refers to wind speeds in m/s. Arrows in center of storm indicate travel direction.

Using 86 pairs of data, the resulting relation (R^2 of 72%) is $B = 0.0166RMW + 0.9735$, where B is dimensionless and RMW is given in km. To account for the forward motion of a tropical cyclone, representing the right-hand side (Northern Hemisphere) intensification of hurricane wind speeds, we used (Jelesnianski, 1966):

$$\vec{U}(r) = \frac{RMW \cdot r}{RMW^2 + r^2}\vec{V}_F \tag{2.10}$$

where $\vec{V}_F$ is the forward velocity of the storm and $\vec{U}$ is the correction term, which was added to the axis-symmetric wind velocity computed from a parametric model. By using Equation 2.10 instead of adding the forward motion vector everywhere, we ensured that these effects are (realistically) limited within the storm. This approach is also used in SLOSH for storm surge calculation (Jelesnianski et al., 1992). The forward motion vector was computed every 3 hours, from H*WIND's latitude and longitude information for Hurricane Rita. For gaps in H*WIND's exceeding 3 hours, we used UNISYS' (2007) positions to compute forward velocities.

Table 2.1: Hurricanes used in determining B=*f*(RMW). The number of H*WIND snapshots available is denoted as *n*.

Hurricane	Year	Landfall	*n*
Lili	2002	Central Louisiana	10
Ivan	2004	Alabama	13
Katrina	2005	SE Louisiana, Mississippi	33
Rita	2005	Louisiana-Texas	30

The angle that forms between the wind direction and the tangent to a circle concentric with the hurricane center due to friction (the "inflow angle") also contributes to the wind field asymmetry, in addition to the effect of forward motion. Using constant values for the inflow

angle, Johns et al. (1985) concluded that it had a negligible effect on coastal storm surge, whereas Peng et al. (2006b) concluded the opposite. Here, we set this angle to a constant 10º based on H*WIND data specific for Hurricane Rita.

In summary, with a set of *X, Y, RMW,* V_{max}, and V_F for each H*WIND snapshot (remaining parameters are *B*, given by *RMW*, and inflow angle set as constant) we assigned a wind vector for every cell in the model, as a function of *r*, the distance to the hurricane center. Parametric wind fields were thus generated for the entire model domain using H*WIND data, and interpolated into 12-minute intervals. The appropriateness of our methodology can be ascertained by comparing Figures 2.3c,d with Figures 2.3e,f. By using time-dependent values for *RMW*, *B* and V_{max} instead of constants, important variations in hurricane characteristics (i.e. size and intensity) are captured, and including the forward motion correction improved Holland's (1980) symmetric model (now shown) by also representing hurricane asymmetry.

2.5 Model Calibration for Tide

To ensure that the model properly represents the characteristics of long-period wave propagation in our domain, a simulation of the tide is first carried out with FVCOM. The model is run without surface wind forcing for 36 days, forced at its open boundary by 9 tidal constituents obtained from Mukai et al. (2002). The last 32 days of hourly model output were used for harmonic analysis of tidal constituents.

Calibrating this application of FVCOM for tidal simulations consisted of varying the bottom friction coefficient, *BFRIC* (Equation 1.5), held constant throughout the entire domain. We found that changing Smagorinsky's horizontal diffusion, the bottom roughness parameter, and the inundation depth (D_{min}) had negligible effects on the model's tidal results. Bottom friction coefficient was varied between 0.0020 and 0.0050, and the best results were produced with *BFRIC*=0.0040. Tidal constituent data (Table 2.2) were obtained from 14 long-term NOAA

tidal stations, along with data from 3 LSU's Coastal Studies Institute stations (http://wavcis.csi.lsu.edu). Most stations are located in areas impacted by Rita's storm surge, from east Texas to southeast Louisiana.

Table 2.2: Stations used in tidal calibration. All stations are NOAA's except the three Coastal Studies Institute (LSU) stations indicated. Each column shows observed Amplitude (in meters), then Amplitude and Phase *differences* (modeled – observed) between modeled and observed values, in meters and hours, respectively, for the three major tidal constituents.

Station Name	**O1** **Amp., Amp., Phase**	**K1** **Amp., Amp., Phase**	**M2** **Amp., Amp., Phase**
Corpus Christi, TX	0.162; +0.004, +0.62	0.160; +0.001 -0.15	0.083; -0.025, -0.08
Freeport, TX	0.147; +0.013, +0.64	0.152; +0.014, -0.11	0.096; -0.013, -0.17
Galveston Pleasure Pier, TX	0.161; +0.004, +0.70	0.171; +0.002, -0.03	0.139; -0.021, -0.16
Eagle Point, TX	0.114; -0.051, +1.41	0.117; -0.052, +0.65	0.034; -0.017, -0.25
Sabine Pass North, TX	0.123; -0.028, +0.19	0.132; -0.029, -0.42	0.123; -0.031, -0.26
Rainbow Bridge, TX	0.083; -0.054, +1.43	0.085; -0.054, +0.29	0.050; -0.033, -0.75
Calcasieu Pass, LA	0.136; +0.040, +0.24	0.144; +0.044, -0.50	0.146; +0.024, -0.16
CSI-03 (LSU)	0.154; +0.010, +0.94	0.169; +0.004, +0.25	0.126; -0.00, -0.10
Lawma, Amerada Pass, LA	0.121; +0.001, +1.10	0.126; +0.007, +0.26	0.084; -0.029, -0.41
CSI-05 (LSU)	0.143; +0.008, +0.83	0.149; +0.005, +0.21	0.027; +0.008, -0.47
CSI-06 (LSU)	0.142; +0.008, +0.87	0.149; +0.003, +0.21	0.024; +0.005, -0.53
Grand Isle, LA	0.114; +0.036, -0.63	0.114; +0.039, -1.25	0.013; +0.013, -1.00
Pilots Station East, SW Pass, LA	0.132; +0.014, +0.62	0.133; +0.015, -0.22	0.017; +0.005, -0.07
Gulfport Harbor, MS	0.157; +0.009, +0.75	0.172; +0.003, +0.03	0.035; +0.013, +0.29
Dock E, Port of Pascagoula, MS	0.149; +0.013, +0.03	0.170; -0.001, -0.61	0.027; +0.016, +0.32
Dauphin Island, AL	0.138; +0.002, -0.47	0.141; +0.002, -1.17	0.015; +0.013, +0.04
Panama City Beach, FL	0.141; +0.008, +0.88	0.145; +0.007, +0.03	0.034; -0.006, +0.59

The diurnal tide is dominant in the northern GoM, where major tidal constituents are O1, K1 (amplitudes of 0.12-0.17 m, with a minimum around southwest Louisiana) and M2 (0.03-0.15 m, with a maximum in southwest Louisiana). The largest errors occurred at Eagle Point, TX and Rainbow Bridge, TX, where FVCOM under-represented the tide, and for Grand Isle, LA where it overestimated tidal amplitudes (Table 2.2). However, these stations are located either very far from the continental shelf, inside Galveston Bay and Sabine Lake, or very far from landfall. Semi-diurnal amplitudes are smaller, and for M2 the two stations with larger errors were Sabine Pass North, TX and Calcasieu Pass, LA, where FVCOM under- and overestimated observed values, respectively, by about 15% (these stations are located inside coastal passes). The semi-diurnal tide was not perfectly captured in our application, but these are smaller amplitude constituents (S2 has 0.01-0.04 m amplitude on these stations; not shown). Typical amplitude prediction errors were about 0.01 m for the most important constituents. Tidal phase errors were small and rarely exceeded one hour for all stations and all constituents, in a region where tides have a ~24 h period. Overall the tidal predictions are satisfactory.

2.6 Model Validation for Storm Surge

Observations by McGee et al. (2006) provided data for Hurricane Rita's storm tide validation (Table 2.3). USGS deployed a total of 23 pressure sensors as Rita approached, along and near the coast ("onshore" in Table 2.3), from Sabine Pass, TX, to Abbeville, LA, at inland distances from 100 m to about 45 km inland. Only 14 USGS stations were used (Figure 2.4); the remainders were either too far north or located on small streams not resolved in the model. Data from three NOAA/NOS and one LSU station were also used for comparison with model results. The model did not do very well on these "offshore" stations. Here, modeled peaks were underestimated (by about 50%) and about 01h30 late (Table 2.3). Unfortunately there were no other "open water" stations with valid data covering Hurricane Rita. The three stations due east are very distant from

landfall (350-500 km), while the station south of Galveston Bay, TX was in the left quadrant of the hurricane, where winds blowing from land "against" the surge are admittedly overestimated.

Table 2.3: Stations used for Hurricane Rita's storm surge validation. All stations are NOAA's except where indicated. Negative timing errors indicate modeled surge ahead of time. Positive peak errors indicate modeled value greater than observation.

Station	Long., Lat.	Type	Max. Obs. Elev. (m)	Peak error (m)	Peak error (hr)
Galveston Pleasure Pier, TX	-94.788, 29.285	*Offshore*	0.94	-0.52	2.0
B15b (USGS)	-93.898, 29.765	*Onshore*	2.85	-0.19	-0.50
LC13 (USGS)	-93.753, 29.764	*Onshore*	3.24	0.15	-1.50
LC11 (USGS)	-93.583, 29.762	*Onshore*	4.54	0.20	-0.75
LC9 (USGS)	-93.471, 29.818	*Onshore*	4.21	-0.05	0.10
LC7 (USGS)	-93.403, 29.890	*Onshore*	3.40	0.20	-0.25
LC8a (USGS)	-93.329, 29.798	*Onshore*	4.07	0.65	-0.50
LC5 (USGS)	-93.228, 30.011	*Inland*	2.11	1.45	-8.50
LA12 (USGS)	29.786 -93.115	*Onshore*	4.52	-0.01	0.50
LC8b (USGS)	-93.080, 29.871	*Inland*	2.25	1.00	-2.50
LA11 (USGS)	-93.015, 29.771	*Onshore*	4.47	-0.45	0.50
LA10 (USGS)	-92.676, 29.707	*Inland*	2.65	-0.16	0.20
LA9 (USGS)	-92.328, 29.745	*Inland*	2.02	0.54	-7.50
LA9b (USGS)	-92.193, 29.783	*Onshore*	3.27	-0.16	-3.75
LF5 (USGS)	-92.127, 29.886	*Inland*	3.07	0.30	-6.50
CSI-05 (LSU)	-90.533, 29.053	*Offshore*	1.18	-0.75	2.00
Grand Isle, LA	-89.957, 29.263	*Offshore*	1.11	-0.75	1.00
Pilots Station East, SW Pass, LA	-89.407, 28.932	*Offshore*	0.82	-0.30	1.50

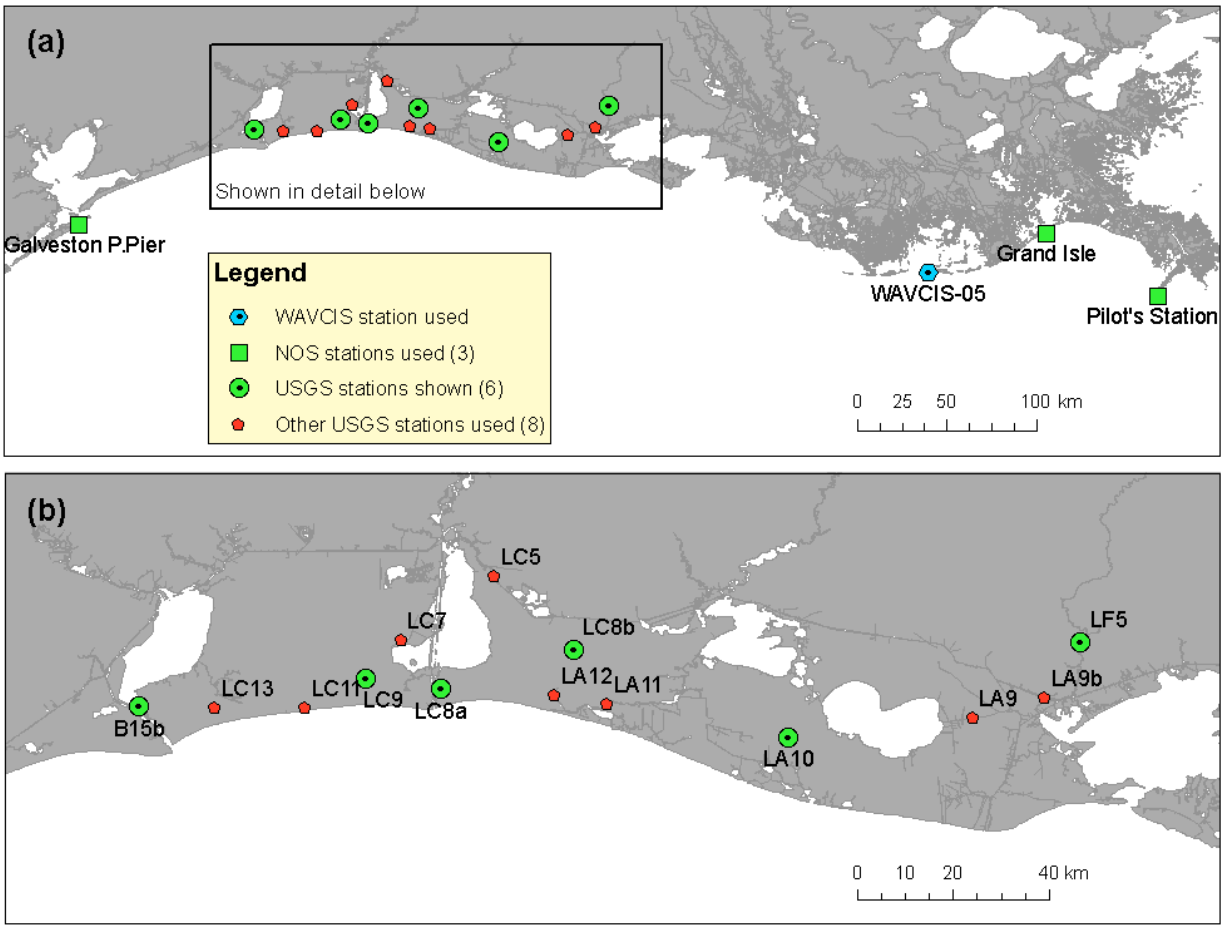

Figure 2.4: (a) Map of the region in the northern Gulf of Mexico most affected by Hurricane Rita, showing all stations used in surge validation. The box indicates the zoom shown below. (b) Detail of USGS stations used in surge validation.

FVCOM results matched very well against USGS observed water levels in coastal land stations inundated by the surge. Peak amplitude errors were typically ± 0.2 m, in records where the storm tide was 3.5-4.5 m (e.g., Figure 2.5c), suggesting a 5% error. The exception was station LC8a (Figure 2.5e), where the model clearly overestimated the surge. This is a 15% error, and although station LC8a is considered "onshore" it is located about 4 km inland from the GoM, on a "loop" of Calcasieu Pass. The large error is probably caused by an increase in drag from the land when flooded. With respect to the timing of the storm tide, coastal results were also very good and typically have a ± half hour shift (e.g., Figure 2.5a). The worst comparison came from station LA9b where the surge was estimated to have arrived three hours earlier than the observations indicated (amplitude error was only 5%). This station is located in Intracoastal City, LA, about 3 km inland from Vermillion Bay and near a network of channels not resolved in our mesh. Inland stations did not do as well, but results are also satisfactory. Either peak elevations were overestimated (e.g., Figure 2.5f) or the peak arrived too early (e.g., Figure 2.5b), but in most stations only one of these issues was a problem. Station LA10 (Figure 2.5d) did not have any of these problems. Overall, modeled surge curves were similar to observed curves. Hindcast simulations of Hurricane Rita using SLOSH and ADCIRC had similar inland issues, and this was attributed to the inability of these applications to properly account for differences in drag that would be felt over marsh as compared to over the seabed (URS, 2006; Guidroz et al., 2006).

Our results also show agreement with other published work on Hurricane Rita's inundation, e.g. USGS's "barrier mapping method" interpolation (Berenbrock et al., 2009), to be compared with our inundation map for the time of peak surge (Figure 2.6b), or FEMA's (2008) simple geographical interpolation of maximum surge contours, to be compared with our map of highest inundations (Figure 2.7). We thus conclude that, overall, FVCOM's representation of the storm tide is satisfactory in the northern GoM.

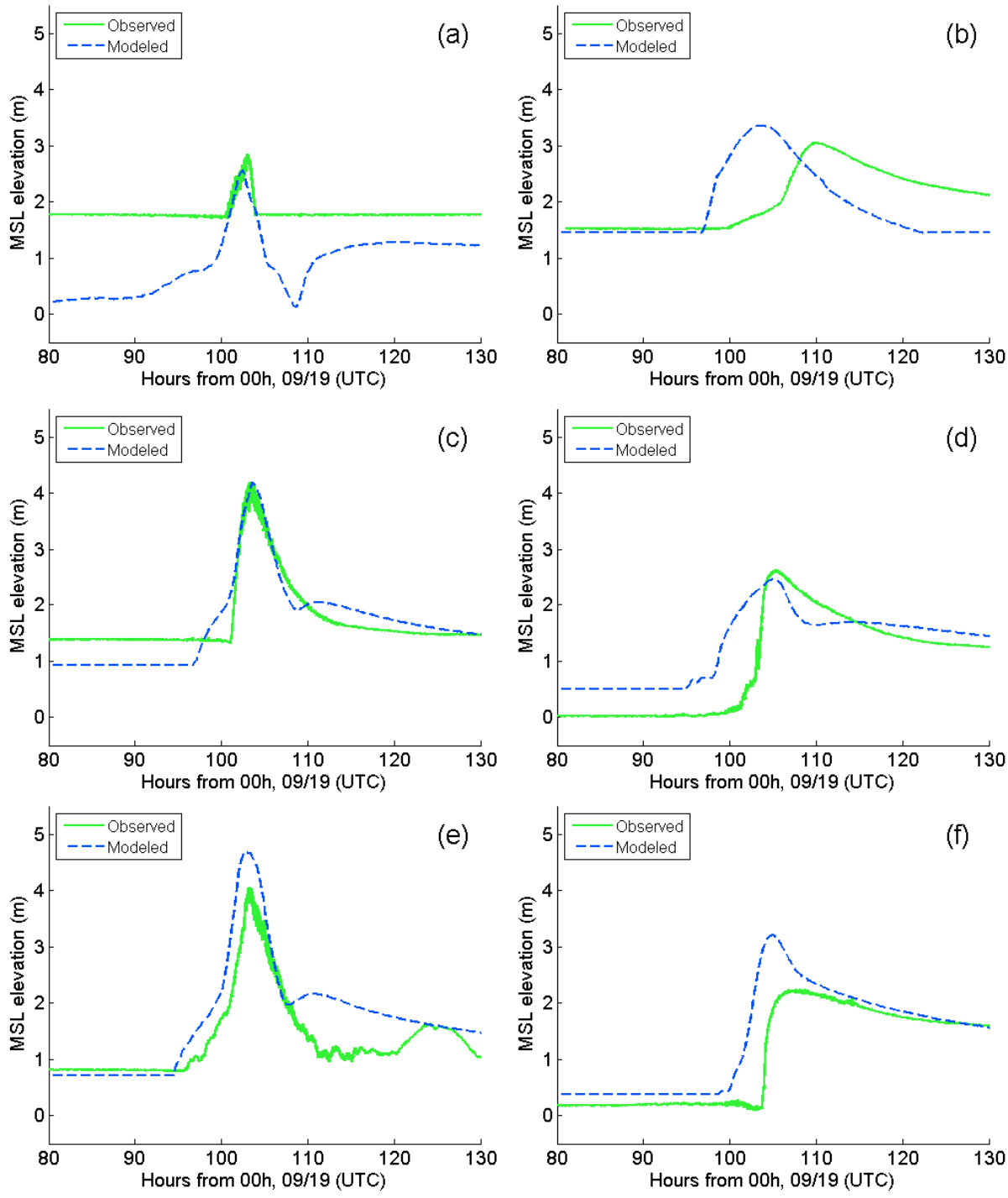

Figure 2.5: Modeled (FVCOM) vs. observed (USGS) water levels for Hurricane Rita, stations: (a) B15b, (b) LF5, (c) LC9, (d) LA10, (e) LC8a, (f) LC8b. All locations were initially dry, except for station B15b on Sabine Pass. Landfall for t = 104h.

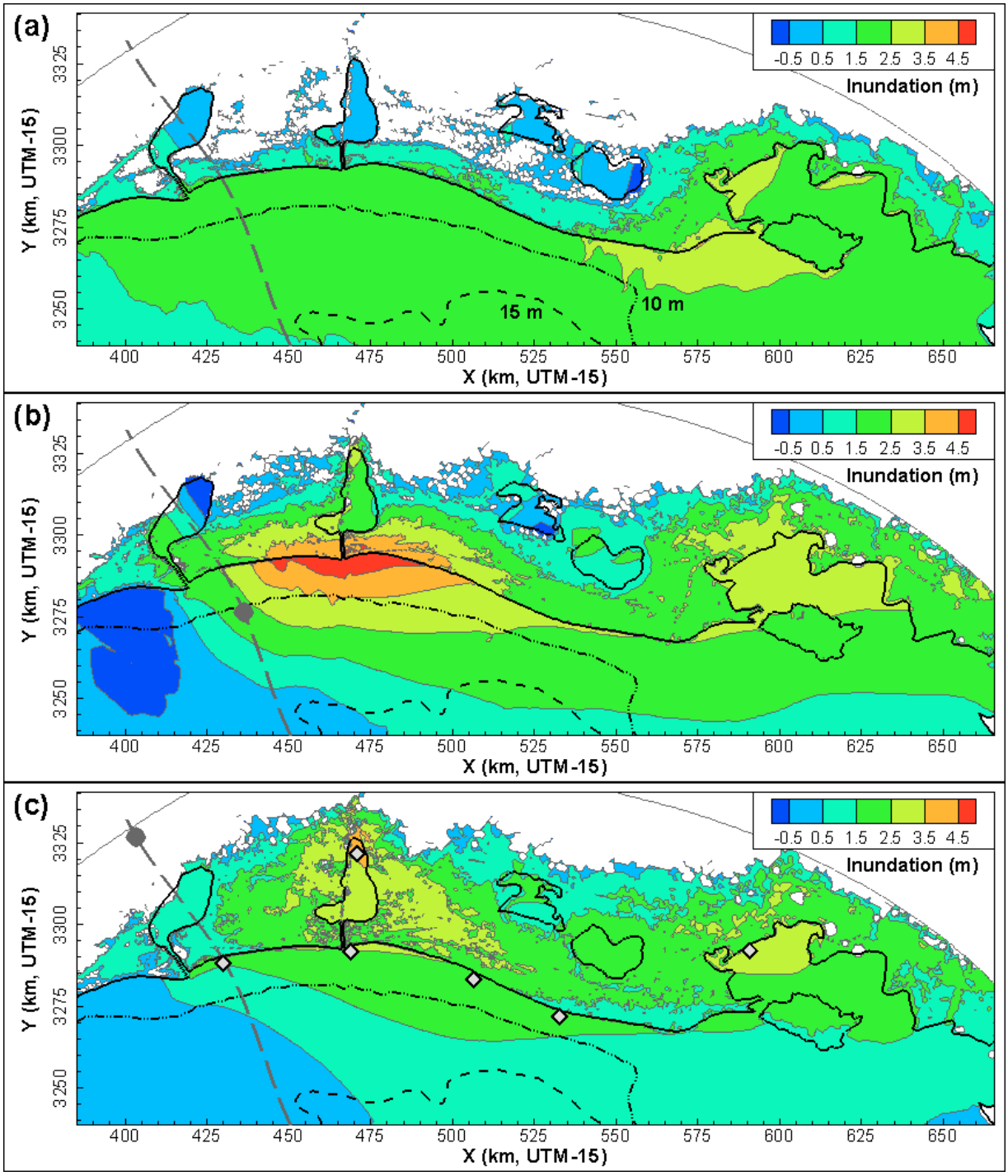

Figure 2.6: Inundation maps from model results: (a) 6 hours before landfall, (b) 1 hour before landfall, and (c) 2 hours after landfall. Hurricane Rita made landfall at 08h UTC, 09/24/2005. Hurricane track (long dashed line) and position (dark grey circle) are shown. Panel (c) indicates 6 locations (grey diamonds) referred to on Figure 2.8.

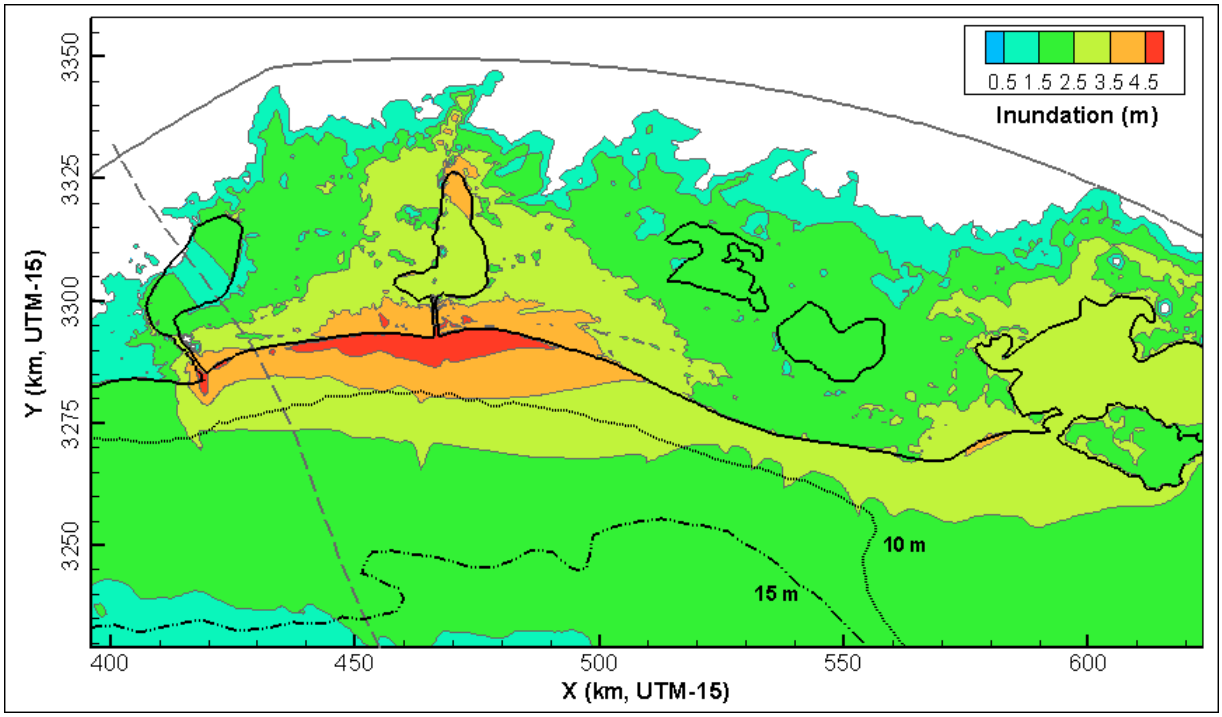

Figure 2.7: Maximum inundation map, illustrating flooding extent and distribution of surge amplitudes. Peak inundation levels for the entire simulation are shown.

2.7 Hurricane Rita's Storm Surge and Inland Flooding

The model indicates that before landfall, at 02h00 UTC, 09/24/2005 there was already significant coastal inundation from Bolivar Peninsula, TX east to Cote Blanche Bay, LA. Inundation reached about 8-10 km inland eastward of Calcasieu Pass, where the storm tide was about 2 m (Figure 2.6a). At this early stage and given the hurricane's northwestward track, the cyclonic hurricane winds blew shoreward over Vermilion Bay and initial surges were highest in the shallows around Marsh Island, about 3 m high (Figure 2.6a). In Vermillion Bay the storm tide peaked almost 2.5 hours before Hurricane Rita's landfall, and here water levels described a relatively slow rise and fall (Figure 2.8e).

The observed USGS water levels for stations LF5 (Figure 2.5b) and LA9 (not shown), however, suggest that the modeled inland flooding speed in this area was overestimated. This has been attributed to the bottom coefficient not taking into account the effect of vegetation over wetland and flooded low-lying land, but it is likely also related to a less-than-perfect representation of far-field hurricane winds. At the point of impact the storm tide curve reached 4 m about 2 hours before landfall (Figure 2.8a). In this location the local winds never really blew perpendicular to the shore; rather, they switched very quickly from easterly to westerly, which explains the lower and briefer surge.

The highest water levels did not occur exactly where the point of maximum winds made landfall, but rather at about 1.1×RMW east of impact one hour before landfall (Figure 2.6b). This is likely explained by the funneling caused by Calcasieu Pass. Here the storm tide peaked around 01h15 before landfall, at about 5.35 m (Figure 2.8b). The storm surge curve here was broader and the "bulge" that dominates the rising water until about 6 hours prior to landfall is also present. This represents the bathystrophic surge which is superseded by the oncoming cross-shore winds that dominate nearer the time of impact.

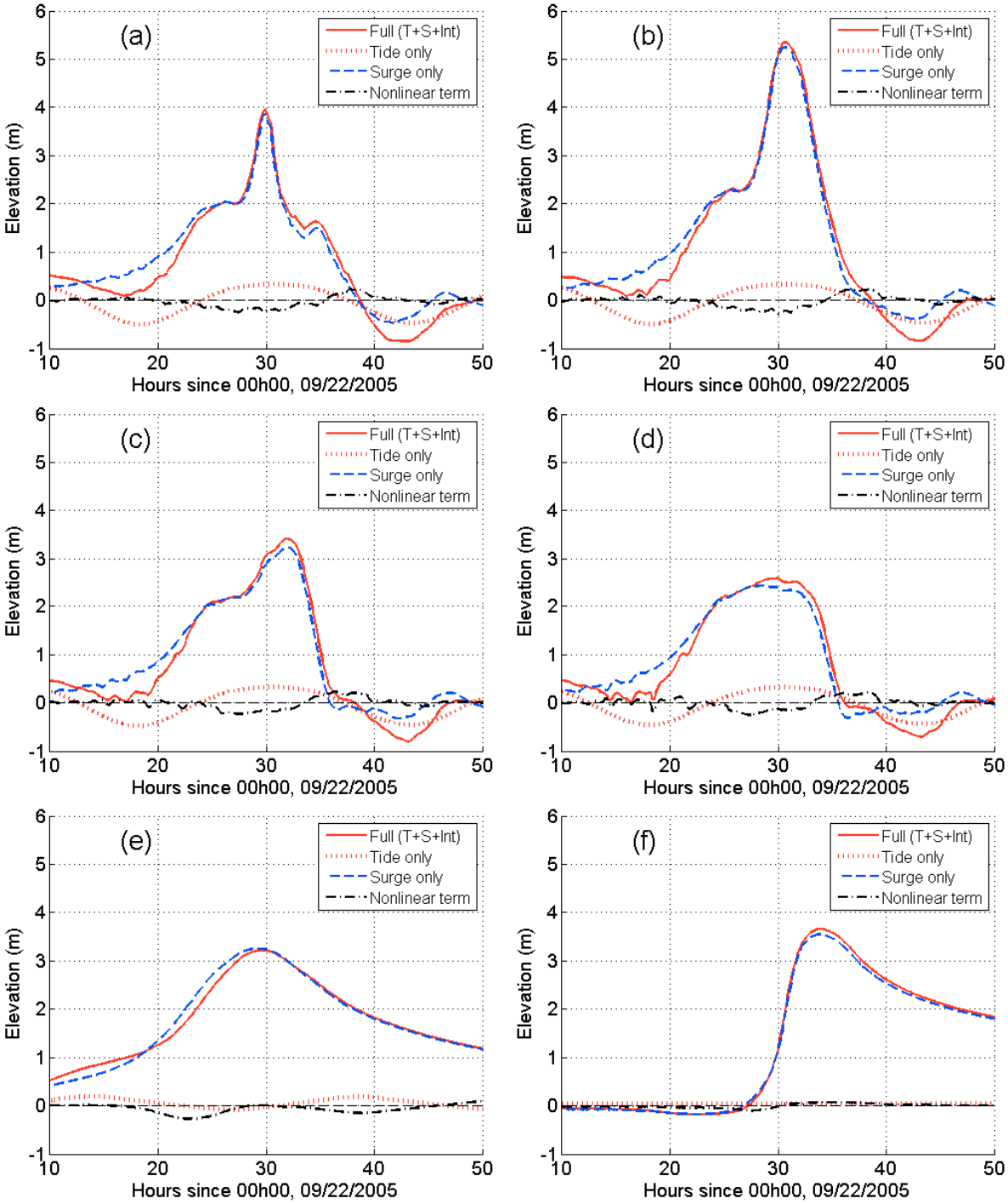

Figure 2.8: Water levels for locations indicated on Figure 2.5c: (a) near landfall, (b) 1×RMW due East, (c) 2×RMW due East, (d) 3×RMW due East; (e) in Vermillion Bay and (f) in Calcasieu Lake. Time shown as hours from 00h, 09/20/2005 (landfall at t = 32h). Locations (a)-(d) are at 4 m depth, the other two are at 2.5 m depth. The four curves represent storm tide (solid line), pure tide (dotted line), surge-only (dashed line), and the nonlinear interaction term (dot-dash line). See Figure 2.6c for locations (grey diamonds).

At about 2×RMW due east of landfall the surge curve is similar (Figure 2.8c): although the peak is considerably reduced, the bathystrophic surge peak of 2.2 m is almost the same as near the RMW. Farther east the surge peaks decrease even further (Figure 2.8d). Here the shore configuration relative to the hurricane track considerably decreased the onshore component of the wind, and surges peak at only 2.6 m and show little more than a bathystrophic surge (Figure 2.8d).

Two hours after landfall, flooding reached 30-50 km inland. At this time the highest water levels (at about 2.5 m) were still located near Calcasieu Pass, but spread east and west along the shore and also north, overland (Figure 2.6c). At the upstream part of Calcasieu Lake the storm tide peaked two hours after landfall, at 3.6 m (Figure 2.8f) and water levels did not go below 1.5 m for more than 30 hours after landfall (not shown). The post-hurricane receding stage is very important from an ecological standpoint and lasted for several days after landfall. This is because (1) there was no wind reinforcement to push them back (gravity "spreading" became the restoring force) and more importantly because (2) unlike the flooding stage when widespread coastal surges of above 2 m elevated the storm tide inundating everywhere over land, receding waters only flow through the existing narrow passes (see Rego and Li, 2009).

Hurricane Rita's landfall having occurred near high tide, the highest water levels to the right of landfall should have been higher than observed, if one merely added tidal elevations to computed surges. To separate the storm tide into astronomical tide, surge residuals, and the interaction component, separate FVCOM simulations were run for tide-only and surge-only scenarios. These are the extra curves shown on Figure 2.8, in which the nonlinear interaction term is computed as $\eta_I = \eta_{T+S} - (\eta_T + \eta_S)$, i.e. one subtracts tide and surge elevations from the storm tide's. If linear superposition were correct, storm tide curves should exceed those calculated for the surge-only case around peak surge (Figures 2.8a-d) by the tidal amplitude of

about 0.33 m, but storm tide elevations are only about half that height above surge-only curves. We conclude that nonlinearity decreases peak storm tide heights along the shoreline east of landfall, where the storm tide was highest (Figure 2.8a-d). This pattern is seen clearly along the Louisiana coast: the nonlinear term opposes the tide, i.e. it reduces storm tide heights near high tide and it enhances the storm tide afterward. The second nonlinearity peak is shorter in duration as the surge decreases rapidly at this time. To test if this pattern holds under a different tide, the same wind forcing was simulated but the tide was changed such that landfall would coincide with low tide, with a tidal amplitude twice as large as before. The same pattern occurred for the nonlinear effect: the nonlinear term opposes the tide by enhancing storm tide heights when the tide is near its lowest (and it reduces the storm tide afterward).

For the case of low- or high-tide landfalls described here, nonlinear effects were constructive or destructive to total storm tide, respectively. For peak "pure" surges between 2.5 and 5 m along the most impacted shore, average peak nonlinearities were 0.25 m at high tide with a 0.33 m amplitude (e.g., Figure 2.8a-d) and 0.45 m at low tide with a 0.68 m amplitude (not shown). These results indicate that nonlinearity is significant, reaching up to 66-75% of the tidal amplitude. Whereas for a hurricane expected to make landfall during high tide one can use the conventional method to obtain an overly conservative estimation for peak storm tide, a significant underestimation will occur if the hurricane hits at low tide (by more than half the tidal amplitude). Other authors have previously reached similar conclusions, but without the quantitative perspective and systematic approach that we perform in the next sections.

2.8 Idealized Simulations

To better understand how surge generation is sensitive to the local tide and continental shelf geometry, different scenarios were ran in which these factors were varied. A standard hurricane was defined, to be used in all idealized simulations. Its only variation will be landfall timing

relative to the tide. An appropriate RMW for a Cat-3 or Cat-4 hurricane is 50 km (Hsu and Yan, 1998). Its maximum sustained wind speed was set to 40 m/s, representing a medium-strength hurricane (Resio and Westerink, 2008). Hurricane forward velocity was set to 5 m/s, the average from those on Table 2.1.

A typical profile representing the continental shelf off southwest and central Louisiana was defined. Here the shelf is wide: the distance from shore to the 50 m isobath is 150 km and the shelf break (as measured by the 100 m isobath) is 45 km further offshore (Table 2.4). A narrower shelf was also defined, three times steeper, representative of the south Texas shelf. The gradient for the continental slope, from the shelf break down to the 1000 m depth, was the same for both cases (Table 2.4). Depths were set to 1000 m everywhere else.

Table 2.4: Gradients for the two typical continental shelves tested here.

Distances from shore, in km	**Typical Louisiana**	**Narrower Shelf**
… to 50 m isobath	150 km	50 km
(upper shelf gradient, $x10^{-3}$)	*(0.333)*	*(1.00)*
… to 100 m isobath	195 km	65 km
(mid shelf gradient, $x10^{-3}$)	*(1.11)*	*(3.33)*
… to 1000 m isobath	265 km	135 km
(continental slope gradient, $x10^{-3}$)	*(12.9)*	*(12.9)*

An idealized computational mesh was developed for these profiles (Figure 2.2b). The model domain fits a semi-circle centered at the point of landfall (*x=0, y=0*), with the open boundary located 300 km away from the center. Depths begin at 0.0 m along the *y=0* line and decrease linearly to *z=–10* m northward to the *y=30* km line (i.e., the inundation area follows the

gradient of the wide shelf slope). Positive depths, representing "wet" nodes, were increased by 1.0 m, to avoid constant wetting and drying during tidal runs. A total of 50234 triangular cells with 25317 nodes comprise the horizontal; 2 sigma layers comprise the vertical. Mesh resolution is 500-2000 m in most of the domain; it is 8 km at the open boundary.

Synthetic tides have amplitude of 0.50 m, slightly larger than the observed tide on the Louisiana-Texas shelf. Since the tide is mostly diurnal in this region, the synthetic tide in the idealized experiments uses K1 except for Scenario C, which will be used for comparison with a semi-diurnal tide. Scenario B has a minimum depth of 5.0 m, allowing for an evaluation of the effect of increasing a shelf's average depth. Simulations under Scenario D were done for the narrow shelf (Table 2.5). For each shelf/tide combination the standard hurricane was made to have landfall at significant tidal phases: High tide, Ebb, Low tide, and Flood (where ebb and flood were defined based on water levels rather than currents). This set of 4×4=16 simulations on a simplified coast (without complex convergences or funneling effects) with simple tides gives us insight into how shelf depth and slope, as well as tidal timing and tidal period affect hurricane-induced storm tides.

Table 5: Four storm tide scenarios tested with standard hurricane. Shelf geometries are summarized on Table 2.4; a "wide" shelf is representative of Louisiana's southwest continental shelf, whereas a "narrow" shelf has 3 times that slope. The depth added immediately seaward of the shoreline (to the entire shelf, thereby maintaining the desired slopes) is also shown. Tidal amplitude was 0.5 m in all cases.

Scenario	Shelf Geometry	Depth added	Tidal Period
A	Wide	1 m	K1 (23.94 h)
B	Wide	5 m	K1 (23.94 h)
C	Wide	1 m	S2 (12.00 h)
D	Narrow	1 m	K1 (23.94 h)

2.9 The Role of Shelf Geometry

Peak surge-only curves, determined along the y=0 line in the synthetic domain, are shown in black in Figure 2.9. Compared to peak surges produced by our "standard" hurricane hitting a wide and shallow shelf (Figure 2.9a), increasing the average depth by 4 m led to the decrease of peak pure surge to about 75% of the original (Figure 2.9b), whereas tripling the shelf gradient led to the decrease of peak pure surge to about 50% (Figure 2.9d). These are the effects of shelf geometry alone. Before introducing the effect of tides in surge simulations, and because we are investigating the role of shelf depth on pure surge, it is worth discussing the vertical structure of the surge currents. A storm surge represents a balance of vertically integrated pressure gradient force (the surface slope) with the difference of the surface and bottom stresses. The surface stress is from the wind; the bottom stress is where 2-D and 3-D models differ. The bottom stress typically follows a quadratic friction law: in the 2-D case this is based on the depth-averaged velocity whereas in the 3-D case it is based on the near-bottom velocity. Hence, by overestimating bottom stress a 2-D model tends to underestimate surge height. This may not be problematic in hindcast because the effective bottom drag coefficient can be calibrated. However, drag coefficients are not physically the same and important physics may not be resolved due to compensation of errors (Weisberg and Zheng, 2008). Our application accounts for this by using 2 sigma layers in the vertical, but most storm surge applications run in 2-D.

Vectors representing surface, depth-integrated and bottom currents are shown on Figure 2.10 for surge-only simulations. Comparing Scenario A (Figure 2.10a) with Scenario B (Figure 2.10b), surface currents in the former are stronger and have larger across-shore components than in the latter. The shallower Scenario A leads to a stronger surge asymmetry, in that surge elevations are higher to the right of the hurricane and lower to its left, as compared to a scenario only 4 m deeper (surge contours given by solid lines).

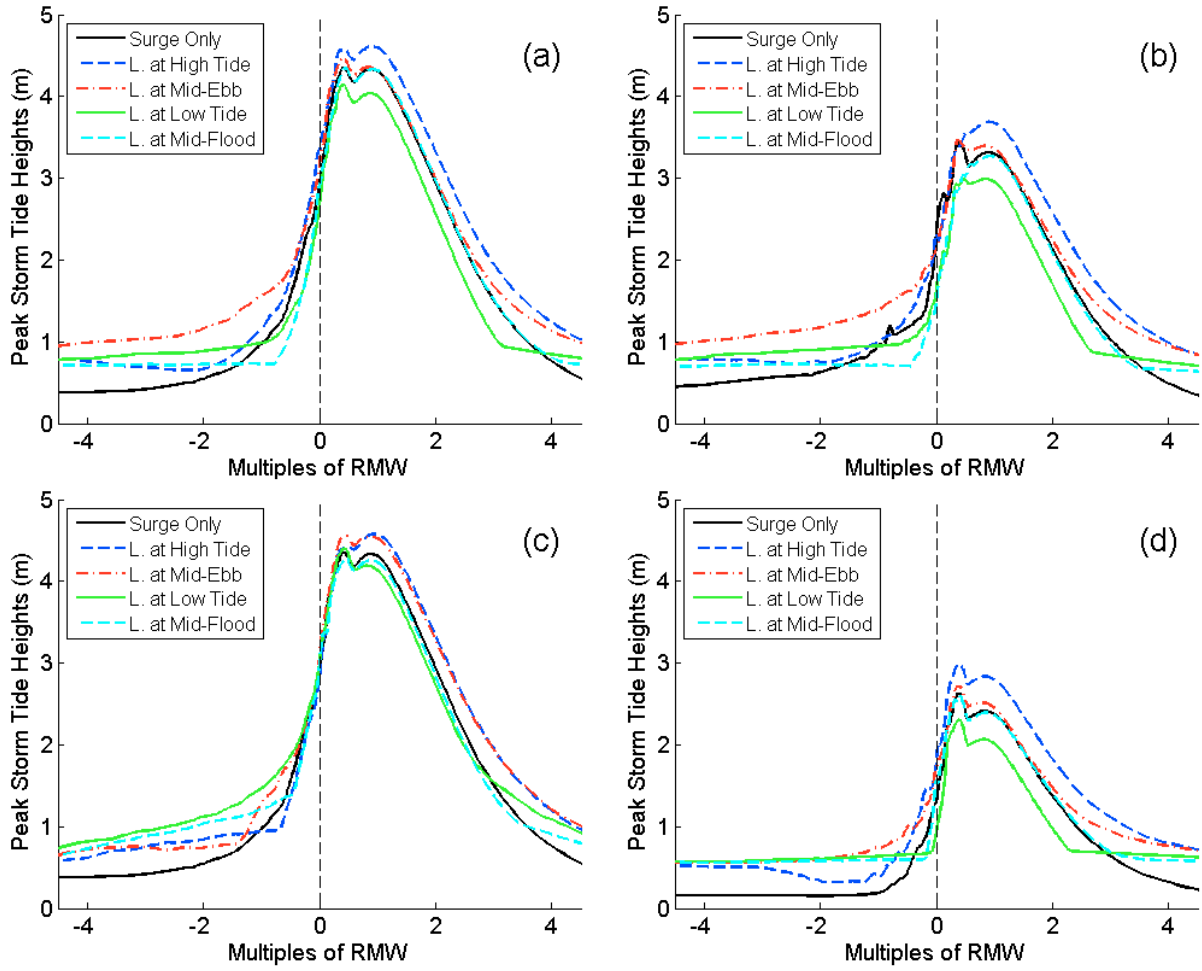

Figure 2.9: Peak storm tide elevations along y=0: (a) Scenario A, (b) Scenario B, (c) Scenario C, and (d) Scenario D (Table 2.5). Different locations have peaks at different times. Surge-only is shown as a dark solid line; other lines represent simulations including tides, for which hurricane made landfalls at different times. Abscissa is distance right (positive) and left (negative) of landfall, in multiples of RMW (=40km).

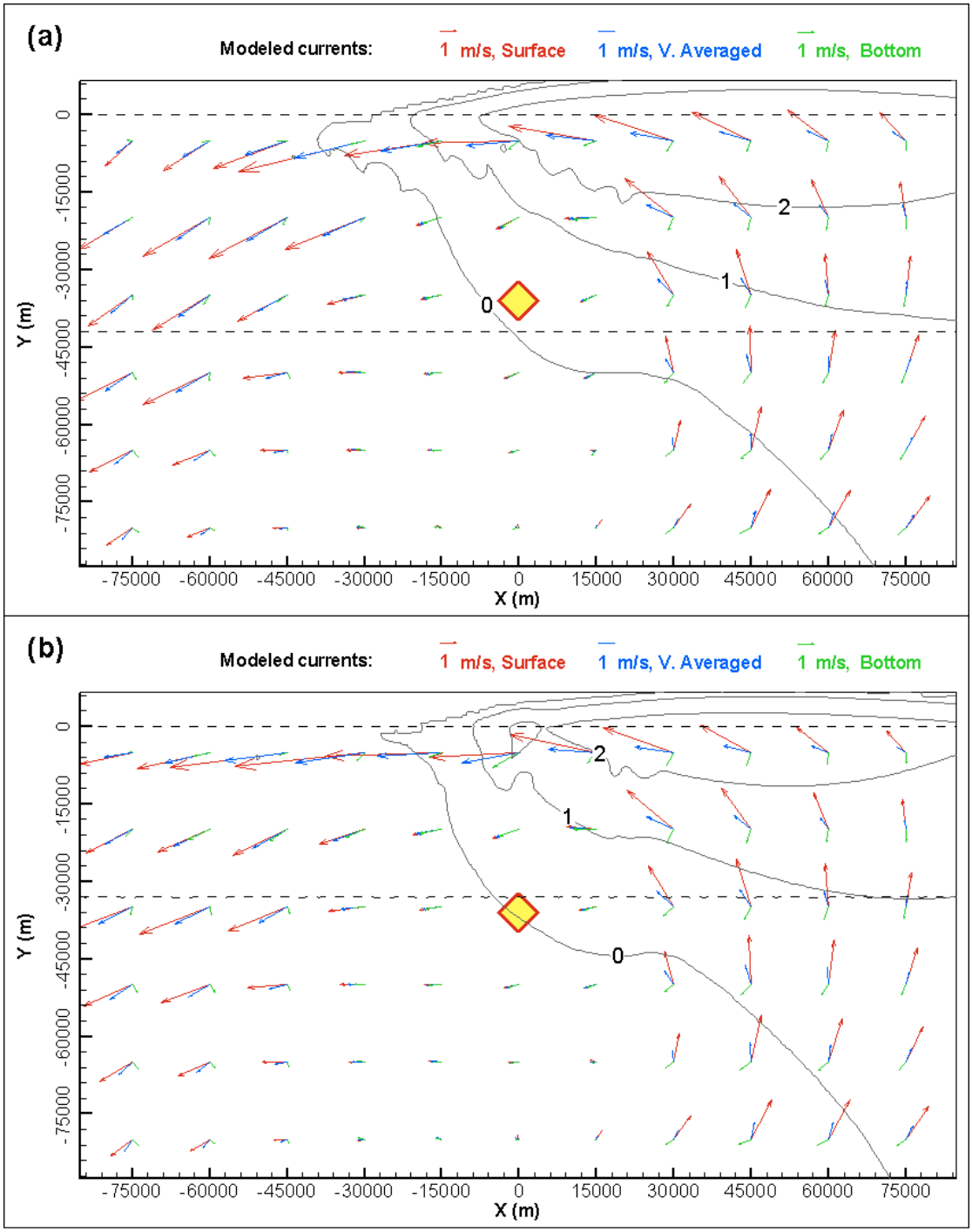

Figure 2.10: Surge-only currents in idealized simulations for (a) Scenarios A (K1 tide, wide shelf), and (b) Scenario B (the same, only 4 m deeper). Red, blue and green vectors represent surface, depth-integrated, and bottom currents, respectively. Coastal currents are shown 2 hours before landfall, for the standard hurricane of RMW=40km. The yellow diamond indicates the center of the hurricane. Currents were resampled into regularly-spaced 15km vectors, for clarity (mesh resolution was 500-2000 m). Dashed lines are the 0 and 15 m isobaths. Solid lines represent inundation heights, in meters.

Bottom currents on the right-hand side of the hurricane are directed to the left of the surface currents, from about 90 to 180º. Here the bottom current vectors point against the surface elevation gradient, nearly perpendicular to the surface elevation contours. This is the bottom return current described in Welander (1961) for the "quasi-steady surge with vertical circulation." It follows that the bottom stress (which opposes the bottom current) has a shoreward component, which contributes to increase the piling up of water against shore. This 3-D effect has a counter-intuitive, enhancing impact on coastal surge, and it is another indication that three-dimensional models are preferable over 2-D models for simulating storm surges (see also Weisberg and Zheng, 2008).

2.10 Effects of Nonlinear Tide-Surge Interaction

The peak height difference between low- and high-tide landfalls may serve as a first approximation for nonlinear effects: measured this way, nonlinear effects are greatest for Scenario C (0.38 m, Figure 2.9c), followed by Scenario A (0.58 m, Figure 2.9a), then Scenarios B (0.70 m, Figure 2.9b) and D (0.76 m, Figure 2.9d). These differences should equal the tidal range, 1 m, if there was no interaction.

All surge and storm tide peak curves are greater to the right of landfall, as expected. For Scenario A, surge-only peaks reach 4.35 m at 0.45×RMW and 0.9×RMW, and are above 2 m in -0.3×RMW<x<+2.6×RMW, (Figure 2.9a). Note that for x<-1.5×RMW and x>+3.8×RMW all the peak storm tide curves are above the surge-only line. This is because these storm tide maxima refer to the local high tide, which does not exist in the pure surge simulation. Indeed, the timing of peak storm tide gradually deviates from the timing of peak pure surge, approaching the time of local high-tide, far from x=+RMW. For locations 4×RMW to the right of landfall given a mid-ebb landfall, for example, local peak storm tide (considerably higher than local peak surge) occurs 4.6 hours before landfall, which is explained by the local K1 high tide 6 hours before

landfall. Given this increase in complexity, but mostly because nonlinearity greatly decreases away from the highest surges, our focus will remain on the -0.5×RMW <x< +2.5×RMW interval. This is consistent with Li (1988), whose approximate analytical solution with both astronomical tide and a meteorological surge give a greater nonlinear effect in the center of the forced wave.

Figure 2.11 summarizes the four scenarios, for each of the four types of landfall timings, at x=+0.9×RMW. Peak pure surge is highest (3.67 m) at 0.9×RMW to the right of landfall. This distance, shorter than RMW in a straight coastline, can be explained by the non-zero inflow angle used in the hurricane wind field (resulting in strongest winds hitting land slightly west of geometric RMW). Note that whereas the nodes used to create Figure 2.9 (along y=0) are over dry land, the nodes used to create Figure 2.11 (4 km offshore), are now at different depths: at 2.4 m for Scenario A and C, at 6.4 m for Scenario B, and at 5.2 m for Scenario D.

Under Scenario A, the effect of nonlinearity for landfalls at high- or low-tide is clear: peak storm tide heights are about 0.30 m lower and higher, respectively, than peak pure surge (Figures 2.11a,i), whereas a linear addition of surge and tide would yield 0.50 m differences. Nonlinearity peaks, in time, between peak surge and highest/lowest tide (these are separated by about a half hour), thus the resulting storm tide curves are similar to the surge-only curves, during rising and falling stages. The second nonlinearity peak, at the time of lowest surge, creates negative storm tides with virtually the same elevation as the pure surge's (always opposing the tide).

For landfalls at mid-ebb or mid-flood, peak storm tide heights are the same as pure surge, suggesting negligible nonlinearity. However, a linear addition of surge and tide for a landfall at mid-flood (Figure 2.11m) would produce a curve with a gentler slope before landfall and a steeper decline afterwards, whereas for a landfall at mid-ebb (Figure 2.11e) linearly adding tide and surge would result in a curve with a steeper slope ahead of landfall and a gentler decline

afterward. The nonlinear effect is relevant (and opposes the tide) in the ±5 hours around peak storm tide (it is zero when tidal elevation is at MSL), and merely alters the "shape" of storm tide curves.

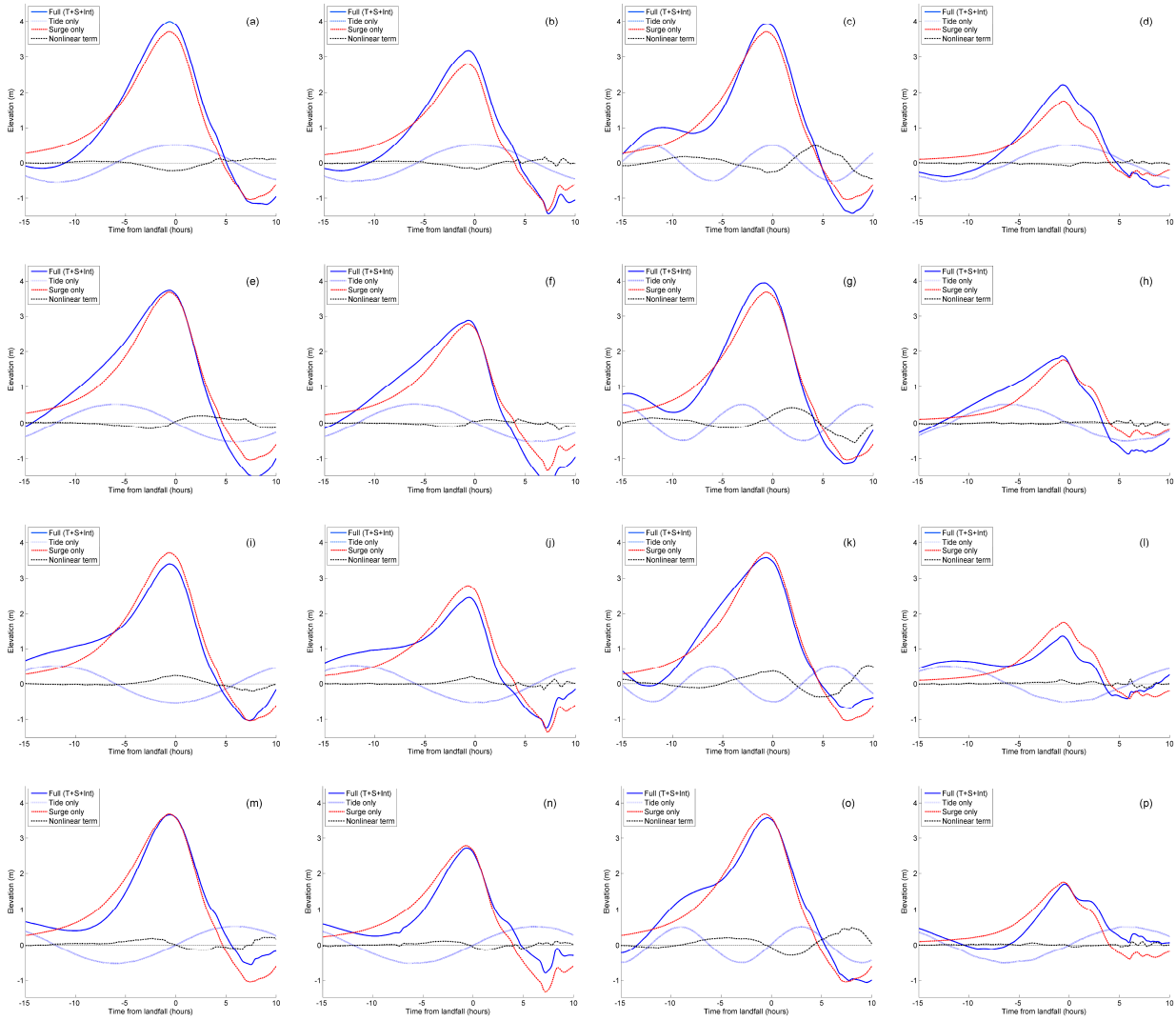

Figure 2.11: Water levels at x=+0.9×RMW. The 4 columns from the left are Scenarios A, B, C, and D, respectively. The 4 rows represent results for landfall at high tide (a-d), mid-ebb (e-h), low tide (i-l), and mid-flood (m-p), respectively. The four curves have the same meaning as Figure 2.8's. All landfalls at t=20h.

Farther away from landfall, at 2×RMW right of landfall (not shown), peak storm surge is about 70% of peak surges near RMW. Here the effect of nonlinearity for high- or low-tide hurricane impacts is to produce peak storm tide heights about 0.4 m lower and higher, respectively, than peak pure surge. This indicates the decreasing effect of nonlinearity as local pure surges decrease. The effect of nonlinearity for all landfall timings tested is the same for Scenarios B and D as for Scenario A, albeit with a decreased magnitude: a change in shape for ebb- of flood-tide landfalls and a change in peak amplitude for high- or low-tide landfalls – with nonlinearity always opposing tide.

Scenario C, with a semi-diurnal tide on the same shelf as Scenario A, yielded the greatest nonlinearities. Although peak pure surges are the same for both scenarios, peak nonlinear effects at these locations are about 50% greater in Scenario C compared to Scenario A. Contrary to all other scenarios, a landfall at mid-ebb produces a peak storm tide higher than the pure surge (Figure 2.11g), because the nonlinear effect actually adds to the tide for about one hour, before landfall. Having landfalls for low- and mid-flood tides yield comparable peak storm tides, both about 0.12 m lower than pure surge (Figures 2.11c,o), which is also unlike the other scenarios. Under Scenario C, storm tide and pure surge curves show 10-15 minutes phase shifts that add to the complexity of this analysis.

Figure 2.12 shows peak magnitudes of the nonlinear effect along $y=0$, averaged between $0.75\times RMW < x < 1.25\times RMW$. Nonlinear effects reach up to about 80% of the tidal amplitude for Scenario C, about 47% for Scenario A, about 41% for Scenario B, and 26% for Scenario D (determined using the average high- and low-tide values). Although they have the same broad and shallow shelf and the resulting same peak storm surge value, 3.7 m, Scenario A with a K1 tide and Scenario C with an S2 tide yielded distinct nonlinearities, the latter producing much larger values.

For all scenarios tested the nonlinear effect is greatest for landfalls at low tide, followed by landfalls at high tide (10-30% smaller) and then by those cases with landfalls at mid-ebb or mid-flood (further 30-45% smaller). The decrease is more pronounced for the case with a narrow shelf, Scenario D, for which both storm surges and nonlinearities were the smallest (Figure 2.12). Not accounting for these nonlinearities may result in peak storm tide overestimation for landfalls at high tide and underestimation for landfalls at low tide, by about 45% of tidal amplitude in Scenarios A and B. But for Scenario C, the semi-diurnal tide on our wide and shallow shelf causes so much nonlinearity (up to 80% of the tidal amplitude) that a simple surge-only simulation would actually produce better estimates for peak storm tide heights than adding pure surge to tidal elevations.

2.11 Nonlinear Residuals in the Momentum Equations

Variations in the nonlinear bottom friction terms, $C_d u\sqrt{u^2+v^2}\,/(h+\eta)$ and $C_d v\sqrt{u^2+v^2}\,/(h+\eta)$, and nonlinear momentum advection terms, $u\,\partial u/\partial x + v\,\partial u/\partial y$ and $u\,\partial v/\partial x + v\,\partial v/\partial y$, generate tide-surge interaction in shallow water and influence the distribution of energy between tide and surge. By examining time-series of these terms, their influence on tide-surge interaction can be better appreciated. The nonlinear terms in the equation for mass conservation play an insignificant role in tide-surge interaction (Welander, 1961; Wolf, 1981; Tang et al., 1996; Jones and Davies, 2008), and will not be considered here. Jones and Davies (2008) made similar investigations to study how extra-tropical surges affect the local tide in the Irish Sea. Their model results indicated that these nonlinear residuals were significantly larger (of order 100) in shallow waters as compared to deep waters (1.8 vs. 45 m depths in their example). Over shallow waters, their bottom friction term peaked at about 5×10^{-4} m·s^{-2}, while their advection term peaked at about 5×10^{-5} m·s^{-2}.

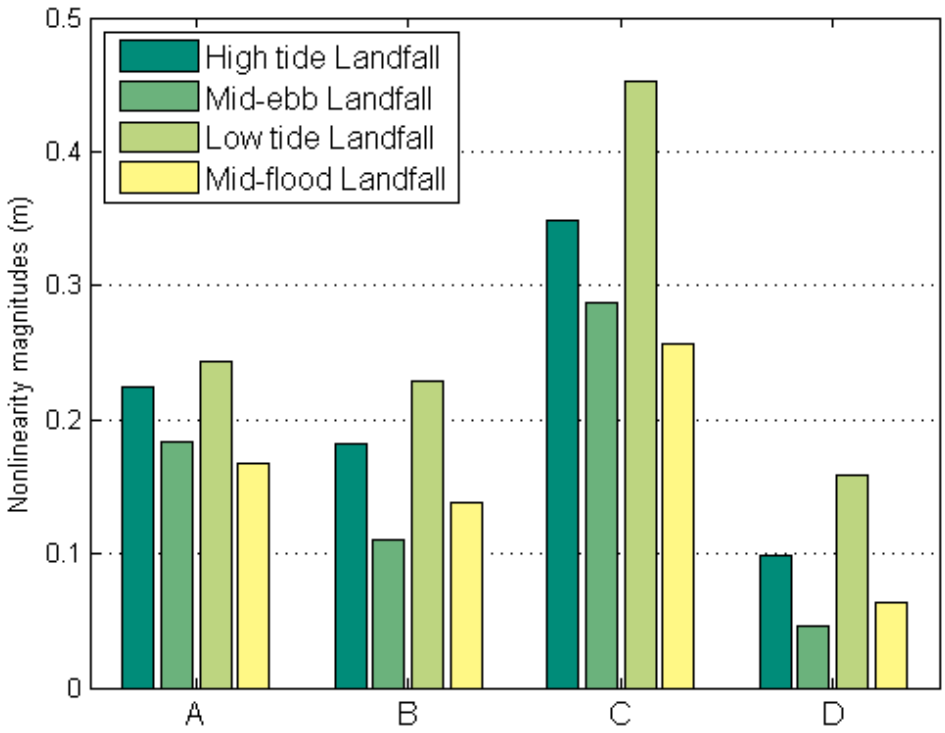

Figure 2.12: Magnitude of nonlinear term maxima for idealized simulations, near x=+RMW for the 4 different landfall timings (4 different color bars). Abscissa represents different Scenarios (Table 2.5). For landfalls at low- or high-tide, only the nonlinear term during peak surge is shown. For landfalls at mid-ebb or mid-flood the average magnitude of two peaks is shown.

Here we examine in detail results at two locations, “Point 1” and ”Point 2” (located 1×RMW and 2×RMW to the right of landfall, respectively) for both real and idealized geometries, and for low- and high-tide landfalls. These are the same points used in Figures 2.8 and 2.11 (over depths of about 4 m in the real mesh and 2.5 m in the idealized mesh). Time-series of the various terms in the y-momentum equation (not shown) indicate that bottom friction and advective terms are the most significant right of landfall, together balancing the pressure gradient force. For the Rita simulation on the realistic Louisiana-Texas mesh, the friction term is greater than advection, but both terms have the same order of magnitude; for the idealized mesh with a straight coastline and monotonically deepening shelf, advection is about 5 times smaller than friction. This is to some extent, expected. As indicated in Li (2006) and Li et al. (2008), advection tends to be much larger when there is a complication of bathymetry and curvature of the coastlines. As much as 45%-70% of the nonlinearity can be from advection when such complication exists. In the x-momentum balance, all terms are an order of magnitude smaller than that in the across-shelf direction and won’t be discussed here.

The change in friction and advective terms, taken as the difference between tide with surge and tide-only plus surge-only, reveals the nonlinear residuals in the simulations. Figure 2.13 shows time series of the difference in these terms for the realistic and idealized cases (top and bottom rows, respectively), having low- and high-tide landfalls; Point 1 is shown on the left, Point 2 on the right.

For the Louisiana-Texas simulations, changes in these terms show significant temporal and spatial variability. Much like in Jones and Davies (2008), nonlinear residuals peak at about 2 and 4×10^{-4} $m\cdot s^{-2}$, also with many fluctuations and no clear pattern. Because the hurricane travels quickly, the relative magnitude of local wind-forced currents and their orientation and phase relative to tidal currents varies quickly, and the advective and frictional terms change

significantly in time and space. In our hurricane simulations the advection term clearly dominates over the bottom friction term, indicating a higher degree of complexity. Comparing the low- and high-tide landfall curves on each plot, they tend to "mirror" each other, but with considerable noise.

Not surprisingly, time-series of nonlinear residuals from the idealized cases (bottom row of Figure 2.13) show less variability. Bottom friction now clearly dominates over advection, which is very small. Here the friction nonlinear residuals peak at only about 2×10^{-4} m·s^{-2}. Overall the nonlinear elevation effects were not that different between idealized and realistic simulations (Sections 4.1 and 4.4); this is attributed to the less oscillating behavior of the bottom friction residuals for the idealized scenarios as compared to the advective residuals for the realistic simulations. The tendency for low- and high-tide landfall curves to "mirror" each other is also clearer.

The variability and dependency upon landfall timing can be appreciated by considering the influence of changes in bottom stress produced by the tide. Since the bottom stress ($C_d vU/D$) is appreciable in nearshore regions and depends upon current magnitude U and total water depth $D= h+ \eta$, even if η and U were constant, the influence of the stress would show significant variability as h changes rapidly near the shore. For a high-tide landfall η increases, and so for a constant U the bottom stress decreases, which in a pure surge simulation would correspond to reducing C_d, leading to an increase in surge amplitude, as less energy is dissipated by bottom stress. However, in a combined tide and surge calculation, U depends on both the storm surge current (a function of wind direction and water depth) and tidal current. Therefore any reduction in bottom stress due to an increase in η in a combined tide-surge simulation can be offset by an increase in U, with an associated increase in bottom stress and reduction in surge energy.

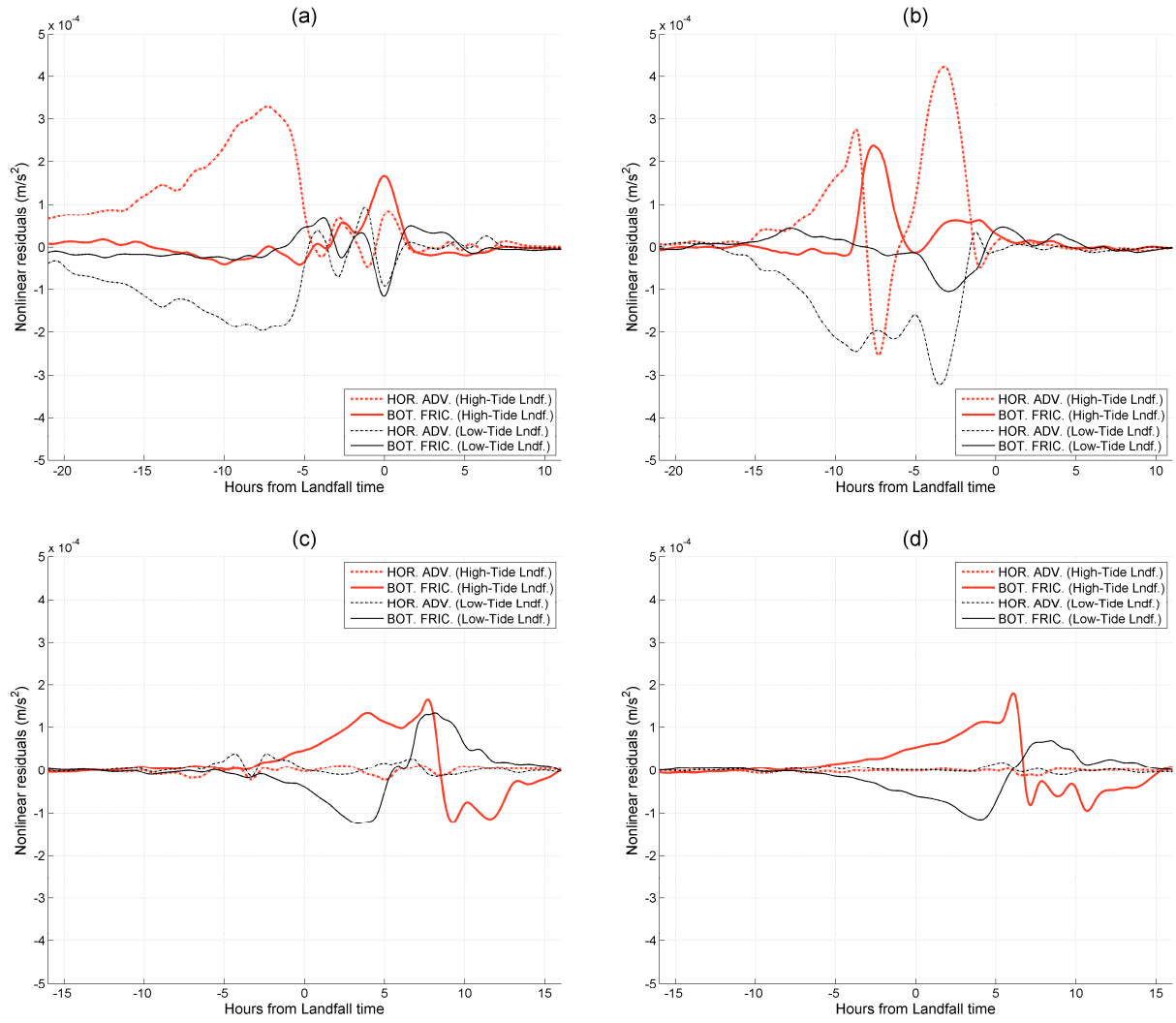

Figure 2.13: Changes in the y-momentum of the two major nonlinear components: bottom friction [$C_d v\sqrt{u^2+v^2}\,/(h+\eta)$, dashed lines] and horizontal advection [$u\,\partial v/\partial x + v\,\partial v/\partial y$, solid lines], both in m·s^{-2}. Each sub-panel shows nonlinear residuals for landfalls at low-tide (fine, black lines) and high-tide (thick, red lines): (a) and (b) represent Hurricane Rita model results, at Points 1 and 2, respectively; (c) and (d) represent Scenario A's results, also for points located 1×RMW and 2×RMW to the right of landfall.

2.12 Conclusions of Chapter 2

An application of the unstructured-grid finite-volume numerical model FVCOM to Hurricane Rita's storm surge in September 2005 was implemented and the resulting inland flooding along the Louisiana-Texas coast studied. The simulated storm surge induced by Hurricane Rita was successfully verified against USGS' measurements in the coastal and inland locations where instruments were deployed prior to the landfall. On the stretch of coastline most affected by Hurricane Rita, from point of landfall to approximately 3×RMW due east, peak storm tide reached 5 m.

The nonlinear effect was computed by subtracting tide and surge-only elevations from the storm tide's. Along the coast east of landfall nonlinearity opposes the tide, reducing storm tide heights when the tide is rising or high, and enhancing the storm tide when ebbing and approaching low tide. For low- or high-tide landfalls, nonlinearity effects are constructive and destructive to total storm tide, respectively. Nonlinearity is significant, reaching up to about 70% of the tidal amplitude in both cases.

In the second part of this study a systematic approach to tide-surge nonlinearities was performed, forcing a typical hurricane on different shelf geometries for different tides and tidal timings (relative to landfall). Compared to peak surges produced by our "standard" hurricane hitting a wide shelf with a 1 m minimum depth, increasing the minimum depth to 5 m decreases peak pure surge to about 75%, whereas increasing (by a factor of 3) the shelf gradient decreases peak pure surge to about 50%. This is the effect of shelf geometry alone.

The analysis of surface, depth-integrated and bottom currents were used to show how the shallow Scenario A leads to a stronger surge asymmetry (higher surge elevations to the right of the hurricane and lower to its left), as compared to a scenario only 4 m deeper. Because the bottom are nearly perpendicular to the surface elevation contours, the bottom return flow is

directed to the left of the surface currents (from about 90 to 180º) on the right-hand side of the hurricane. The bottom stress then has a shoreward component, which contributes to increase the piling up of water against shore. This counter-intuitive three-dimensional effect has an enhancing impact on coastal surge, and suggests that 3-D models are preferable over 2-D models for simulating storm surges.

When tides are included in simulations, nonlinear interaction is shown to be important in the region -0.5×RMW <x< +2.5×RMW (where *x=0* is landfall), since this is where surges are higher and also where local peak storm tides are coincident in time with local peak pure surges. For landfalls at mid-ebb or mid-flood the main nonlinear effect is to oppose the tide in the 5 hours before and after peak storm tides, generating storm tide curves with moderately different shapes but having the same peak height (as a linear superposition of surge and tide). For landfalls at high- or low-tide the nonlinear effect opposes the tide, i.e. peak storm tide heights are lower and higher, respectively, than a linear superposition.

Nonlinearity effects reach up to 80% of the tidal amplitude on a wide shelf under a semi-diurnal tide. This demonstrates the effect of amplification of nonlinearity over a wide shelf: the semi-diurnal tide has larger nonlinear effect compared to the diurnal tide because the former has a shorter wavelength and "sensed" the shelf as being wider when the same geometry is used. Under diurnal tides, nonlinearity effects reach up to 47% for a wide shelf, 41% for a wide shelf 4 m deeper, and 26% for a narrow shelf. The nonlinear effect is the greatest for landfalls at low tide, followed by landfalls at high tide and then by landfalls at mid-ebb or mid-flood. Not accounting for such tide-surge interaction may result in a significant overestimation of peak storm tide heights for a landfall at high tide and a significant underestimation for a landfall at low tide.

The change in the storm tide was found to be appreciable in shallow water and was produced by changes in non-linear bottom friction and momentum advection due to the presence of the tide. A detailed examination of these residuals showed that the nonlinear residuals of advection dominate in the realistic simulations, while the nonlinear residuals of the quadratic bottom friction dominate in idealized simulations (see also Li et al., 2008). Because bottom friction is the most important nonlinear term, it would be physically more correct to have a spatially variable drag coefficient and a comparison against simulations having spatially-varying values should be of interest. While there are applications where lower values are used "offshore" and higher values for shallower waters (e.g. Retana, 2008), our study produced very good validations with a "high" drag value used throughout the domain (like e.g. Jones and Davies, 2008), probably because our focus was on nearshore areas. Unfortunately, such an increase in complexity would complicate even more any attempt to summarize storm surge mechanisms and its interaction with tides and shelf geometry. This complication is not addressed here and is left for future studies.

CHAPTER 3

ON THE RECEDING OF STORM SURGE ALONG LOUISIANA'S LOW-LYING COAST[2]

3.1. Introduction

Since it is the initial surge impact that causes the largest part of human deaths and destruction, most surge hydrodynamics studies focus on peak coastal surge timing, elevations and currents, and the return to sea of storm waters is often overlooked. However, this receding surge is reportedly important from an ecological standpoint (e.g., Nichols, 1994) in that the longer surge inundation lasts, the more environmental damage will take place (endangering animals, fish and plants by keeping excessive amounts of saltwater in marshes). Nichols (1994) studied the response of Chesapeake Bay estuaries to storms and concluded that the "recovery" stage extends from 7 to 26 days. Gong et al.'s (2007) model results for the York River estuary suggest that the influence of Tropical Cyclone Isabel's (September 2003) storm surge itself on estuary transport mainly occurs within the first 48 h, whereas the recovery of the estuary to its natural state required about 20 days. The study by Gong et al. (2007), however, focused on salt flux mechanisms during storm surge and subsequent high river pulse event, and did not attempt to explain the surge hydrodynamics.

Hurricane Gustav occurred three years after Hurricane Rita (described in Chapter 2). After devastating large parts of Cuba, Gustav reached its maximum strength with maximum sustained winds of 240 km/h and a minimum pressure of 941 mbar (becoming the second major hurricane of the 2008 Atlantic hurricane). On 09/01/2008 at 15h UTC the center of Gustav made landfall in the United States along the Louisiana coast near Cocodrie (Figure 3.1) as a very strong Category 2 hurricane, with winds of 175 km/h (Beven, 2008). Here we use USGS surge

[2] Reprinted by permission of the Journal of Coastal Research (see Rego and Li, 2009a)

data, our modeling results from Hurricane Rita, and our data covering Hurricane Gustav to study the receding stage of surge waters. We quantify typical longer term hurricane-induced inundation patterns and describe why surge inflow and outflow dynamics are so different on this coast. This is relevant to the general problem of storm surge coastal impacts and clearly warrants investigation.

3.2. Methods

The model domain, designed to study Hurricane Rita's storm surge, extends from the Mexico-U.S.A. border to Apalachicola Bay in Florida, with a 1,300 km long open boundary arching in between. The mesh has a total of 178,675 triangular cells with 90,099 nodes comprising the horizontal and 2 sigma layers in the vertical. Mesh resolution increases from 10 km on the open boundary toward the region of Hurricane Rita's impact; the finest resolutions (200 m) are on Sabine and Calcasieu Passes (Figure 3.1), which connect the area's major lakes to the Gulf. In this application floodplain cells have a 500-2000 m resolution; the flooding threshold depth was set to 10 cm. Bathymetry data is a combination of the National Geophysical Data Center's US Coastal Relief Model, the ETOPO-2 Global Relief model and LSU's LIDAR dataset. The model was forced by wind stress and tides. With an external timestep of 0.6 s and running on 64 processors of the Shell Coastal Environmental Modeling Laboratory (LSU's SC&E), a 10-day simulation takes approximately 25 hours to complete.

Following the methodology of Chapter 2, we use the parametric wind model by Holland (1980) with the observed gridded wind speed data from NOAA's Hurricane Research Division, the H*WIND dataset (Powell et al., 1996). Jelesnianski's (1966) "correction" to account for the asymmetry due to the forward motion of a hurricane (increasing the wind speed in the right quadrants) is used. Holland's peakedness parameter, B, is given as a function of the RMW.

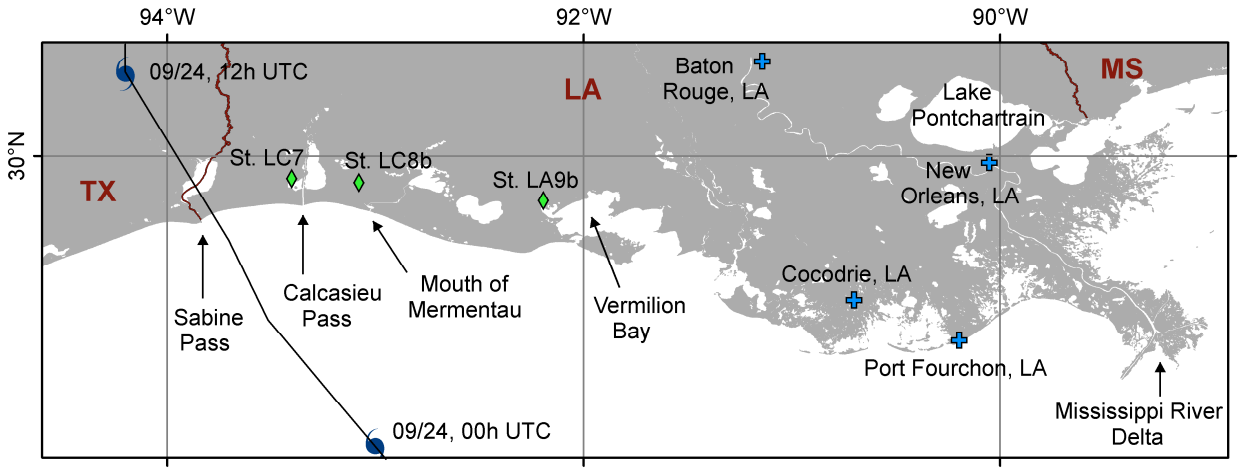

Figure 3.1: Map of south Louisiana. Hurricane Rita's path, features mentioned in the text and USGS stations from Figure 3.2 are shown.

The "inflow angle" is set to a constant 10º. Having a set of X, Y, RMW, Vmax, and forward speed for each H*WIND snapshot, we assign a wind vector for every cell in the model as a function of the distance to the hurricane center. Our improved Holland model provides a better fit against observed winds and allows for hurricane wind field interpolation at short intervals; here, wind fields are interpolated into 12-minute intervals.

A simulation of the tide was first carried out with FVCOM. The model was forced at its open boundary by 9 tidal constituents obtained from Mukai et al. (2002) and run without wind forcing for 36 days. Hourly model output was used for harmonic analysis of tidal constituents. Calibrating FVCOM for this application consisted of varying the bottom friction coefficient, constant in the entire domain; the best results were obtained with BFRIC=0.0040. Tidal constituent were obtained from 14 NOAA tidal stations and three Coastal Studies Institute (CSI) WAVCIS stations (LSU). The tidal phase errors are small and rarely exceed one hour for all stations and all constituents, in a region where tides have a ~24 h period. Excluding three upstream stations, the typical amplitude prediction error is about 0.01 m for the most important constituents, O1 and K1. Overall the tidal predictions are very satisfactory.

Observations by McGee et al. (2006) provided data for Hurricane Rita's storm tide validation. A total of 23 USGS pressure sensors were deployed along and near the coast, from Sabine Pass, TX, to Abbeville, LA, at inland distances ranging from a few hundred feet from the coast to about 30 miles inland. Data from three NOAA/NOS and one LSU/CSI stations were also used, for storm tide comparison in GoM open waters. Comparison between FVCOM results (simulating surge and tide, for an observed landfall near high tide) and USGS water levels for coastal stations on southeast and central Louisiana yielded very good matches (see Chapter 2). Peak amplitude errors were typically ± 0.2 m, in records where the storm tide was 3.5-4.5 m, suggesting a 5% error.

With respect to the timing of the storm tide, coastal results were also very good and the typical situation is a ± half hour shift. Inland stations had slightly larger errors. Either peak elevations were overestimated (*e.g.*, Figure 3.2b) or the modeled peak arrived too early (*e.g.*, Figure 3.2c), but in most stations only one of these issues was a problem. Inland stations LC7 (Figure 3.2a) and LA10 (not shown) did not have any of these problems. Hindcast simulations of Hurricane Rita using SLOSH and ADCIRC had similar inland issues, and this was attributed to the inability of models to account for differences in bottom friction between water and marsh (URS, 2006). Our results also show good agreement with other published work on Hurricane Rita's inundation (FEMA, 2008; Berenbrock et al., 2009).

More importantly, our modeled receding surge curves match very well with observed curves, with small errors in peak heights or peak timing. Such a successful representation of Rita's storm tide allows us to proceed with confidence in looking at storm surge dynamics and coastal inundation.

3.3. Discussion

The USGS surge data is valuable (*e.g.*, Figure 3.2), but has some disadvantages: it only covers a few locations, clustered around roads and bridges; only 2 stations (inside our mesh, B15b and LC8b) start with a 0 MSL elevation, with most stations placed at about 1 m elevation. The former is offset by the use of our validated numerical model, which gives us water levels and currents for the entire domain at any time (*e.g.*, Figure 3.3), whereas the latter is countered by the use of our own data from two channels, covering Hurricane Gustav (Figure 3.4). Having time-series that only record down to 1 m implies that receding times can only be stated with confidence for the ~35% level (*i.e.*, the time it takes for the surge to reach down to 35% of its local peak).

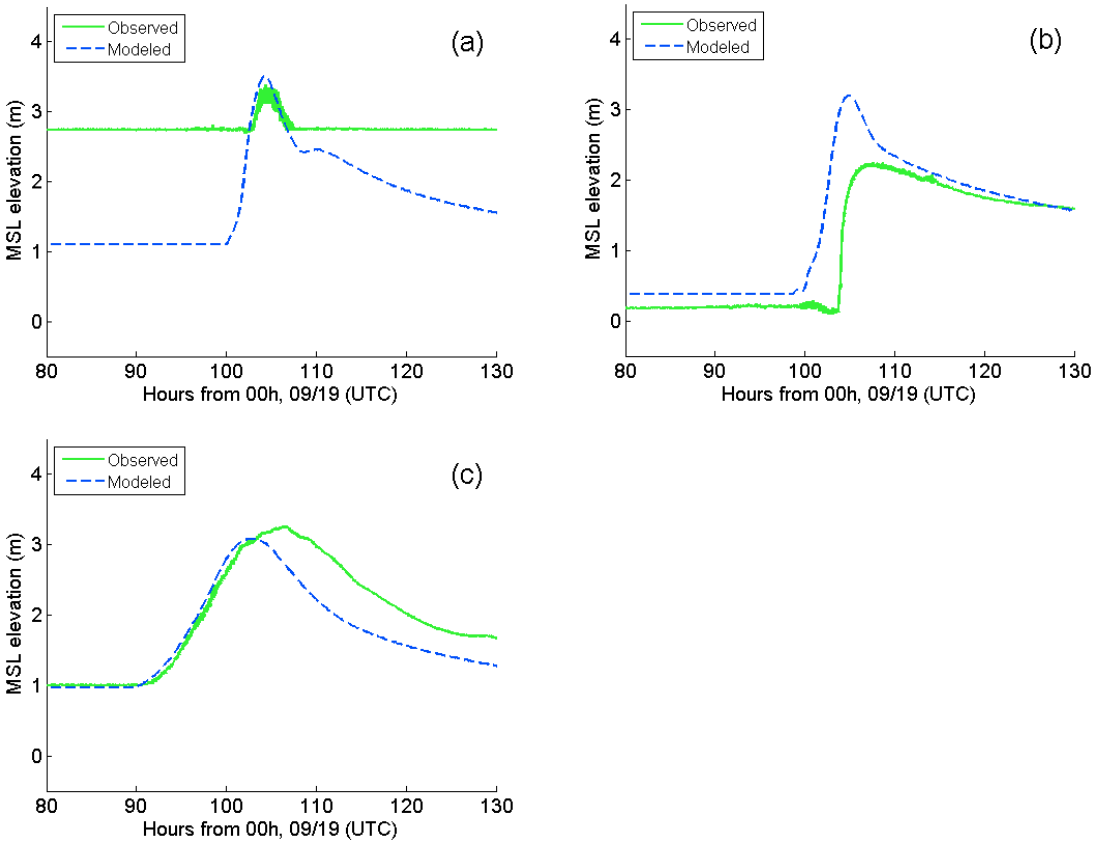

Figure 3.2: Validation curves for USGS stations (a) LC7, (b) LC8b, and (c) LA9b. Sensors were initially dry (location on Figure 3.1).

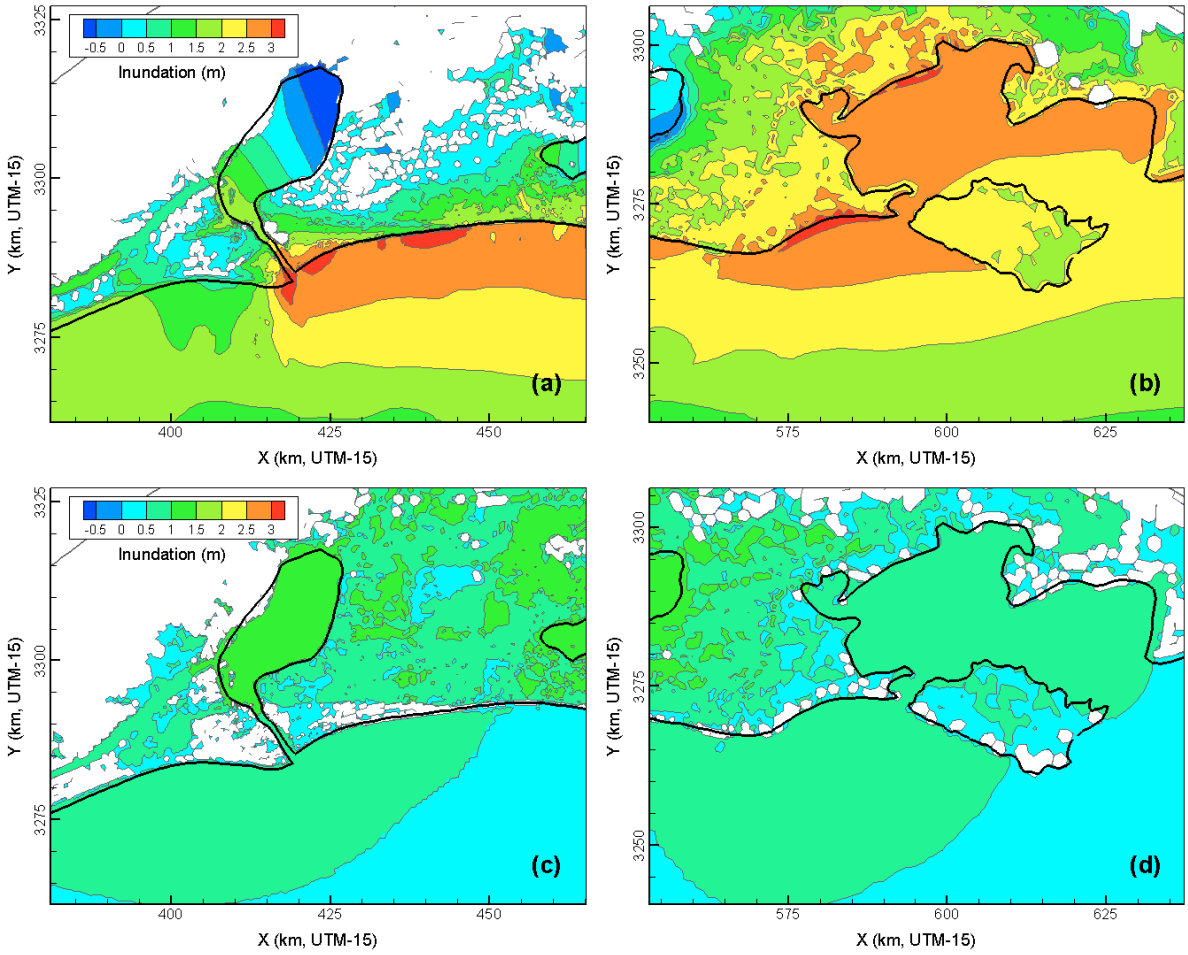

Figure 3.3: Inundation maps for southwest Louisiana: 3 hours before landfall (a) Sabine Pass and (b) Vermillion Bay areas; (c) Sabine Pass and (d) Vermilion Bay, 24 and 26 hours after landfall, respectively.

The USGS data only recorded water levels for about 4.5 days after landfall. We run FVCOM for a longer period but only looked at results, with confidence, for about 6 days after landfall. After that we had little to compare against, and other mechanisms not modeled here would have an increasing influence (e.g., evaporation, rainfall).

It is typical of surge curves from any hurricane (*e.g.*, Figure 3.2) that the surge build-up is much shorter and more intense than the receding, waning stage. For Hurricane Rita, the former lasts 5-15 hours, tending to the lower value for stations near the coastline. Water levels may take between 140 hours from landfall to reach a normal level (station B15b, on Sabine Pass, captures the entire receding period) to more than 7 days (station LC8b, about 10km inland, still has a 0.9 m water level after this time).

Having only one USGS station recording water levels on a coastal pass (B15b on Sabine Pass), we also compare FVCOM's Hurricane Rita results with observed data for "similar" channels – curves in Figure 3.4a represent channels just east and far east from Rita's landfall, while Figure 3.4b's represent channels just east and far east from Gustav's landfall. Based on the data from these 5 stations, we can determine that on this low-lying coast, water levels on coastal passes take about 100-140 hours to return to normal. The coastal stations that do recede the most (LC9, LC8a) take about 100 hours to reach 20% of the local peak surge height (these sensors were placed at about 0.9 m MSL elevation). Most of the coastal stations (*e.g.*, LC11, LA12, LA9b) take about 100 hours to reach 35% of local maxima. Inland stations (*e.g.*, LC8b, LA10, LA9) take longer, about 6.5 days to reach this 35% threshold.

This significant difference becomes more important for low-lying coasts, because here the flooding volumes and the distance they travel inland are very large. Contrasting surge dynamics during peak inflow, which occurs just before landfall, and during peak outflow, which takes place about a day after landfall, can explain it. Figure 3.3 shows FVCOM snapshots for

two of the four main outflow points in the impacted region (the other two being Calcasieu Pass and Mermentau River; Figure 3.1). Coastal surges peak at about one hour before landfall, and 2 hours before that coastal flooding is already widespread near Sabine Pass and the southwest pass of Vermilion Bay (Figure 3.3a,b).

FVCOM clearly shows that when a hurricane approaches a coast, flooding occurs along large parts of the shoreline (tens of kilometers). Three hours before impact near landfall, surge heights are 2.5-3.5 m and flooding as measured by the 2 m contour begins to spread inland (Figure 3.3a). Notice how the beach ridges east of Sabine Pass are represented in the model and do retard (but do not ultimately avoid) the surge flooding in that area. At the same time, farther east (where cyclonic winds started flooding earlier) surge heights are also 2.5-3.5 m, and the 2 m contour extends about 15 km inland on both sides of the southwest pass of Vermilion Bay (Figure 3.3b). Pushing against the coast, eventually this elevated "dome" of water (in which bottom friction has a decreased effect) results in widespread flooding: a brief, massive landward transport of water.

In contrast, the outflow of surge waters takes place on smaller space scales and over a much longer period. Having spread over about 8,500 km^2 of low-lying marshes and inland lakes, the large volume of surge waters that flooded the entire coastline now flows back to the GoM constrained by the existing channels. Most cells along the coastline are now dry and surge outflow occurs exclusively through the narrow passes. At peak outflow, about one day after landfall, surge waters flow out of Sabine Pass (Figure 3.3c) and Vermilion Bay's southwest pass (Figure 3.3d) in plume-like patterns defined here by the 0.5 m elevation contour.

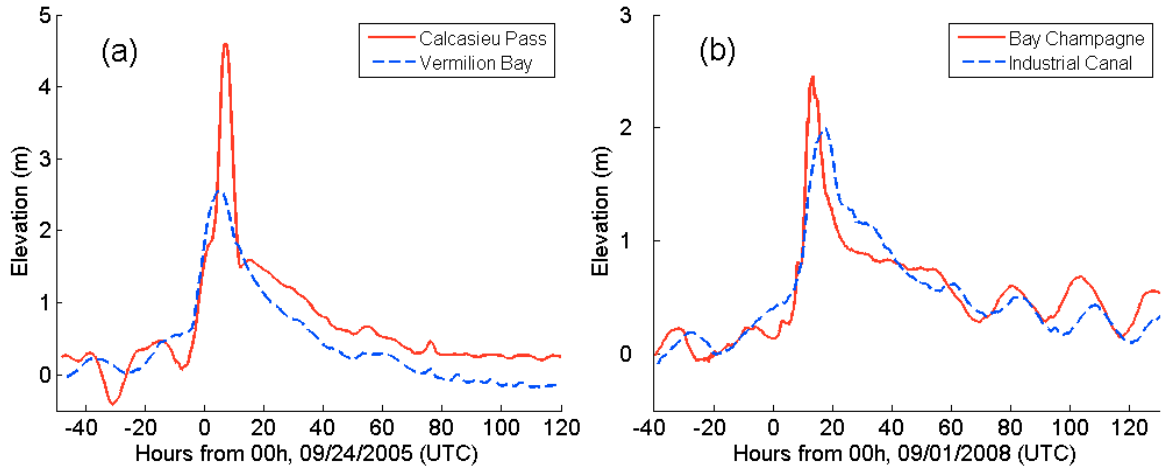

Figure 3.4: Water-levels at representative locations for (a) Hurricane Rita (modeled), and (b) Hurricane Gustav (observed curves).

3.4. Conclusions of Chapter 3

We combine data and our modeling results from Hurricanes Rita and Gustav to study the receding stage of surge waters on Louisiana's low-lying coast. We quantify typical longer-term hurricane flooding, based mostly on USGS's and our own observed data. On this low-lying coast water levels on coastal passes take about 100-140 hours to go back to normal. The coastal stations that recede the most take about 100 hours to reach 20% of the local peak surge height; most coastal stations take about 100 hours to reach 35% of local maxima. Inland stations take longer, 6.5 days and more to reach this 35% threshold.

Surge curves from any hurricane show much briefer surge build-ups than the receding, waning stage. For Rita, the former lasts 5-15 hours, tending to the lower value for stations near the coastline, while the latter takes more than 4 days (even more for inland locations). Based on FVCOM's results, we explain how distinct surge inflow and outflow dynamics create this difference. When a hurricane approaches, flooding occurs along large parts of the shoreline; coastal surge heights reach up to 3 m and flooding (as measured by the 2 m inundation contour) spreads several kilometers inland. These flood waters do not "feel" the bottom (friction) as much, resulting in a brief, vast landward transport of water. In contrast, the surge flows back to the GoM constrained by the existing channels. Indeed, at peak outflow surge waters flow out of the region's major coastal passes in plume-like patterns defined by the (much lower) 0.5 m elevation contour.

CHAPTER 4

ON THE IMPORTANCE OF THE FORWARD SPEED OF HURRICANES IN STORM SURGE FORECASTING: A NUMERICAL STUDY[3]

4.1. Introduction

Linear theory predicts that the ocean's response to an atmospheric traveling disturbance is proportional to $(1-U^2/gh)^{-1}$, *i.e.* when the speed of the traveling disturbance, U, is very close to that of the propagation of a long wave, there is resonance and the elevation becomes very large (Proudman, 1953). Jelesnianski's (1972) numerical experiments with a standard hurricane over representative shelves suggested that a "critical speed" exists, greater than 30 mph, which gives the highest possible surge. Peng et al.'s (2004) numerical experiments on a North Carolina estuary suggested that both storm surge heights and inundation areas decreased as hurricane translation speed increased (for 1.74-13.88 m/s). Peng et al. (2006a), using a modified inundation scheme, concluded for Charleston Harbor in South Carolina that while slower hurricanes invariably induce greater inundation areas, whether or not they induce higher storm surges depends on their track and speed (only 5.07 and 10.14 m/s were tested). Irish et al. (2008) created an idealized, straight coastline basin representing the northern GoM with different slopes to investigate the effect of varying storm sizes on coastal peak surges. They also varied the storm motion (2.6-10.3 m/s) and concluded that for moderate bottom slopes a 50% increase in forward speed translates to a 15-20% increase in peak surge.

This paper applies the FVCOM to Hurricane Rita's storm tide (the total height of the surge plus the astronomical tide) over the Louisiana-Texas shelf with a successful validation. Hurricane Rita was chosen for two reasons: the relatively simple coastline and shelf geometry of the landfall area (allowing for a simplified, quasi-idealized look into surge results) and the

[3] Reprinted by permission of the American Geophysical Union (see Rego and Li, 2009b)

unique dataset from the USGS, which recorded flooding along the southwest Louisiana coast (permitting the report of differences to a "base case" that is fully validated against observations). Our conclusions are thus representative of powerful hurricanes over mild slopes, impacting low-lying coasts consisting of marshes and inland lakes. Among other parameters, we focus on the impact of the forward speed of the hurricane, a factor that has been overlooked in previous studies.

4.2. Methods

Our model domain extends from the Mexico-U.S.A. border to Apalachicola Bay in Florida. A total of 178,675 triangular cells comprise the horizontal, with 2 sigma layers in the vertical. Mesh resolution increases from 10 km on the open boundary toward the region of Hurricane Rita's impact; the finest resolutions (200 m) are on coastal passes that connect the area's major lakes to the GoM. Bathymetry data is a combination of the NGDC's US Coastal Relief Model, the ETOPO-2 Global Relief model and Louisiana State University's (LSU) LIDAR Atlas. The model was forced by wind stress and tides.

Following the methodology of Chapter 2, we use the parametric wind model by Holland (1980) with NOAA's observed wind speed data (Powell et al., 1996). Jelesnianski's (1972) "correction" accounts for the asymmetry due to the forward motion of a hurricane (increasing the wind speed in the right quadrants). Another parameter is the inflow angle, which previous authors have argued to have negligible (Johns et al., 1985), important (Peng et al., 2006b), or complex effect on storm surge (Phadke et al., 2003). Here we set this angle to 10º on the "standard" hurricane simulations. A wind vector is then assigned to all cells in the domain as a function of the radial distance. The surface wind stress is computed from $\vec{\tau}_S = C_d \rho_a \left|\vec{V}_W\right| \vec{V}_W$, where ρ_a is the air density, $\vec{V}_W$ is the wind speed at 10 m height, and C_d is a drag coefficient

dependent on wind speed, assumed constant when $\vec{V}_W > 25 m/s$ (Large and Pond, 1981). Powell et al. (2003) and Jarosz et al. (2007) suggest that C_d decreases for $\vec{V}_W > 40 m/s$, by about 15-20%. However, these authors recommend conflicting values for C_d with $20 < \vec{V}_W < 40 m/s$ winds. Given this lack of consensus, and given that our sensitivity analyses using Powell et al.'s (2003) strong winds correction showed little effect on surge results, Large and Pond (1981) is used.

Tidal constituent were obtained from 14 NOAA tidal stations and three Coastal Studies Institute (CSI-LSU) WAVCIS stations. The model was initially forced at its open boundary by 9 tidal constituents obtained from Mukai et al. (2002) and run without wind forcing for 36 days. Calibrating FVCOM for this application consisted of varying the bottom friction coefficient, constant in the entire domain; the best results are obtained with C_z=0.0040. The errors for tidal phase are small and rarely exceed one hour for all stations and all constituents, in a region where tides have a 24 h period.Typical amplitude prediction error is about 0.01 m for the largest constituents, O1 and K1. Overall the tidal predictions are very satisfactory.

Observations by McGee et al. (2006) provided data for Hurricane Rita's storm tide validation. Comparison between FVCOM results and USGS water levels for coastal stations on central Louisiana demonstrated very good matches (see Chapter 2). Peak amplitude errors are typically ± 0.20 m, for a storm tide of 3.5-4.5 m, suggesting a 5% error. With respect to timing, coastal results are also very good and the typical situation is a ± half hour shift. Inland stations have slightly larger errors; either peak elevations are overestimated or the peak arrives too early, but in most stations only one of these issues is a problem. Hindcast simulations of Hurricane Rita using SLOSH and ADCIRC had similar inland issues, which were attributed to the inability of models to account for differences in bottom friction between water and marsh (URS Group,

2006). Our results also show good agreement with other published work on Hurricane Rita's inundation (FEMA, 2008; Berenbrock et al., 2009).

Upon a successful representation of Rita's storm tide, storm surge dynamics and coastal inundation are studied. Different scenarios are simulated in which 5 major parameters are varied: (1) wind intensity, (2) RMW, (3) landfall timing relative to the tide, also varying the tidal amplitude, (4) forward speed and (5) wind inflow angle (Table 4.1). In addition to these simulations, a "standard" simulation representing the observed Hurricane Rita (*i.e.*, 100% intensity and RMW, ~5 m/s forward speed, 10° inflow angle) without tidal forcing is run. Wind intensity is varied in 15% increments (used here to represent a one-category difference in the Saffir-Simpson scale); since Rita was a very powerful hurricane, a 7.5% increase is also tested. Hurricane Rita was a medium-size hurricane while over the shelf, and RMWs are varied in larger, 25% increments.

Table 4.1: Parameters used in the experiments. Changes relative to the base case.

Intensity (relative to H. Rita)			
A: 70%	B: 85%	C: 107.5%	D: 115%
RMW (relative to H. Rita)			
A: 50%	B: 75%	C: 125%	D: 150%
Tide: Landfall timing & Forced amplitude			
A: High, 2x Amp.	B: High, Obs. Amp.	C: Low, Obs. Amp.	D: Low, 2x Amp.
Forward speed			
A: 2 m/s	B: 3.5 m/s	C: 8 m/s	D: 12 m/s
Wind vector inflow angle			
A: 0°	B: 5°	C: 20°	D: 40°

Storm tide is simulated with hurricane landfalls forced at high and low tides, having the observed tidal amplitudes of about 0.33 m (B and C, respectively, on Table 4.1), and with tides having twice the observed amplitudes (A and D, respectively). The hurricane's forward speed is varied from very slow (2 m/s) to very fast (12 m/s). The tested inflow angles (0 to 40°) reflect typically used values. The mesh, bathymetry and storm track are the same in all 21 simulations.

4.3. Discussion

Total inundation volumes are computed using maximum inundation heights for each model cell in an area-weighted sum for all land cells affected by the hurricane. Given FVCOM's proven wetting and drying module, these volumes and maximum heights can be used to compare the effects of varying the parameters in Table 4.1. Maximum inundation maps (Figure 4.1) illustrate flooding extent and distribution of surge amplitudes. Total volumes are summarized on Figure 4.2a for all 5×4 simulations, compared to the "standard" run representing Hurricane Rita without tide (dashed line). Figure 4.2b shows peak surge heights, which depend to some extent on where the right-sided RMW hits land.

The effect on total flooded volumes of varying wind intensity and RMW is the largest (Figure 4.2a). They are also similar in magnitude, indicating that a 70-115% change in intensity is roughly equivalent to a 50-150% change in RMW (the chosen test range). For both parameters, scenarios A and D yield about 3 and 22 km^3, respectively, whereas the standard case floods about 14 km^3. Increasing each parameter also results in the increase of both volumes and peak heights (Figure 4.2b). Varying wind intensity has a more significant impact on peak surges (2.9-6.3 m) as compared to varying the RMW (3.6-5.6 m). Flooded volumes peak for about 125% of the observed Hurricane Rita's RMW. In this application, a 25% larger RMW means that the strongest winds act on an area of convergence (near Calcasieu Pass), enhancing local peak surges but having little influence on overall flooding.

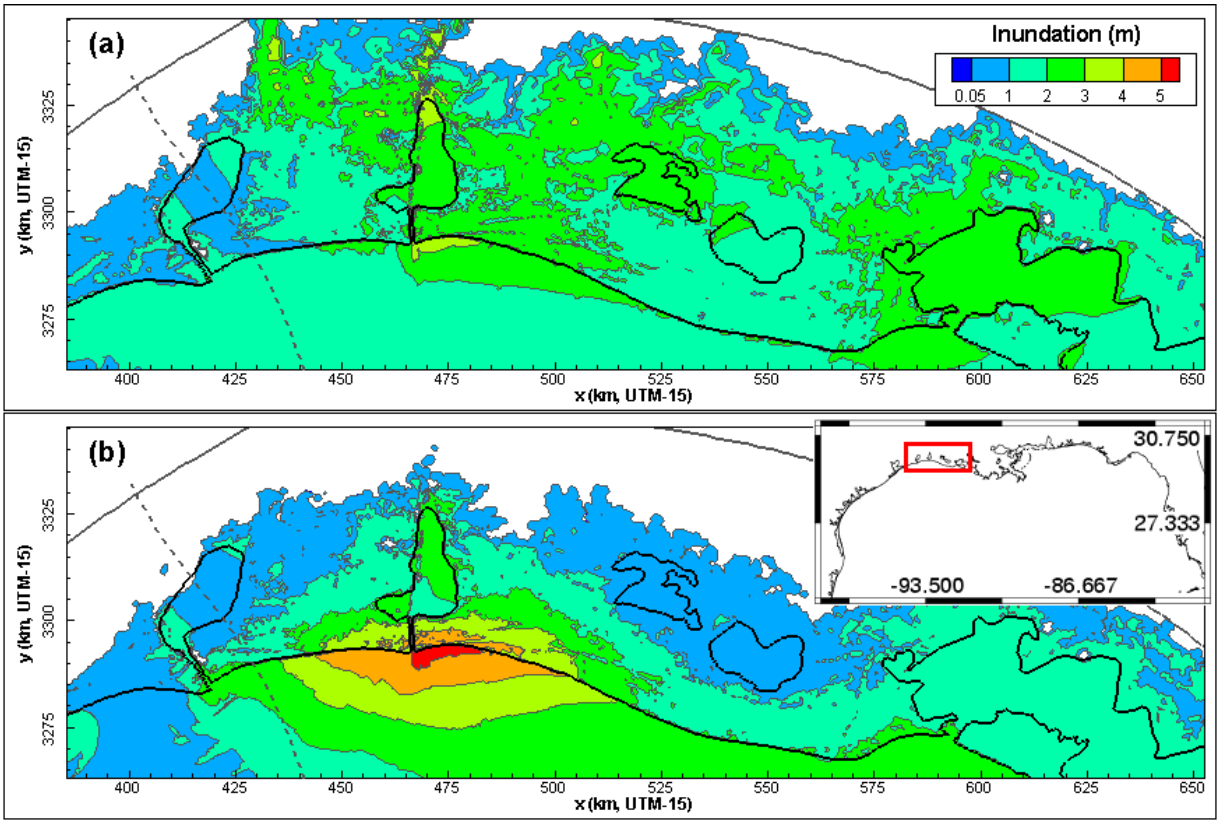

Figure 4.1: Maximum inundation maps for hurricanes having forward speeds of (a) 2 m/s, and (b) 12 m/s. Track shown as dashed line. Inset shows location on regional map.

Tidal timing also affects flooded volumes and peak surges in the same manner: hurricanes landfalling at high tide yield both greater flooded volumes and peak surges than those landfalling at low tide. Variations in this case are only about ±16% of the "standard" volume (Figure 4.2a). Tide-surge nonlinearity decreases the impact of high- or low-tide landfalls: peak storm tides for high tide and double high tide should be greater than the no-tide case by about 0.33 and 0.66 m (the tidal amplitude) and they are not. This is because nonlinear tide-surge interaction is stronger during low-tide and peak surge, opposing the tidal signal by up to 70% on the Louisiana-Texas shelf (Chapter 2).

Conversely, varying a hurricane's forward speed and wind inflow angle have opposite effects on flooded volumes and peak surge elevations. Increasing the forward speed from the standard value decreases flooded volumes (by up to 40%) while increasing peak surges (by up to 7%); decreasing the forward speed increases flooded volumes (by up to 9%) while decreasing peak surges (by up to 30%) in the range considered. The same pattern holds for different inflow angles, albeit with an influence of only about 15% (Figure 4.2).

The impact a hurricane's forward speed has on coastal flooding is thus shown to be very interesting: consistent with theory it has a significant positive effect on peak surge heights, but a significant negative effect on total maximum flooded volumes, which had not been recognized before. A slower storm produces lower peak surges (below 4 m) that travel far inland (Figure 4.1a), whereas a faster hurricane will move swiftly across the shoreline generating higher surges (above 5 m) but flooding a relatively narrower section of the coast (Figure 4.1b). Slower hurricanes (here represented by 2 and 3.5 m/s speeds) are usually feared the most because, having considerable more time to impact coastal waters they tend to produce heavier flooding – which is consistent with our results.

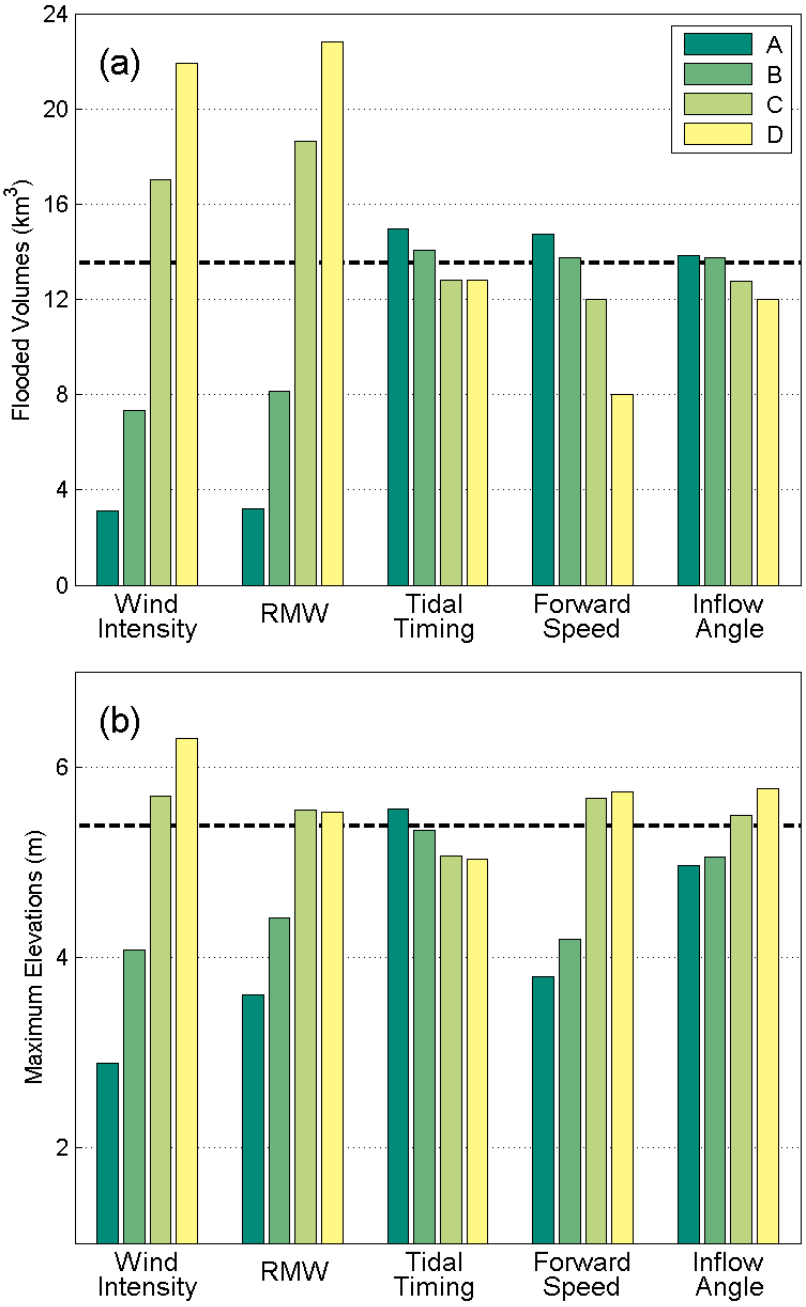

Figure 4.2: (a) Total flooded volumes and (b) maximum surge heights. Bars show results for scenarios A, B, C and D (Table 4.1). Dashed line indicates "standard" run values.

But considering highest surge elevations alone, faster hurricanes are shown here to be more dangerous, causing higher surges. Local surge curves have considerably different shapes depending on the hurricane's forward speed. For the Louisiana-Texas shelf, 5-12 m/s moving hurricanes produce higher, narrower surge curves, compared to those by 2-3.5 m/s moving hurricanes. A threshold separating broad and narrow surge curves is identified between 3.5 and 5 m/s, implying a representative depth of about 2 m (Proudman, 1953). On this coast the 2 m isobath is typically 1000-3000 m offshore.

These are significant results, as the effect of hurricanes' forward speed is typically overlooked in surge studies. Previous analyses focus mostly on the two major parameters: wind intensity and RMW. Some authors describe wind inflow patterns with more or less validation, whereas the timing of landfall (relative to the tide) is commonly mentioned as a source of added uncertainty (and most studies fail to address it). Here we show how a storm's forward motion speed is more important than the latter two factors, with a distinct effect on the coast: slower hurricanes yield greater flooded volumes than faster hurricanes (by up to 49%) while producing reduced peak surges (by up to 37%).

4.4. Conclusions of Chapter 4

A systematic investigation of storm surge impact to the coast of Louisiana was conducted using FVCOM (Chen et al., 2003). An application to Hurricane Rita's storm surge event is described, and flooding along the Louisiana-Texas coast is used for model validation. We then conduct idealized experiments to quantitatively evaluate the impacts of each parameter influencing coastal inundation over a wide and shallow continental shelf. The effects on total flooded volumes of varying wind intensity and RMW are the largest, and our results indicate that a 70-115% change in intensity translates approximately to a 50-150% change in RMW. For both variables, extreme scenarios yield total flooded volumes of about 25 and 160%, respectively,

compared to the standard case. Landfall timing is another factor for which flooded volumes and peak surges vary together: those hurricanes landfalling at high tide yield both greater flooded volumes and peak surges than those landfalling at low tide. The variations in this case are smaller, about ±16% of the base case volume.

Conversely, varying a hurricane's forward speed has opposite effects on flooded volumes and peak surge elevations. Increasing the forward motion speed of the storm decreases flooded volumes while increasing peak surges, by about 40%. Regarding surge levels, this is consistent with Irish et al.'s (2008) results on a northern GoM continental shelf, while contradicting Peng et al. (2004), who studied surges for the much narrower North Carolina shelf. These authors have not investigated variations in flooded volumes. We show that a slower moving storm produces lower peak surges that travel far inland, whereas a faster hurricane moves swiftly across the shoreline generating higher surges that flood a narrower section of the coast. We conclude that a storm's forward motion may account for variations in flooded volumes equivalent to an upgrade or downgrade of about 1 category on the Saffir-Simpson scale (Figure 4.2a), providing new insight into coastal surge dynamics. This represents a larger impact than tidal timing, amplitude, or wind inflow angle, more likely to be the focus of previous studies.

CHAPTER 5

STORM SURGE PROPAGATION IN GALVESTON BAY DURING HURRICANE IKE[4]

5.1. Introduction

Storm surge is a long-period wave caused by extreme wind and atmospheric pressure differences. Numerical modeling of coastal surge has played an important role in engineering design, disaster planning and coastal management since the 1970's, and the rate of new publications indicates a renewed interest in surge modeling around the world (Shen and Gong, 2009). Tropical cyclones, with lower interior pressures and higher wind speeds, typically produce significantly higher surges than extratropical cyclones (Resio and Westerink, 2008). But the impact of a hurricane's surge on the coastal region depends not only on the characteristics of the forcing (a storm's intensity, size and speed) but also on the path of the storm and on the geometric properties of the waterbody. In this chapter we use the FVCOM with a high-resolution unstructured mesh to study Hurricane Ike's storm tide along the Texas-Louisiana coast. The exceptional USGS surge dataset allowed for validation of the model and in-depth discussion of this powerful hurricane-induced surge in the semi-enclosed Galveston Bay. The estuaries in Chapter 1 all have wide openings, without barrier islands protecting them from storm surges. Here we examine Hurricane Ike's flooding along the Texas-Louisiana coast, and focus on the impact of barrier systems to surge propagation into and within Galveston Bay, with a new set of simulations using different coastal geometries to represent increasing degrees of coastal erosion.

5.2. Hurricane Ike

Hurricane Ike caused extensive damage and over 100 deaths across Hispaniola, Cuba, and along the coasts of Texas and Louisiana. It reached peak intensity with 230 km/h winds and minimum

[4] Submitted to the Journal of Marine Systems

central pressure (MCP) of 935 mbar over the open waters of the central Atlantic Ocean before hitting the island of Cuba. Ike was the most intense storm in the 2008 Atlantic hurricane season (Berg, 2009) and had the highest Integrated Kinetic Energy ("IKE"; Powell and Reinhold, 2007) of any Atlantic storm in the past 40 years. On a scale where 6 is the highest destructive potential, Ike reached IKE=5.4 over the Gulf of Mexico (GoM) (Hurricane Research Division, 2009), while Hurricanes Wilma and Katrina in 2005 peaked at IKE=5.1 (Powell and Reinhold, 2007). Hurricane Ike re-intensified after battering Cuba and reached its maximum strength over the GoM at 00h00 UTC September 11 (winds of 215 km/h, MCP of 944 mbar). Ike made landfall as a strong Cat-2 hurricane (MCP of 950 mbar) along the eastern part of Galveston Island, Texas at 07h30 UTC, 09/13/2008, traveling at about 5.7 m/s (Figure 5.1). The hurricane's center continued northwestward bordering Galveston Bay, then northward across eastern Texas and Arkansas, where Ike weakened to an extratropical storm (Berg, 2009).

Maximum storm surge heights of 1.5-3 m were observed along the coast of south-central Louisiana, increasing to 3-4 m along the southwestern Louisiana and extreme upper Texas coast near Sabine Pass (Berg, 2009). Even as far east as the Rigolets in southeast Louisiana (the channel leading to Lake Pontchartrain) storm surge reached almost 2 m (Li et al., 2009). USGS sensors indicate that areas in Jefferson County, Texas, and Cameron Parish, Louisiana, had surge heights up to 5.2 m, referenced to NAVD88 (East et al., 2008).

The highest overall surges occurred on the Bolivar Peninsula and in parts of Chambers County, in Texas. FEMA's highest water mark was 5.4 m referenced to NAVD88, about 18.5 km inland in Chambers County. Storm surge levels on Galveston Island and on the west side of Galveston Bay were about 3-4 m, and farther south along the Texas coast surges of 1.5-3 m were recorded down to Freeport, TX (Berg, 2009).

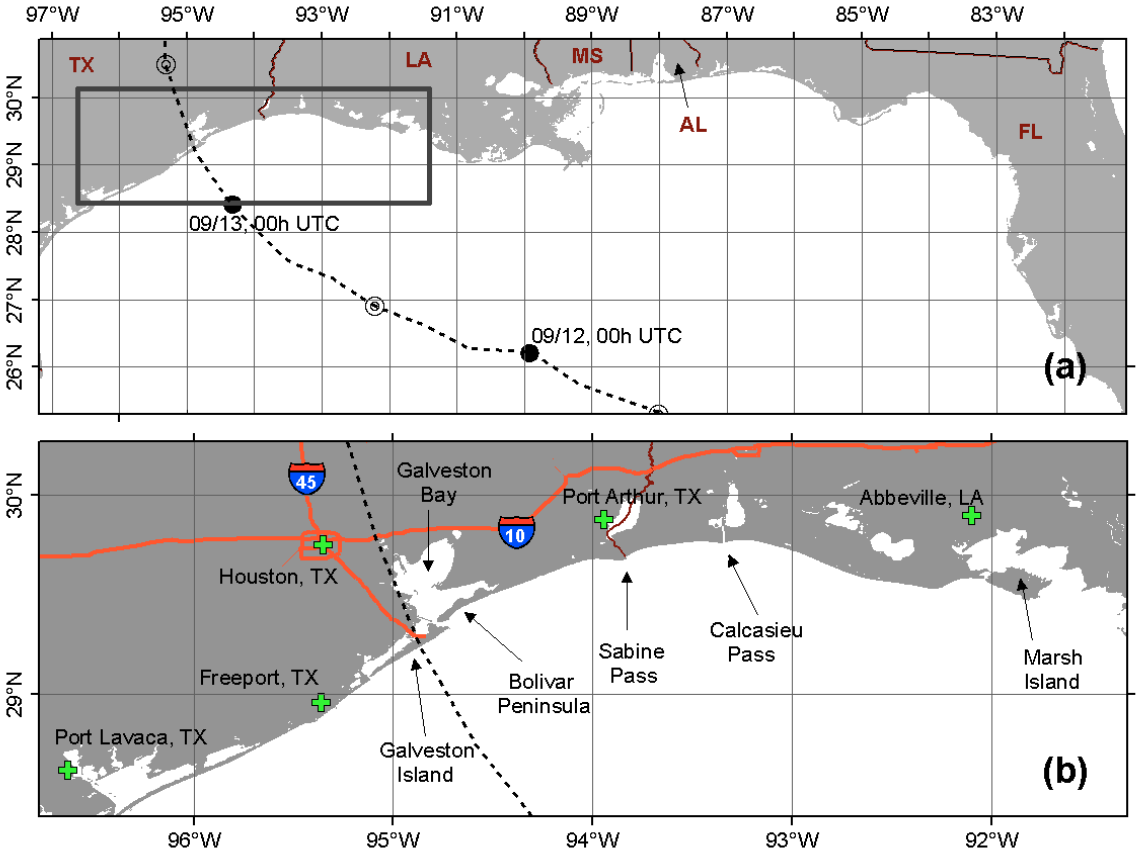

Figure 5.1: (a) Regional map of northern Gulf of Mexico, (b) Study area with features mentioned in the text. The dashed line marks Hurricane Ike's track.

5.3. Model Implementation

Our model domain extends from the Mexico-U.S.A. border to the Mississippi River Delta in Louisiana, with an 850 km long open boundary arching in between, covering water depths of 1,000-3,000 m in the most part (Figure 5.2a).

A total of 206,711 triangular cells comprise the horizontal, with 2 sigma layers in the vertical. The mesh resolution increases from 9 km on the open boundary toward Hurricane Ike's landfall. Mesh resolution on the upper continental shelf between Freeport, TX and Calcasieu Pass, LA is about 500 m. The finest mesh resolution (200 m) is around Galveston Bay entrance (Figure 5.2b). On the West Louisiana coastal region and around Galveston Bay our model domain extends well beyond the land-sea interface, to the 6 m elevation contour, approximately. Land cells have typically a coarser 500-1000 m resolution (deemed sufficient by *e.g*. Dietsche et al., 2007) and D_{min}, is set to 0.05 m. Bathymetry data is a combination of the National Geophysical Data Center's US Coastal Relief Model, Louisiana State University's LIDAR Atlas and the USGS National Elevation Dataset.

5.4. Hurricane Wind Field

A common practice for creating hurricane winds in storm surge modeling (*e.g*. Peng et al., 2006a,b; Weisberg and Zheng, 2008) is to reconstruct the wind field by fitting the analytical cyclone model from Holland (1980). The radial distribution of wind relative to the storm center and the maximum wind speed are specified such that:

$$V_w = \sqrt{\frac{B\left(P_{amb} - MCP\right)}{\rho_a}\left(\frac{RMW}{r}\right)^B \exp\left(-\frac{RMW}{r}\right)^B} \tag{5.1}$$

$$V_{\max} = \sqrt{\frac{B\left(P_{amb} - MCP\right)}{\rho_a e}} \tag{5.2}$$

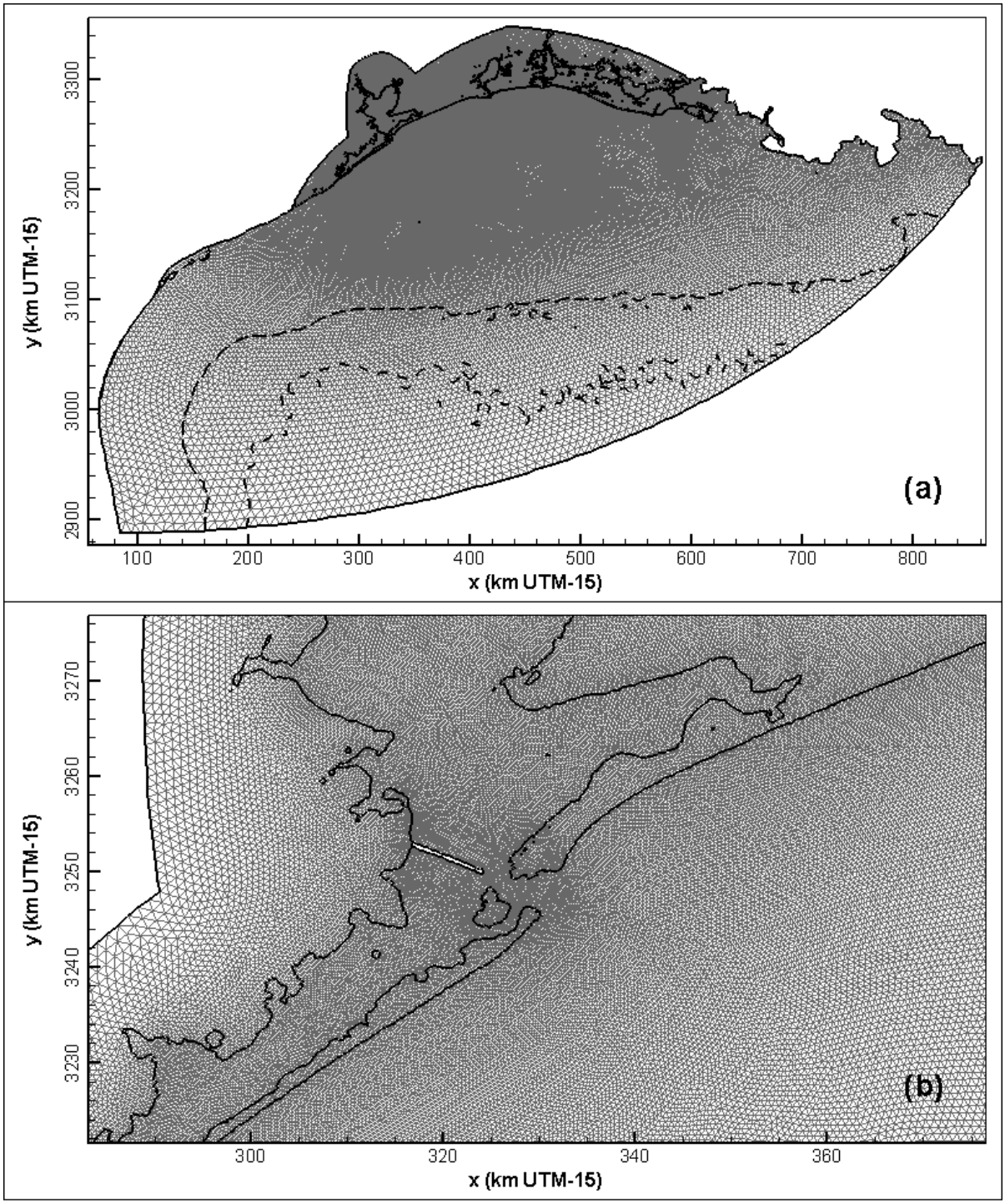

Figure 5.2: (a) Mesh used in the simulations; (b) Zoom in on landfall location.

where r is the radial distance from the hurricane center, V_w is the wind speed as a function of r, ρ_a is the air density (=1.15 kg/m^3), p_{amb} and MCP are the ambient and minimum central atmospheric pressures, respectively, e is the natural logarithm base (=2.718…), RMW is the Radius of Maximum Winds, V_{max} is the maximum sustained wind speed, and B is the "peakedness" storm scale parameter, $1.0 < B < 2.5$.

Many past studies use a constant B without comparing against observed data (Peng et al., 2006a,b; Weisberg and Zheng, 2006a). Here we apply Holland (1980) with the gridded H*WIND dataset of Powell et al. (1996), in much the same way as in Chapter 2. Terms ($p_{amb} - MCP$) and B are determined iteratively using Equations 5.1, 5.2 and the combination of these terms that produces a wind profile with the smallest Root Mean Square Error as compared to H*WIND's profile is chosen at each snapshot.

We improve wind representation further to account for hurricane asymmetries and most importantly to account for land effects around landfall. Unlike Hurricane Rita, which made landfall on a relatively simple coast, Hurricane Ike made 3 landfalls near a major bay (Figure 5.1). Thus, for a critical 6 hours, about half of the hurricane-strength winds were over land while the remaining half was either over the GoM or Galveston Bay. We determine hurricane parameters RMW, V_{max} and B separately for 8 "cones" of 45°, hereby accounting for land effects in our model. Open water winds are stronger in the "relative" East, Southeast, South and Southwest cones (*e.g.* relative North is forward on the hurricane's track, relative West to its left) (Figure 5.3a). Between first and second landfalls (Figure 5.3b) variations in RMW and V_{max} are much larger than those over the Gulf. This approach is more accurate than merely applying a decay rate factor after landfall to the whole wind field (DeMaria et al., 2006), more straightforward than other similar methods (Xie et al., 2006), but less comprehensive than directional land-masking procedures based on land roughness data (Westerink et al., 2008).

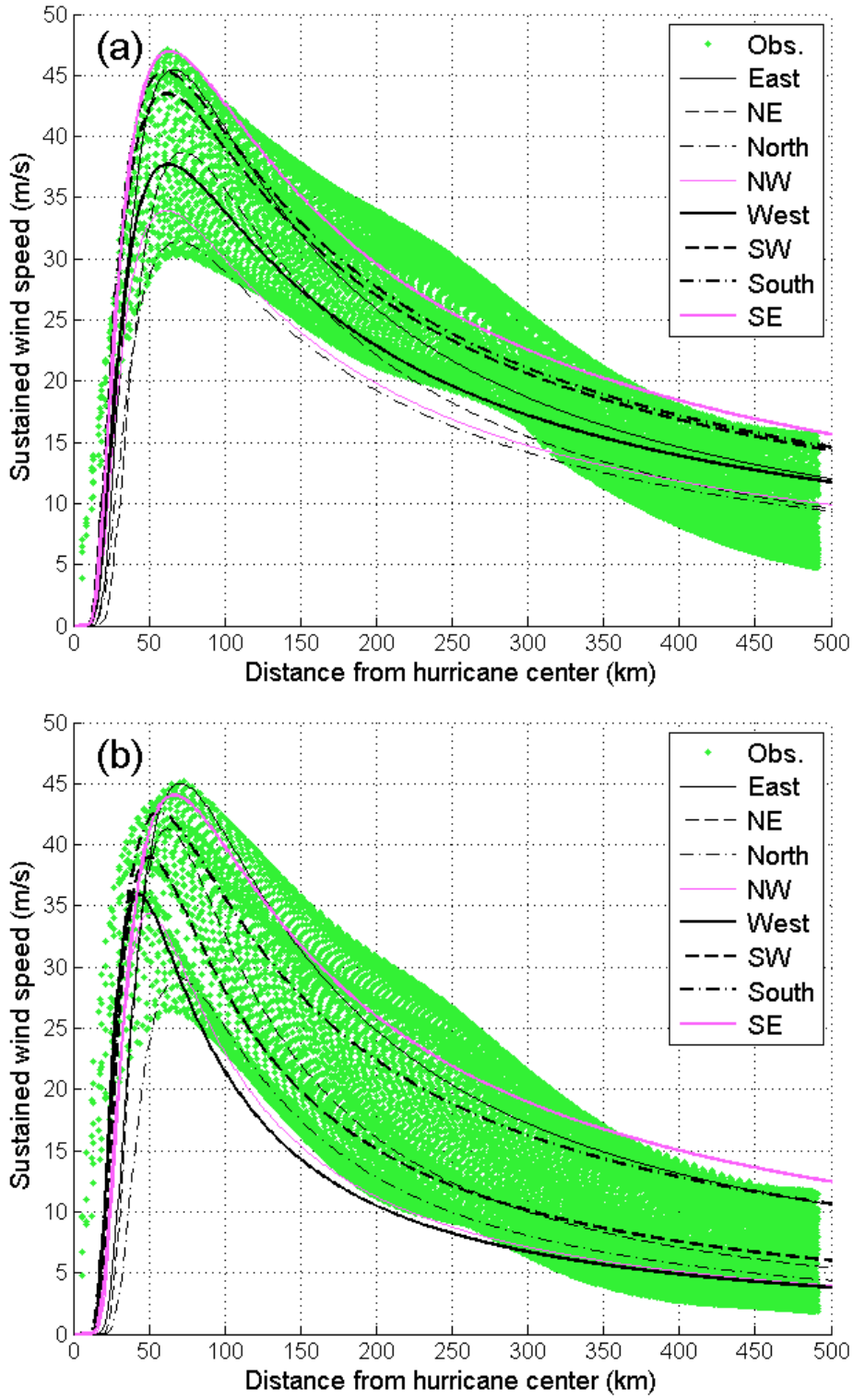

Figure 5.3: Wind profiles fitted to H*WIND dataset: (a) 16h30 UTC 09/12 and (b) 07h30 UTC 09/13/2008. Factors *RMW*, V_{max} and *B* determined separately for 45° cones.

The 1-minute averaged H*WIND winds are then multiplied by a factor of 0.89 to adjust to a 10-minute average period (Powell et al., 1996). Jelesnianski's (1972) forward motion correction is also used (increasing the wind speed in the right quadrants). The inflow angle is harder to estimate. In Phadke et al. (2003) it varies linearly from 10º at the center to 20º at RMW, while Peng et al. (2006b) admit this is an "elusive" parameter for forecasters and test constant of 0-40º. Here the inflow angle is set to 10º everywhere.

5.5. Model Calibration for Tide and Storm Surge

The model is first run without surface wind forcing for 36 days, forced at the open boundary by 9 tidal constituents obtained from Mukai et al. (2002). Calibrating the tidal application of FVCOM consisted of varying the bottom friction coefficient (constant in the entire domain), with a coefficient of 0.005 yielding the best results. We found that changing Smagorinsky's horizontal diffusion and the inundation depth had negligible effects on the model's tide representation. Tides in the northwest GoM are diurnal except along the southwest Louisiana coast where they are mixed. Major tidal constituents are O1, K1 (0.12-0.17 m amplitudes) and M2 (0.10-0.14 m). Tidal constituent data were obtained from 8 long-term NOAA stations near Ike's landfall (Table 5.1).

Overall the tidal predictions are satisfactory. The largest modeling errors (Table 5.1) occur at Eagle Point, TX and for Sabine Pass North, TX where modeled amplitudes are under- and overestimated, respectively (by 0.02-0.05 m in both cases). Other than these stations (located inside Galveston Bay and Sabine Lake), the typical amplitude prediction error for the most important constituents is about 0.01 m on GoM stations and 0.03 m on upstream stations. Overall tidal phase errors are small and rarely exceed one hour for all stations and all constituents (in a region where tides have a ~24 h period); the exception is Round Point, TX station where the modeled tide is almost 2 hours late.

Table 5.1: NOAA/NOS stations used in tidal calibration. Each column shows Observed Amplitude (Ao, in m), Modeled Amplitude (Am, in m), and Phase Difference (Pd, modeled – observed, in hours), for the three major tidal constituents in the region.

Station Name; ID #	K1 Ao, Am, Pd	O1 Ao, Am, Pd	M2 Ao, Am, Pd
Uscg Freeport, TX; 8772447	0.153, 0.166, -0.03	0.145, 0.159, +0.70	0.095, 0.078, +0.03
Galveston Pleasure Pier, TX; 8771510	0.171, 0.173, +0.05	0.161, 0.163, +0.74	0.139, 0.108, +0.08
Galveston Bay Entrance, TX; 8771341	0.144, 0.165, -0.35	0.135, 0.156, +0.22	0.113, 0.108, +0.05
Eagle Point, TX; 8771013	0.117, 0.067, +0.66	0.114, 0.065, +1.33	0.034, 0.019, -0.17
Clear Lake, TX; 8770933	0.105, 0.073, -0.21	0.105, 0.070, +0.60	0.037, 0.024, -0.88
Round Point, TX; 8770559	0.108, 0.076, +0.94	0.103, 0.073, +1.81	0.051, 0.029, +0.34
Sabine Pass North, TX; 8770570	0.132, 0.181, -0.80	0.123, 0.167, -0.28	0.123, 0.150, -0.13
Calcasieu Pass, LA; 8768094	0.144, 0.188, -0.10	0.136, 0.173, +0.60	0.146, 0.151, +0.46

Observations by East et al. (2008) provided data for surge validation. The USGS deployed a temporary monitoring network of pressure sensors at 65 sites to record the timing and magnitude of inland flooding and coastal surge generated by Hurricane Ike, and sensors were recovered at 59 of these sites. Water levels, referenced to NAVD88, were converted into MSL using National Geodetic Survey (2009). Only 33 stations are used here; the remainders were located either too far from landfall or on areas not resolved in our model. Data from four NOAA/NOS stations was also used (Table 5.2).

The inverse pressure adjusting method was used at the open boundary to partially account for meteorological forcing (Jones and Davies, 2004; Shen et al., 2006), and a seasonal component not given by Mukai et al. (2002) was taken into account by adding 0.1 m to the open boundary levels (the average sum between tidal components SA and SSA given for NOAA/NOS stations). Lastly, noticing that observed water levels in this region were consistently 0.20-0.30 m

higher than predicted levels for the ~10 days before and after landfall, an extra 0.25 m was added to account for what appears to be a low-frequency weather effect. Stations used to demonstrate model validation are shown on Figure 5.4; curves for these 12 stations on Figure 5.5 (a 5-minute filter was applied to USGS time-series). Results for all 37 stations are shown on Table 5.2.

Table 5.2: Stations used for Hurricane Ike's storm tide validation. Negative timing errors indicate modeled surge ahead of time. Positive peak errors indicate modeled elevation value greater than observation (both in m above MSL).

Station	Obs. Peak (m)	Peak error (m)	Peak error (hr)
NOS Uscg Freeport, TX	1.98	-0.24	+4.0
NOS Eagle Point, TX (Fig. 5d)	3.46	0.13	+0.1
NOS Sabine Pass North, TX	4.13	0.02	0
NOS Calcasieu Pass, LA	3.27	-0.04	-1.5
USGS TX-MAT-009	1.66	-0.14	+2.5
USGS TX-BRA-004	1.60	-0.05	+3.0
USGS TX-BRA-009 (Fig. 5a)	1.91	+0.01	+4.0
USGS TX-BRA-008	2.01	-0.15	+2.5
USGS TX-BRA-002	2.00	+0.24	+1.2
USGS TX-BRA-001	2.14	+0.22	+5.0
USGS TX-GAL-015 (Fig. 5b)	2.45	-0.30	-2.0
USGS TX-GAL-011	3.38	-0.93	-2.0
USGS TX-GAL-010	3.62	-0.73	-1.0
USGS TX-GAL-016 (Fig. 5c)	3.55	-0.64	-2.0
USGS TX-GAL-008 (Fig. 5g)	3.81	-0.08	+1.0
USGS TX-GAL-019	2.85	+0.80	+0.15
USGS TX-GAL-022	3.52	+0.82	-0.25
USGS TX-HAR-002 (Fig. 5e)	3.63	+0.31	-0.15
USGS TX-HAR-004	3.64	+0.24	-4.5
USGS TX-CHA-004	4.58	-0.25	-1.0
USGS TX-CHA-003 (Fig. 5f)	3.64	-0.09	-1.0
USGS TX-GAL-002	3.92	-0.53	+1.0

(Table 5.2 continued)

(Table 5.2 continued)

USGS TX-GAL-001 (Fig. 5h)	4.84	-0.03	-0.5
USGS TX-GAL-005 (Fig. 5i)	4.65	-0.26	-0.5
USGS TX-JEF-001	4.82	-0.18	0
USGS TX-JEF-002 (Fig. 5j)	5.00	0.01	+0.25
USGS TX-JEF-004	4.68	-0.12	+0.15
USGS TX-JEF-005	4.75	-0.09	0
USGS TX-JEF-006	4.30	-0.04	-0.5
USGS TX-JEF-007 (Fig. 5k)	3.83	-0.39	-0.5
USGS TX-JEF-008	3.17	+0.06	0
USGS TX-JEF-009	4.01	+0.97	-0.5
USGS LA-CAM-001	4.54	-0.49	+0.15
USGS LA-CAM-002	4.30	-0.57	-0.5
USGS LA-CAM-003 (Fig. 5l)	3.02	+0.01	-1.25
USGS LA-CAM-010	3.04	-0.20	0
USGS LA-CAM-012	3.06	-0.22	-0.5

FVCOM results matched very well against observed water levels in most stations. Peak amplitude errors are typically below 15%, in records where peak storm tide was 2-5 m (Table 5.2). Exceptions are USGS stations TX-GAL-010, TX-GAL-011 and TX-GAL-016 (Figure 5.5c), where modeled peak levels were 0.7-0.9 m below observations. These three stations are on or “behind” Galveston Island, very close to Hurricane Ike’s path and to its left. Two factors can explain this difference: our exclusion of air pressure effects (relatively important on the storm’s path), and our admittedly overestimated winds blowing from land “against” the surge (since we don’t explicitly include land effects). Other exceptions are USGS stations TX-GAL-019 and TX-GAL-022 (see Figure 5.5e for a similar case) where the model overestimates peak levels by about 0.80 m; this is where observed surge shows a complicated triple-peak not fully captured by the model which can be attributed to poor bathymetry data in the area.

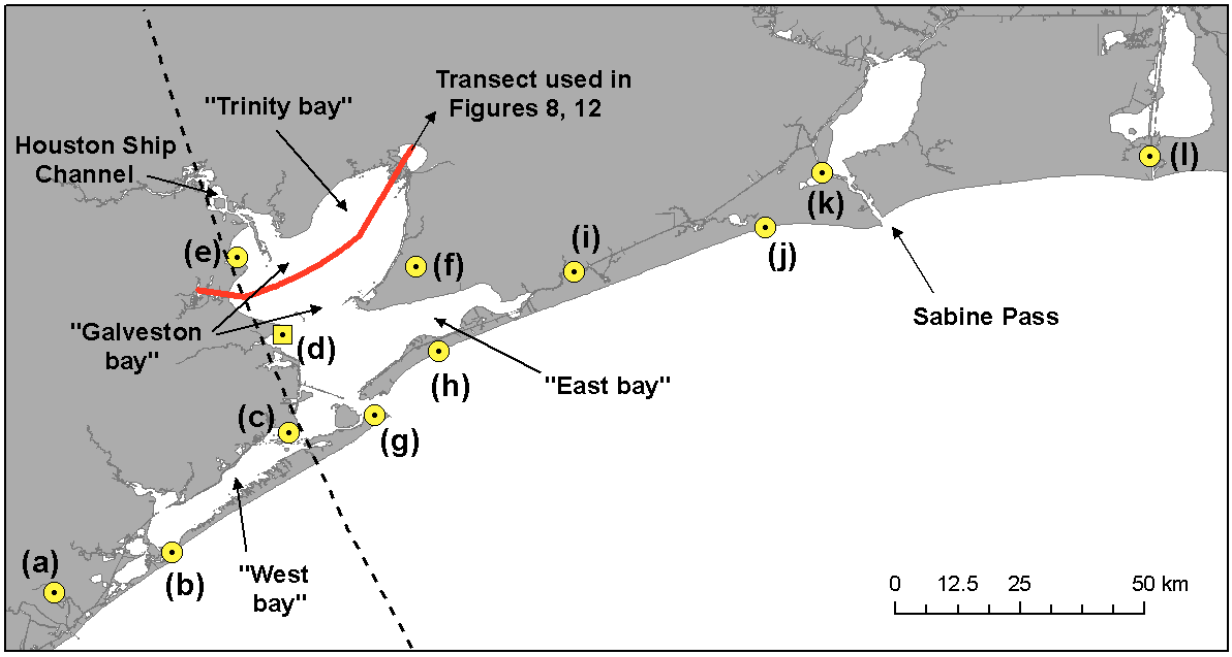

Figure 5.4: Map showing surge validation stations: (a) TX-BRA-009, (b) TX-GAL-015, (c) TX-GAL-016, (d) Eagle Point, TX, (e) TX-HAR-002, (f) TX-CHA-003, (g) TX-GAL-008, (h) TX-GAL-001, (i) TX-GAL-005, (j) TX-JEF-002, (k) TX-JEF-007 and (l) LA-CAM-003. All stations are USGS except (d) which belongs to NOAA/NOS.

For USGS station TX-JEF-009, peak surge levels were apparently overestimated in the model by almost 1 m. Observed levels should be seen with caution though, as this station is very near TX-JEF-002, which is farther from landfall and recorded peak surges 1 m higher than the former.

With respect to the timing of storm tide, modeling results are also very good and typically have a ± half hour shift (or smaller). Exceptions are some stations further south where modeled curves lag observations by 2.5-5.0 hours (with peak errors of only ±0.20 m and smaller). It can be shown that because surge curves are rounder here, a very close match can yield a misleading large lag (Figure 5.5a).

The other only exception is USGS TX-HAR-004, which is 4.5 hours ahead of time. In this area (see Figure 5.5e for a similar case) there were multiple short-scale peaks and the model only captured the major curve. Even when the model slightly over- or underestimates peak surges (Figure 5.5i,j,k), it does accurately capture the local surge's curve. Even as far away from landfall as USGS station LA-CAL-003, the model did a very good job in representing surge (Figure 5.5l). The stations where the highest surges were recorded, east of Galveston Bay entrance (Figures 5.5g,h,i,j), show a very good match with observations.

There is, nevertheless, a pre-peak prominence not fully captured by the model; also, the modeled surges recede slightly earlier than observations. These issues have been noticed in studies with much more comprehensive meshes (*e.g.* Westerink et al., 2008). Our results also show good qualitative agreement with inundation maps from the National Weather Service (2009) for Chambers and Jefferson counties (Texas) and for Cameron, Calcasieu and Vermilion parishes (Louisiana). Overall, we conclude that FVCOM's storm tide is satisfactory.

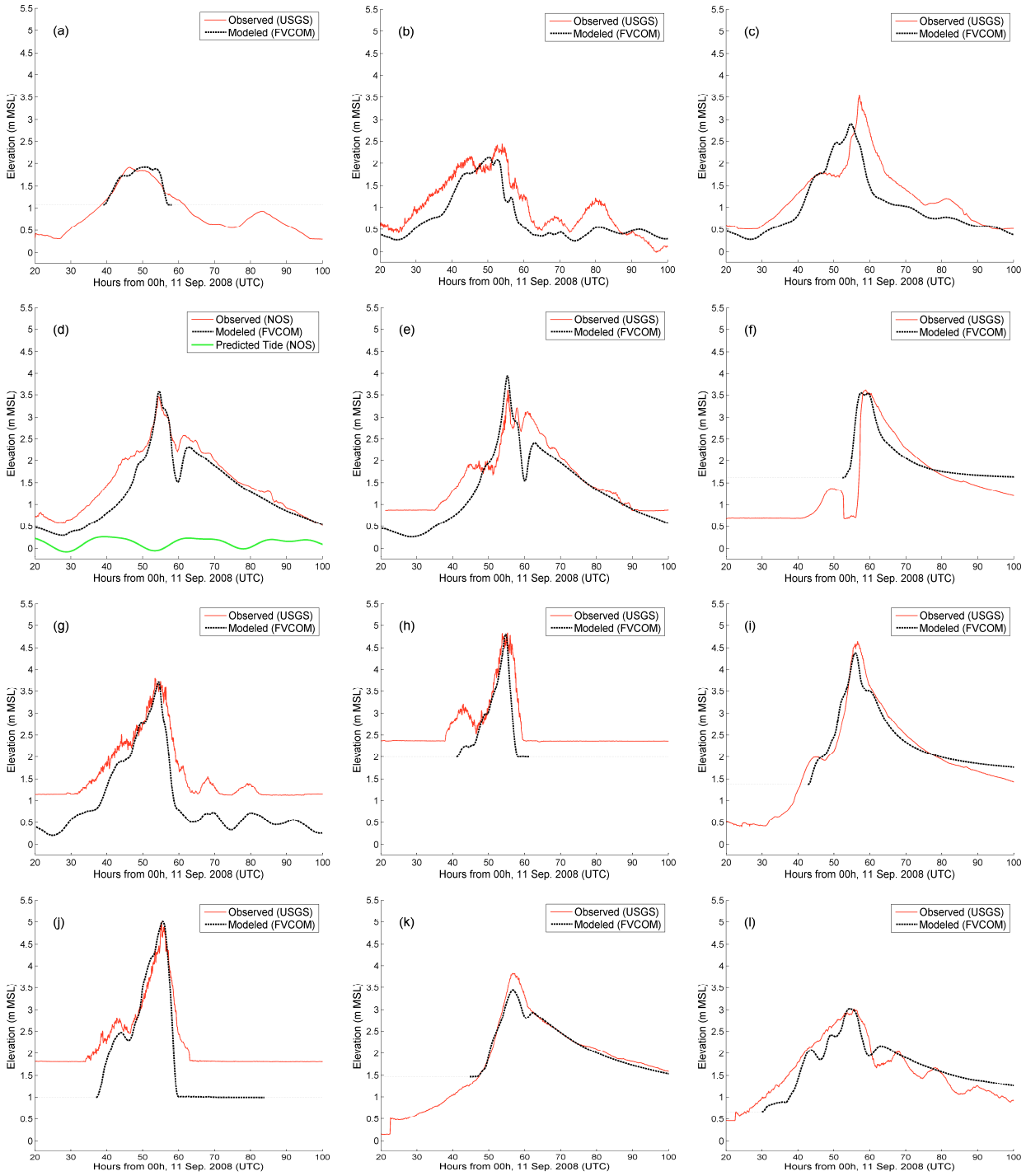

Figure 5.5: Validation plots: observed (solid light line) vs. modeled (dark dashed line) storm tide curves. (a) through (l) have the same meaning as in Figure 5.4.

5.6. Scenarios Tested

Insight into how surge propagation is affected by the geometry of Bolivar Peninsula is gained by running different scenarios in which only this factor is varied. The same winds and tides of Hurricane Ike are used in all simulations summarized in Table 5.3, where the single parameter varied is the bathymetry (representing advancing stages of erosion).

Table 5.3: Summary of scenarios defined in Section 6 and tested in Section 8. Bathymetry changes computed around Bolivar Peninsula over an area of about 132 km^2.

Scenario	Bathymetry simulated	Peninsula: Volume above MSL (10^6 m^3)	Galveston Bay: Total flooded volume (10^6 m^3)
A	Existing	162.0	3583 (100%)
B	Eroded dune	118.9	4276 (119%)
C	Further erosion and 2 breaches	73.5	4625 (129%)
D	Plateau 0.05 m above MSL	5.6	5249 (147%)
E	Plateau 0.30 m below MSL	-40.6	5780 (161%)

Figure 5.6a shows original elevations: most of the peninsula is at least 1 m above MSL, with a strip about 500 m wide of higher ground, 1.5-3 m above MSL, stretching alongshore for 28 km. Scenario B (not shown) represents a typical after-hurricane situation: elevations on the peninsula are reduced to 2/3 of their original heights except in the 500 m behind the dune, where elevations are increased by 0.3 m. For a quantitative estimate of the specific value to be deposited landward of the foredune, we use USGS Hurricanes and Extreme Storms Group (2009), who compared airborne LIDAR surveys of pre- (09/2005) and post-storm (09/17/2008) topography on the Texas coast. In Bolivar Peninsula erosion along the shoreline reached about 1 m, while landward there are areas of ~0.3 m deposition, indicating movement of at least some of

the eroded sediment towards land. This pattern follows Santa Rosa Island's (Florida) pre- and post-storm profiles for Hurricane Opal (October 1995), given by Stone et al. (2004), and is also consistent with Otvos and Carter's (2008) description of erosion caused by Hurricane Rita (August 2005) in the Mississippi-Alabama chain of barrier islands. This demonstrates the fact that tropical storms can be both "constructive" and "destructive" on barrier environments with respect to their sediment budget (Stone et al., 2004).

Scenario C (Figure 5.6b) represents a situation of severe coastal erosion: peninsula elevations from Scenario B are all reduced by a further 2/3 and two breaches have opened up, 0.60 m deeper but still 0.1-0.5 m above MSL. These 600 m wide breaches are similar to the one created by Hurricane Charley on North Captiva Island (Weisberg and Zheng, 2006b). Scenario C could happen if another similar hurricane had passed on the same track soon after Ike, before the barrier system had time to replenish itself. Although an unlikely scenario, Allison et al., (2005) did present a study of two powerful storms affecting the same region of Louisiana's central coast, separated by only 7 days in 2002. Scenario D and E (not shown) are extreme cases for which the peninsula is reduced to a leveled plateau 0.05 m above and 0.30 m below MSL, respectively.

5.7. Hurricane Ike's Surge and Inundation in Galveston Bay

Hurricane Ike made landfall on the eastern part of Galveston Island, along a NNW track that followed the western side of Galveston Bay, with its center virtually alternating between land and water for about 60 km (Figure 5.7). Here inundations refer to the elevation above the still water levels (*i.e*. above MSL for bay points and above topography for land points), a simple way to illustrate surge over both water and land.

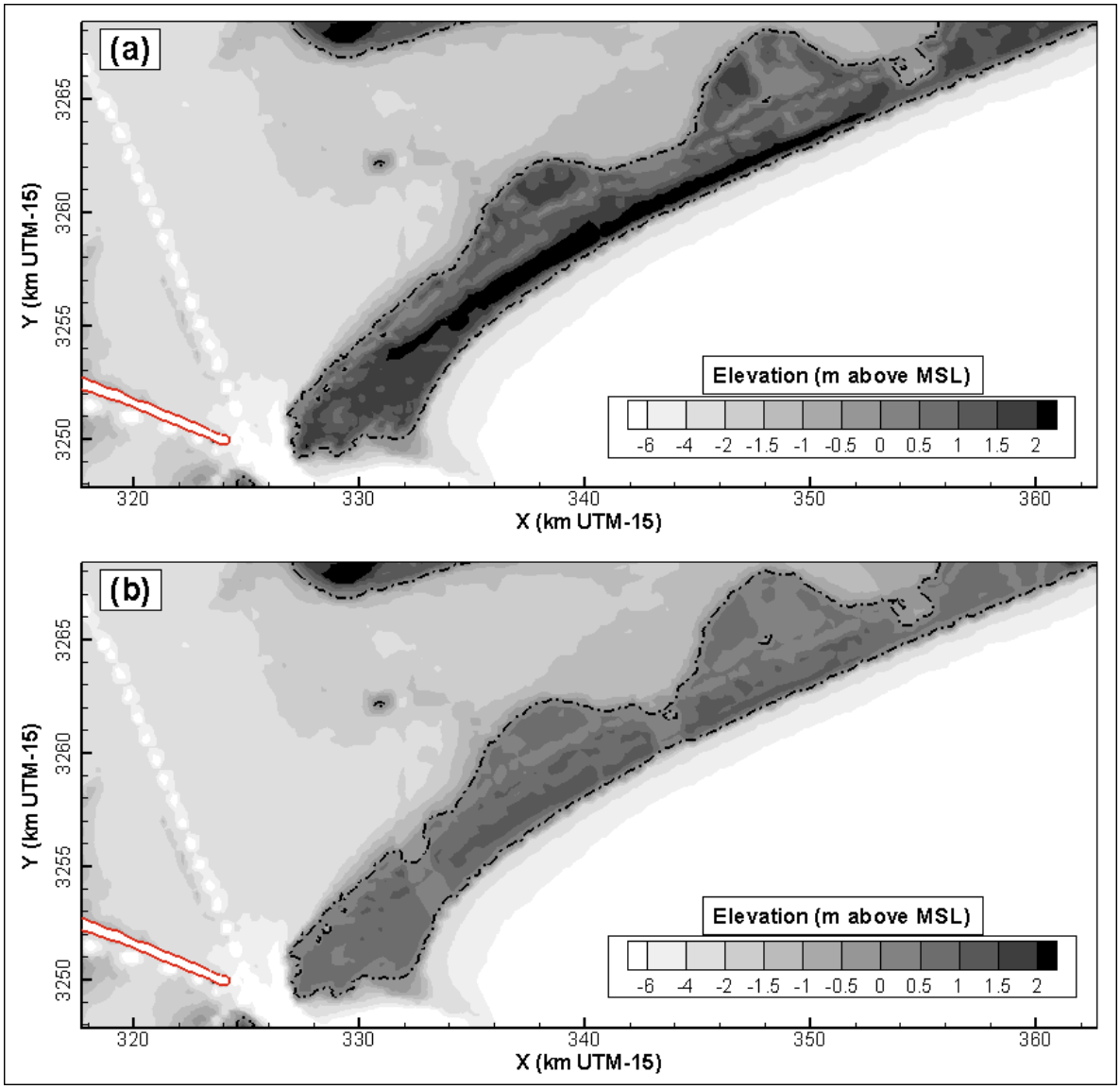

Figure 5.6: Tested model bathymetries: (a) Scenario A, and (b) Scenario C.

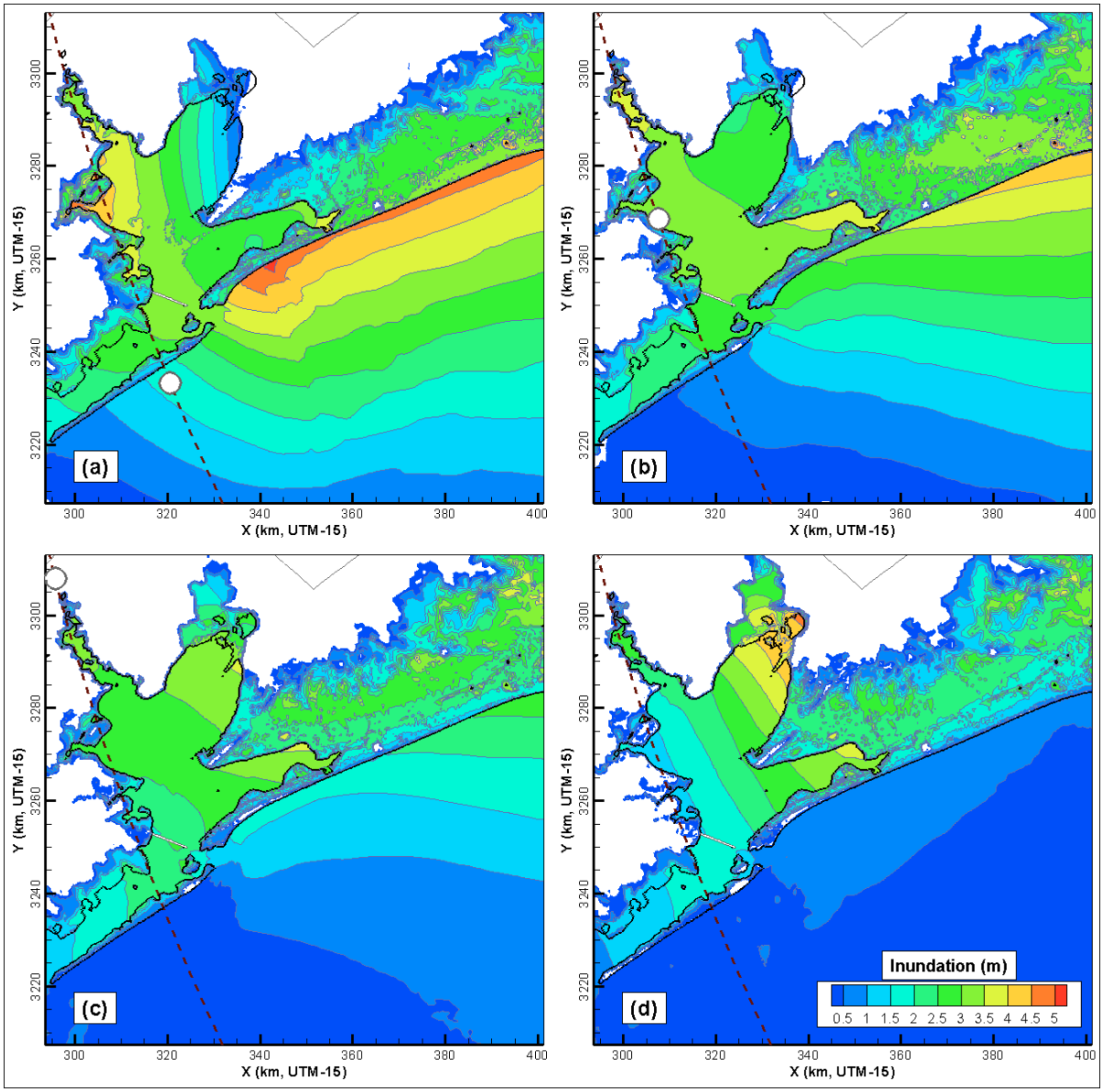

Figure 5.7: Scenario A inundation snapshots: (a) 07h00, (b) 08h30, (c) 10h00 and (d) 11h30 UTC, 09/13/2008.

At 07h00 UTC, 09/13/2008 (about half an hour before landfall), the highest nearshore water levels of about 5.2 m were offshore Bolivar Peninsula, which was completely flooded (Figure 5.7a). A strip of 4.5-5 m inundations stretched due east along the shore from this location. Inundation levels in East Bay, behind the peninsula, were just 2.5-3.2 m at this time. On the left-hand side of Ike's track, nearshore inundation levels were 0.7-2.7 m increasing eastward, and in West Bay behind Galveston Island, they were 1.8-3.1 m. The 3-3.5 m inundation band reached from offshore up to the north coast of the bay, uninterrupted. Given the specific relationship between bay geometry and hurricane track, a clear gradient of water elevations occurred inside the bay, 0.5-4.0 m increasing westward, along a distance of about 38 km (Figure 5.7a). One and a half hours later (Figure 5.7b), nearshore water levels dropped to 2.6-3.4 m along Bolivar Peninsula, increasing eastward. The highest levels of 4-4.5 m propagated east, deflected by the Peninsula and forced by the ENE alongshore winds. Inundation in East Bay increased to 3-3.6 m. On the left-hand side of Ike's track, nearshore inundation levels decreased to 0.2-1.2 m, and in West Bay increased slightly to 1.7-2.7 m. Over most of Galveston Bay winds blew northwestward at this time, and the across-bay gradient virtually disappeared.

Another 1.5 h later (Figure 5.7c), nearshore water levels decreased further to 1.4-1.8 m along Bolivar Peninsula and to 0.4-0.5 m along Galveston Island; some patches started to dry over both barrier systems. The highest levels of 2.5-3 m propagated alongshore due east and reached Sabine Pass. Inundation levels in East Bay were 2.5-3.5 m, and in West Bay 1.2-2.5 m. At this time, water levels in the bay were higher than on the continental shelf. Over most of Galveston Bay, hurricane winds blew northeastward and a weak (reverse) eastward gradient formed. At 11h30 UTC (Figure 5.7d), nearshore water levels were 0.4-0.5 m along Galveston Island and about 0.8 m from the bay entrance to Sabine Pass. Over Bolivar Peninsula and Galveston Island, greater portions were dry. Inundation levels continued to decrease in East Bay

(1.8-3.6 m) and in West Bay (0.9-1.8 m). Hurricane Ike's weakening winds blew ENE over Galveston Bay; in the upper bay, the eastward gradient strengthened to 1.3-4.2 m.

The surge propagation described above could be inferred from NOAA and USGS data, but with a narrower perspective. For coastal surge magnitude and timing, compare data from stations USGS TX-GAL-008, TX-GAL-001 and TX-JEF-002 (Figures 5.5g,h,j). Peak surge increases west to east, from 3.7 to 4.8 and 5 m, whereas time-of-peak increases from 6h20 to 6h50 and 7h30 UTC, respectively, indicating an eastward coastal surge propagation. Although closer to the hurricane's track, peak surge behind Galveston Island was lower, increasing eastward from 2 to 3.5 m (stations USGS TX-GAL-016 and TX-GAL-016, Figures 5.5b,c). On the right-hand side of Ike's path, even stations much farther away had higher or comparable peak surges, *e.g*. USGS TX-JEF-007 with 3.8 m and LA-CAM-003 with 3 m (Figures 5.5k,l). Cross-bay elevation gradients could be implied from data in stations NOS Eagle Point, TX (Figure 5.5d) and USGS-TX-HAR-002 (Figure 5.5e), compared to stations USGS TX-CHA-3 (Figure 5.5f) and TX-CHA-004 (not shown). It should be noted that modeled water levels in west Galveston Bay show an exaggerated decrease after peak surge, by about 0.4-0.8 m (Figure 5.5d,e), most likely a result of incorrect bathymetry and the uncertainty in tropical storms' inflow angle which make negative surges inherently more difficult to model than positive ones (Peng et al. 2006b). On the east, the model anticipates the arrival of the peak by about half an hour earlier (Figure 5.5f), a less important flaw. But overall the model captures both nearshore and in-bay surge propagation.

These westward quickly followed by eastward elevation gradients that occur between west Galveston bay and east Trinity bay (and East bay) are very interesting oscillations that had rarely been described. Other studies have mentioned similar phenomena, but for larger basins with rather wide openings. In this paper we use FVCOM on a high-resolution mesh, aided by

very good observations, to go a step further and analyze the "sloshing" (in fluid dynamics, the movement of a free-surface liquid inside another object) created by a hurricane bordering on a semi-enclosed bay. This effect is shown on Figure 5.8, where elevations above MSL (and not inundations; this is only different over land points) are shown over time along the 52 km line defined in Figure 5.4. Figure 5.8a shows the more intuitive, 3-D surface, while Figure 5.8b presents a more analysis-ready form. As the hurricane approaches (hours 45-50 after 00h UTC, 09/11), waters are gradually pushed westward inside the bay, and a sharp peak is reached at about 55 hours; at this time a sharp westward elevation difference exists, from 0.5 to 4.5 m. As the hurricane advances, water is quickly pushed eastward, and a reversed gradient peaks just 5 hours after the first peak. It is also shown (Figure 5.8b) that the build-up inside the bay is much faster than the set-down. The 1 to 4 m build-up (hours 45-55) is much more intense than the subsequent 2.5 to 2 m set-down (hours 63 and 70).

The initial westward gradient (of about -0.09 m/km) is slightly stronger than the subsequent eastward gradient (of about +0.08 m/km); this was predictable as storm winds decay with time after landfall. It is worth noting that, given the hurricane's track relative to the bay and its counterclockwise winds, this phenomenon is not entirely unexpected. Other studies had superficially mentioned similar gradients. Based on a thorough and successful validation against observed surges, our contribution is its quantification, both in space (from -0.09 to +0.08 m/km) and in time (a 5 hour interval). The former is mostly a function of the storm's intensity and proximity to the bay, but also of the bay's geometry; the latter is a direct result of the hurricane's traveling speed.

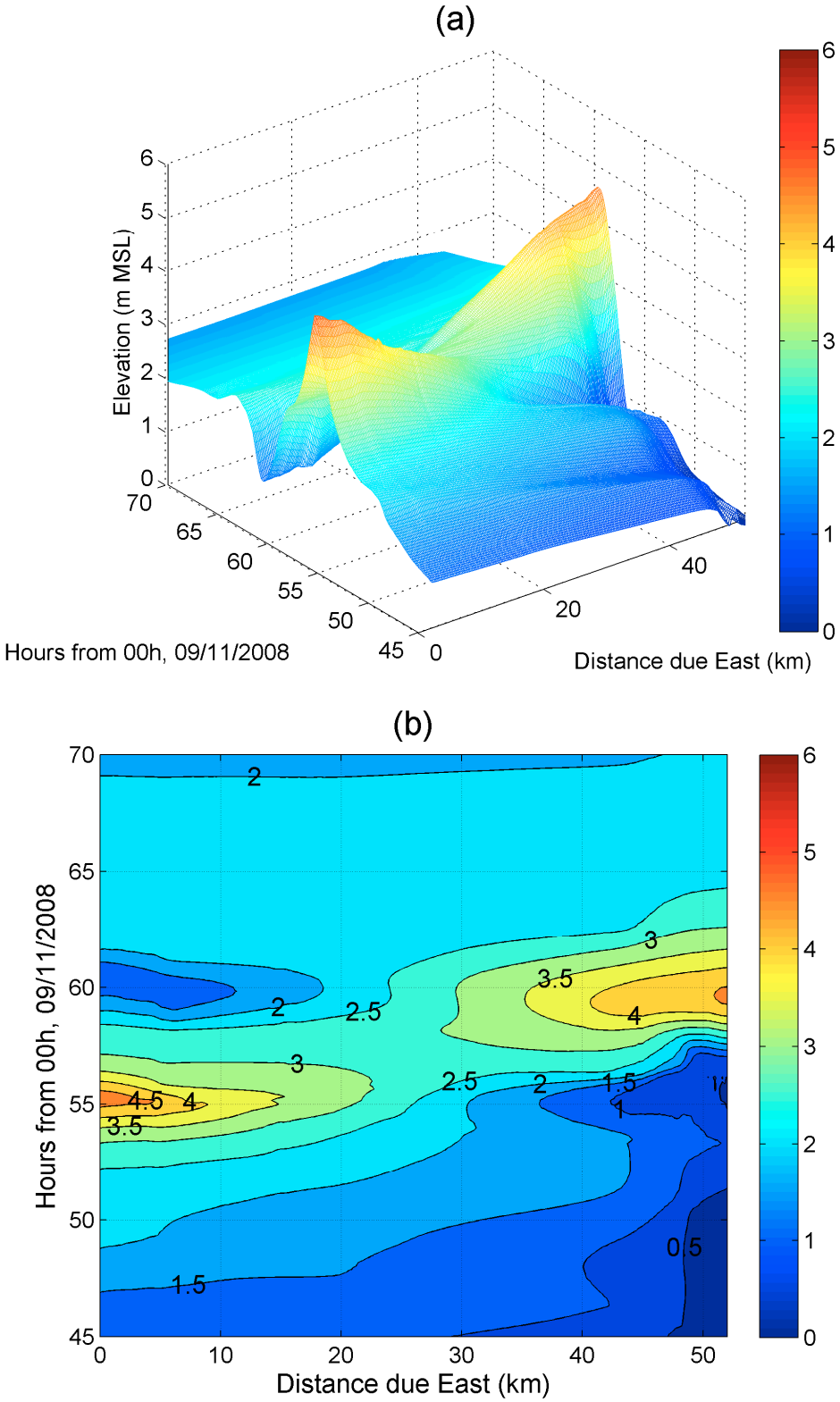

Figure 5.8: Modeled storm surge development along the line defined in Figure 5.4, under Scenario A: (a) intuitive 3-D form and (b) flattened down form.

5.8. Quantifying the Effect of Barrier Systems

Having shown that nearshore surge propagated alongshore due east, towards Louisiana, and that Bolivar Peninsula contributed to this "deflection" and had a significant role in protecting the bay (although landfall was on Galveston Island), an evaluation of how this system's major barrier impacts surge propagation into and within Galveston Bay is discussed next. Magnitude and evolution of total inundation volumes (computed as totals for Galveston Bay and its surrounding inundation areas) for the 5 tested scenarios are shown on Figure 5.9a. The 4 vertical dashed lines indicate the instants when Figure 5.7's snapshots were taken. Instant (a) is half-hour before landfall on Galveston Island; instant (d) is approximately the time when Bay-Gulf outflow begins and flooded volumes decrease for Scenario A. Inundation areas varied from an average of 200 km^2 under normal circumstances, up to a peak of 1700-1900 km^2 (depending on the scenario) during peak storm surge. Results are summarized on Table 5.3.

Scenarios B and C produce total peak flooded volumes greater than Scenario A's by 19 and 29%, respectively. Scenarios D and E yield total peak flooded volumes 47% and 61% greater than that caused under Scenario A (Table 5.3). Also, scenarios having smaller barrier system lead to earlier and more severe flooding, but also to faster flushing out of flooded waters: curves for Scenarios D and E rise earlier and higher than all other curves, but also drop faster and lower than the others (Figure 5.9a).

Consistent with the "sloshing" effect described in the previous section, there are two peaks for the highest inundation levels, separated by about 5 hours (Figure 5.9b). Under Scenarios A-D the first peak of highest levels represents inundations in western Galveston Bay and onshore Bolivar Peninsula (*e.g.* Figure 5.7a).

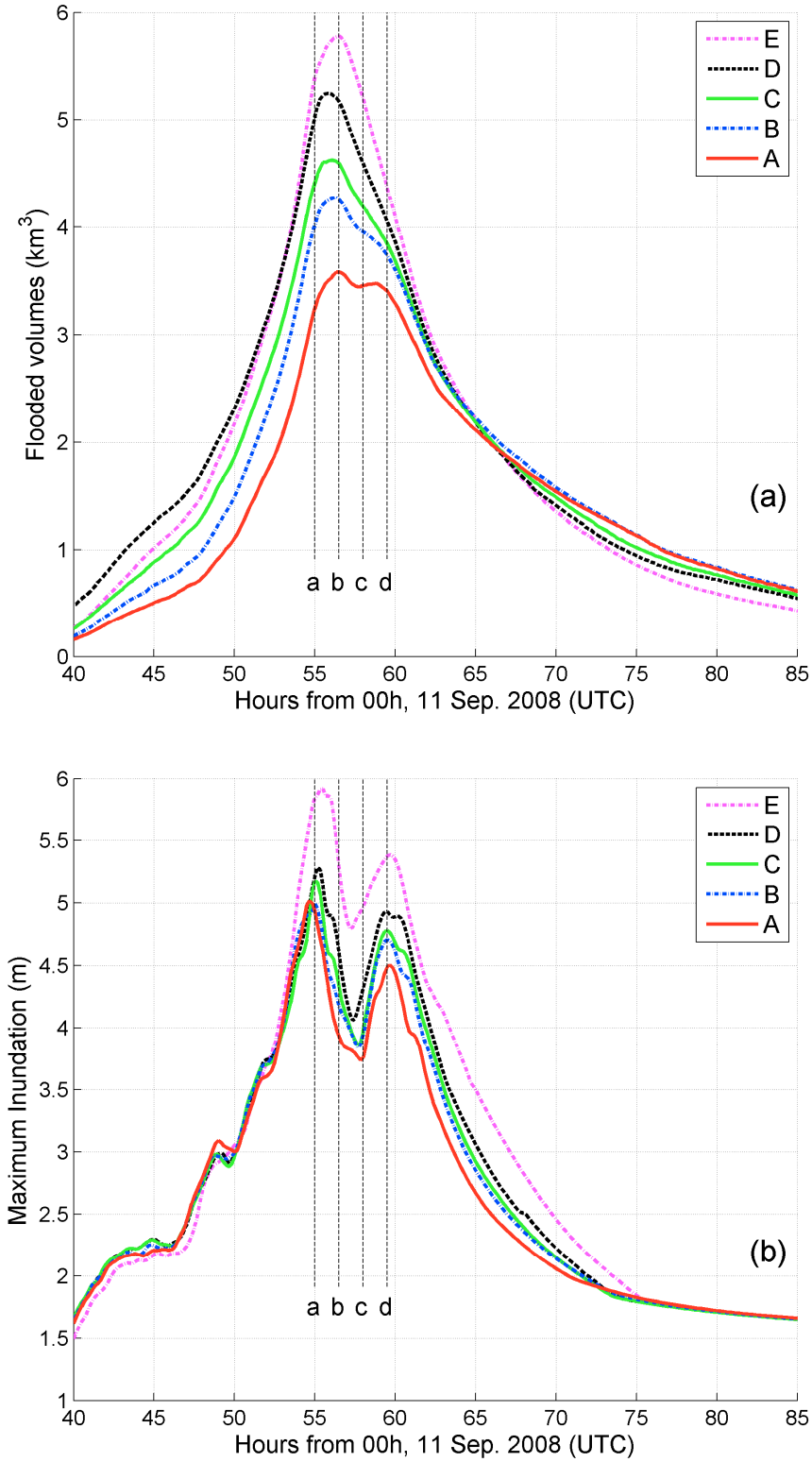

Figure 5.9: Comparison of Galveston Bay region-wide (a) total flooded volumes, in km^3 and (b) maximum elevations, in m, under Scenarios A through E.

For Scenario E (with no barrier), this first peak of highest levels represents inundations in western Galveston Bay and on the northern East Bay. The second peak's inundations are located up in Trinity Bay for all Scenarios (e.g. Figure 5.7d). It is worth noting that highest inundation level curves (also decreasing in the expected fashion from E to A), are not as separated as total flooded volume curves, indicating how these peak water levels are relatively localized.

The original results from Figure 5.7 are compared with those of Scenarios C (Figure 5.10) and D (Figure 5.11), for a better look into the varying dynamics within the bay under different scenarios. The severely eroded dune with breaches is (expectedly) a less effective barrier than the original peninsula, and East Bay water levels are about 1 m higher compared with Scenario A's before landfall (Figures 5.7a and 5.10a). The 0.05 m high peninsula in Scenario D offers little resistance to the passage of storm surge, but East Bay water levels are "only" about a half meter higher than those in Scenario C, before landfall (Figures 5.10a and 5.11a). For instant (b), the time of peak flooded volumes, inundation levels are 3.0, 3.6 and 3.8 m in Galveston Bay and 3.7, 4.4 and 4.6 m in the Houston Ship Channel for Scenarios A, C, D, respectively.

We conclude that in this respect the major change is from Scenario A to C, and that the change to Scenario D has relatively less impact. Thus a Peninsula with a height (or volume) reduced to about 45% of original values and two breaches exposes the interior bay to dangerously high water levels almost as much as a Peninsula that is leveled at just 0.05 m above MSL. Figures 5.10a,d and 5.11a,d also indicate that the same kind of eastward followed by westward surface gradients exist for Scenarios C and D, but about 0.5 m higher than under Scenario A.

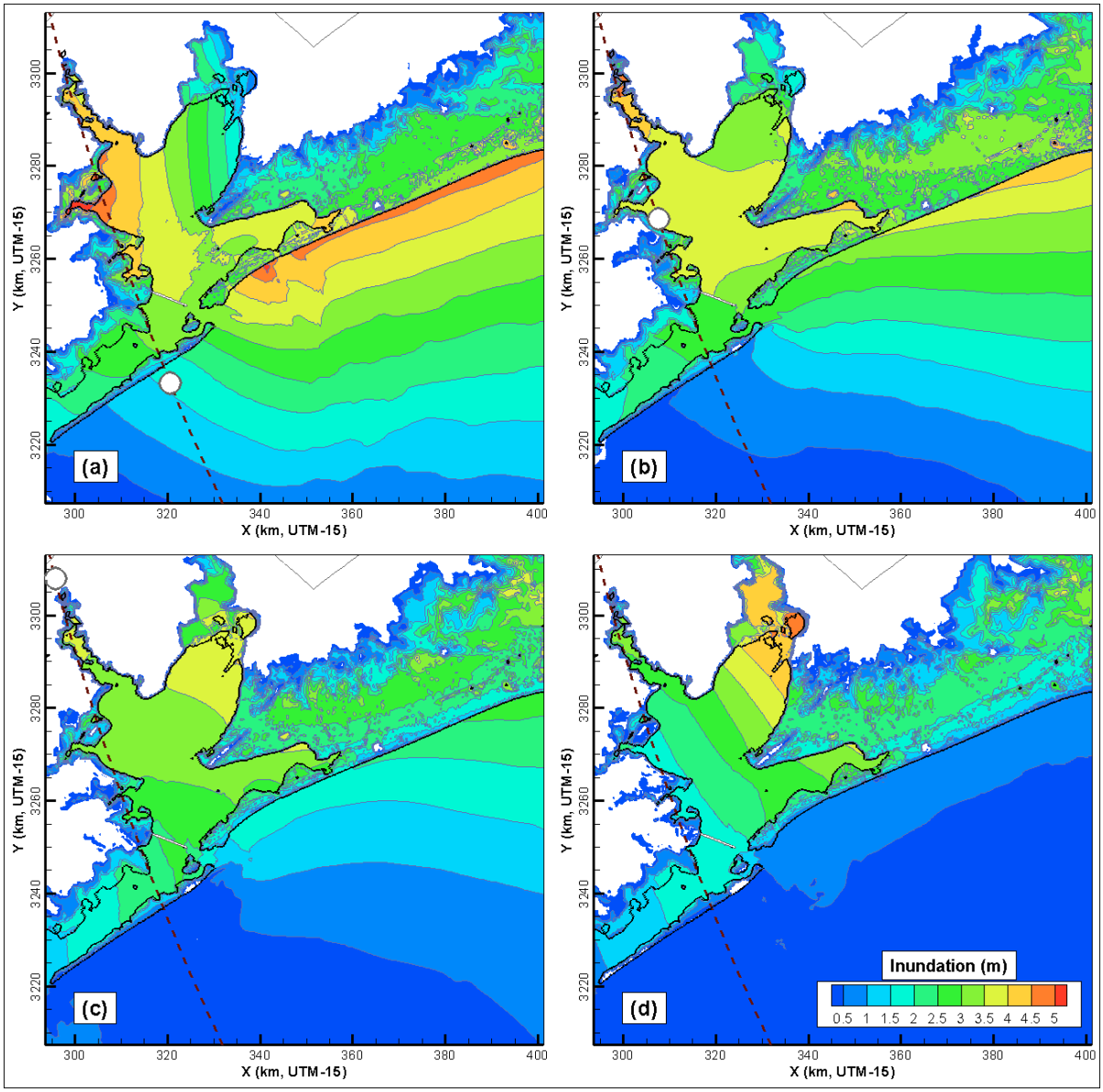

Figure 5.10: Same as Figure 5.7, but under Scenario C.

Figure 5.12 shows inundation levels along the line defined in Figure 5.4, for the same four snapshots (covering a 4h30 period), for all scenarios; it shows how varying barrier geometries affect the sloshing of Figure 5.8. At each instant, the upper bay gradients are similar for varying scenarios (exceptions are land points in the east). Scenario A's gradients (westward of -0.09 m/km, eastward of +0.08 m/km) are slightly stronger than those from idealized scenarios (westward of -0.08 to -0.07, eastward of +0.07 to +0.06, Scenarios B-E), because as water depth increases inside the bay the wind becomes less effective at raising water levels.

Finally, it is noted that in Figures 5.12a,b the curves for various scenarios are the farthest apart, while in Figures 5.12c,d they are the closest together: this is consistent with the evolution of total inundation volumes, which peaked for instant (b) and are converging for (d) (Figure 5.9a). These results suggest that changes in the barrier system geometry do not change the basic dynamics of the upper-bay sloshing (similar gradients), but that considerable 1-2 m variations in the background level still occur, with potentially destructive consequences.

5.9. Conclusions of Chapter 5

We use FVCOM with a high-resolution mesh to study Hurricane Ike's storm tide along the Texas-Louisiana coast, where coastal surge heights up to 5.2 m NAVD88 were measured. The exceptional surge data collected by the USGS during Ike allowed for the validated modeling of this unique situation during which a powerful hurricane traveled next to and to the left of a medium-sized, semi-enclosed bay. A hurricane's coastal surge depends to a large extent on the path of the storm and on the geometric properties of a waterbody, and we focus on how the surge wave propagates into and within Galveston Bay and on the importance of its barrier system. FVCOM results match very well against observed water levels at most stations, with peak amplitude errors mostly below 15% and timing errors typically under ± 0.5 hour. Even when slightly over- or underestimating peak surges, the model accurately capture surges' curves.

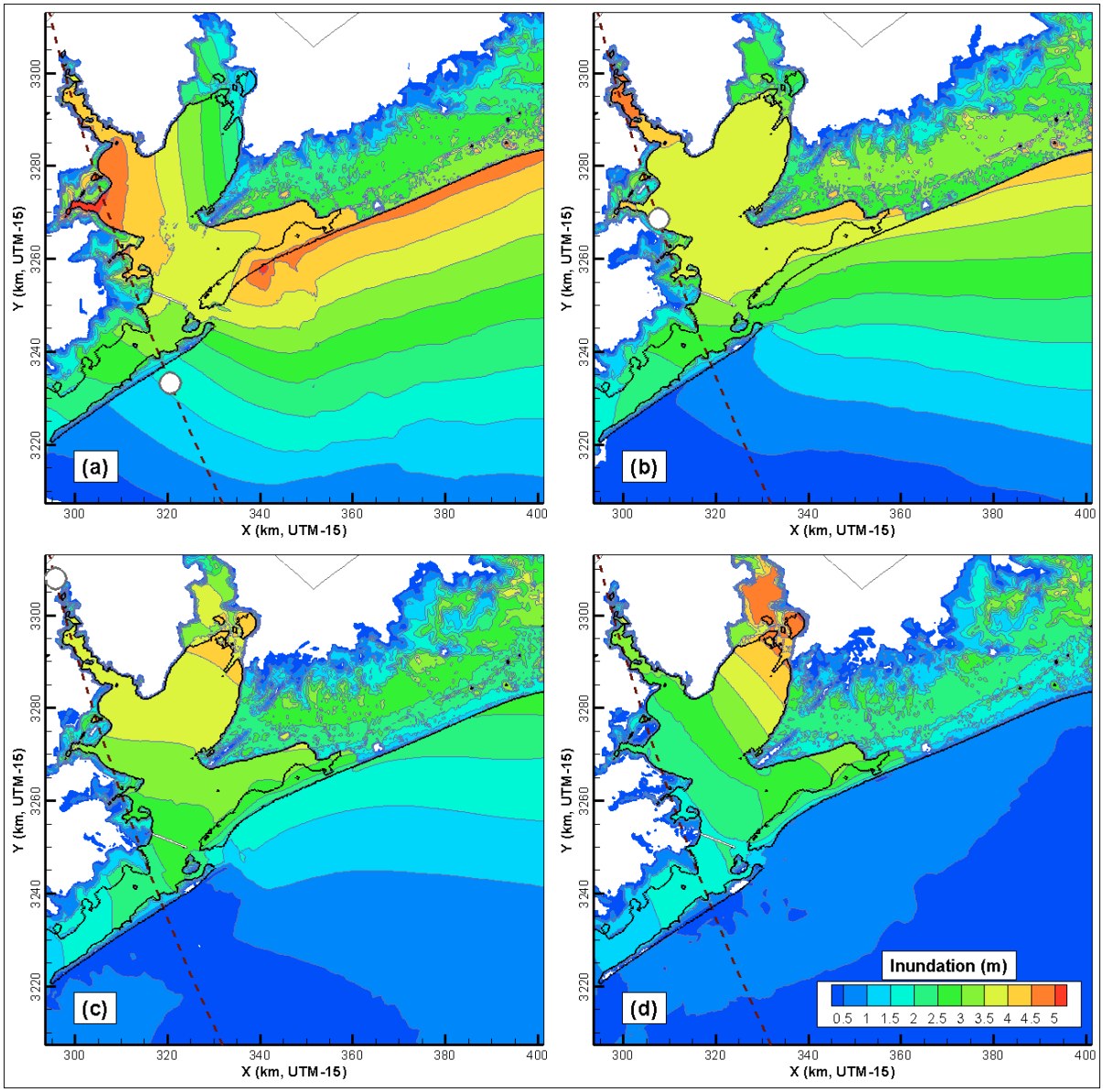

Figure 5.11: Same as Figure 5.7, but under Scenario D.

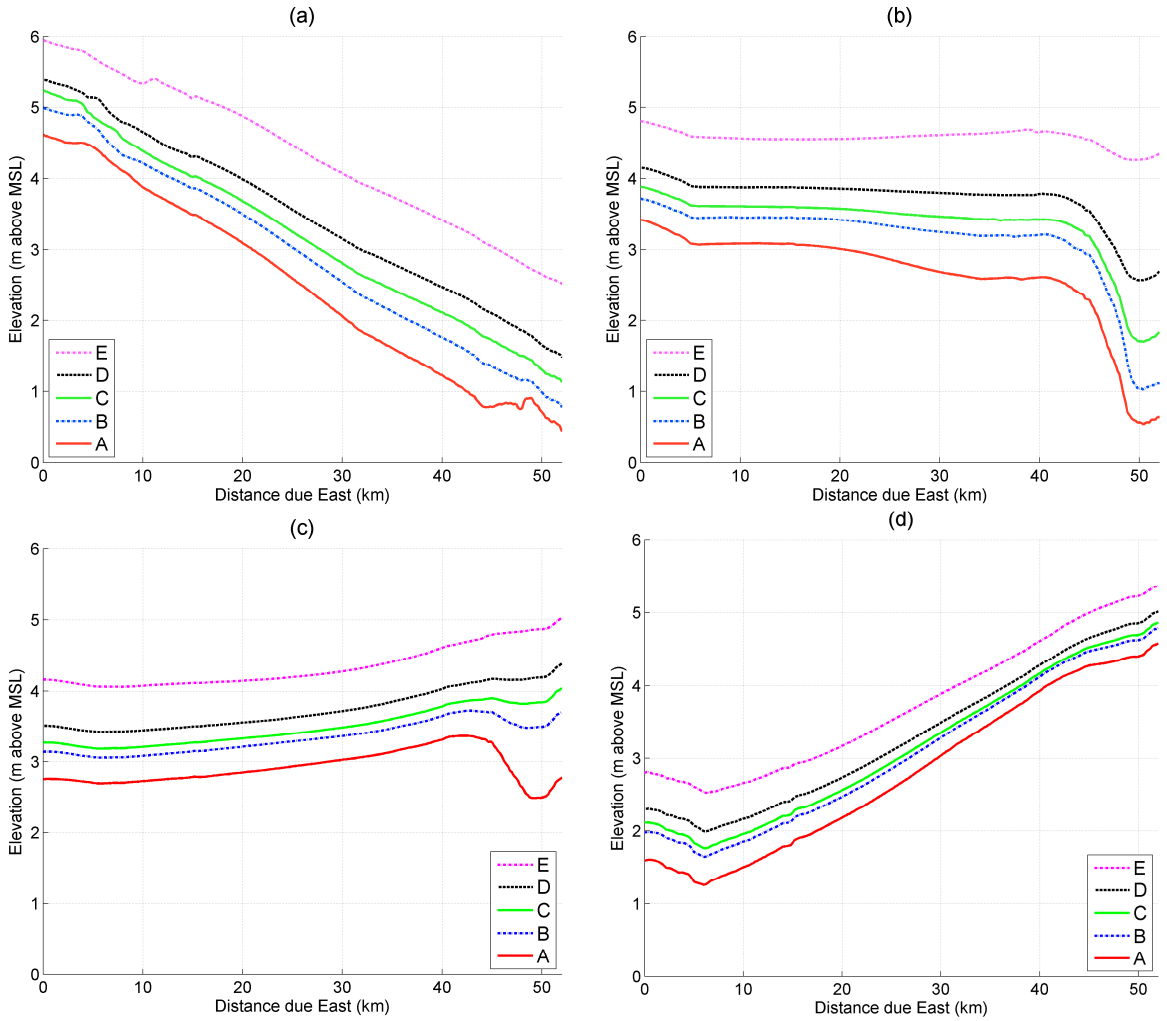

Figure 5.12: Water levels (m above MSL) along the line defined in Figure 5.4, for the same four instants used in Figures 5.7, 5.10 and 5.11.

For the specific relationship between Hurricane Ike's track and Galveston Bay's geometry, we show that coastal surge propagated alongshore towards Louisiana, and that Bolivar Peninsula contributes to this deflection and had a significant role in protecting the bay (although landfall was on Galveston Island). We identify a fast-reversing cross-bay elevation gradient in upper Galveston Bay, and analyze the "sloshing" that formed as the hurricane traveled northward bordering the western side of this semi-enclosed bay. The westward followed by eastward elevation gradients between west Galveston bay and east Trinity bay (and East bay) are very

interesting and had not been fully described. These sharp, opposing surface gradients (of about 0.08 m/km) occur in just 5 hours.

Insight into how this system's major barrier impacts surge propagation into and within Galveston Bay was gained by running different scenarios in which only Bolivar Peninsula's bathymetry was varied (representing increasing degrees of coastal erosion). Compared to the original bathymetry, scenarios B-D yielded 19, 29, 47 and 61% greater total peak flooded volumes, respectively. For the time of peak flooded volumes, we show that the major change is from Scenario A to C, and that the change to Scenario D has relatively less impact. This suggests that a realistic erosion scenario to this peninsula exposes the interior bay to dangerously high water levels almost as much as a peninsula that is leveled to just 0.05 m above MSL.

CHAPTER 6

SYNTHESIS AND CONCLUSIONS

As detailed in previous chapters, a systematic investigation of hurricane induced storm surges along the coasts of Louisiana and Texas was conducted using FVCOM (Chen et al., 2003). It includes an application to the storm surge event during Hurricane Rita (September 2005) using data of flooding along the Louisiana coast for model validation and another application to the storm surge during Hurricane Ike (September 2008) using data of flooding along the Texas coast for validation. Various idealized scenarios were also simulated using FVCOM, to gain insight into specific surge mechanisms. The following conclusions are applicable to hurricane induced storm surges over wide and shallow shelves with small tidal amplitudes.

6.1. Storm Surge Simulations on the Louisiana Shelf

One of the well-known results, as confirmed by many observations and this study, is that storm surges are much briefer in their build-up stages than in the receding, or waning stage. The receding of surge waters on Louisiana's low-lying coast during Hurricanes Rita and Gustav was studied here. It is demonstrated in this dissertation that it takes 100-140 hours for the surge to go back to normal in tidal passes, but about 7 days or longer in inland areas to reduce the surge to about 1/3 of peak inundation. Based on the model results from FVCOM, this dissertation explained the processes that distinguish surge inflow from outflow, creating the contrasting and asymmetric flooding and receding stages. When a hurricane approaches, flooding occurs along large parts of the shoreline with low-lying lands and wetlands. Surge heights along the coast can reach 3 m and flooding spreads several kilometers inland. Flood waters are forced by winds with higher water levels and do not "feel" the bottom (friction) as much, resulting in a brief and vast landward transport of water. In contrast, the surge water coming back to the GoM is constrained

by the existing channels. At the peak outflow, surge waters flow out of the region's major coastal passes in much weaker plume-like patterns, as the wind forcing rapidly diminishes.

The roles of a storm's various parameters were investigated by several idealized experiments while maintaining Rita's track and Louisiana's bathymetry and tides. It was shown that wind intensity and RMW have the largest effect on flooded volumes and peak surge heights: for both variables, extreme scenarios yield total flooded volumes of about 25 and 160% (weakest and smallest vs. strongest and largest, respectively), of that of the standard case. Varying the landfall timing (relative to the tide) also influences the flooded volumes and peak surges in the same way but in a less dramatic fashion: hurricanes making landfall at high tide yield both greater flooded volumes and peak surges than those landfalling at low tide. Variations in this case are only about ±16% of the base case.

On the other hand, varying a hurricane's forward speed has opposite effects on flooded volumes and peak surge elevations. Increasing the forward motion speed of the storm within a realistic range (2-12 m/s) decreases flooded volumes while increasing peak surges, both by about 40%. This peak surge result is consistent with some literature, but contradicts studies on narrower shelves (see Chapter 4). Variations in flooded volumes had not been studied before. A slower moving storm produces lower peak surges but reaches farther inland, whereas a hurricane moving swiftly across the shoreline generates higher surges that only flood a narrower section of the coast. A storm's forward motion may account for variations in flooded volumes equivalent to an upgrade or downgrade of about 1 category on the Saffir-Simpson scale, a larger impact than tidal timing, amplitude, or wind inflow angle, which are emphasized by previous studies.

6.2. The Role of Shelf Geometry

A systematic approach of forcing a typical hurricane on the shelf and estuarine waters with different geometries, varying tides and landfall timing, allowed for in-depth investigation of tide-

surge nonlinearities. These conclusions are thus not limited to Hurricane Rita's storm surge. Compared to peak pure surges produced by this "standard" hurricane hitting a wide shelf with a 1 m minimum depth, increasing the minimum depth to 5 m decreases peak pure surge to about 75%, whereas increasing (by a factor of 3) the shelf gradient decreases peak pure surge to about 50%. This is the effect of shelf geometry alone.

The analysis of surface, depth-integrated and bottom currents were used to show how the shallow Scenario A leads to a stronger surge asymmetry (higher surge elevations to the right of the hurricane and lower to its left), as compared to a scenario only 4 m deeper. Because the bottom are nearly perpendicular to the surface elevation contours, the bottom return flow is directed to the left of the surface currents (from about 90 to 180º) on the right-hand side of the hurricane. The bottom stress then has a shoreward component, which contributes to increase the piling up of water against shore. This counter-intuitive three-dimensional effect has an enhancing impact on coastal surge, and suggests that 3-D models are preferable over 2-D models for simulating storm surges.

6.3. Nonlinear Tide-Surge Interaction

The numerical model simulation of Hurricane Rita's storm surge showed that peak storm surge elevation surpassed 5 m along the major flooded areas of the coast (from point of landfall to approximately 3×RMW due east), where tidal range is about 0.66 m. The nonlinear effect was computed by subtracting the sum of tide and surge-only elevations from the total elevation. East of the landfall point, the nonlinearity opposes the tide, reducing storm tide heights when the tide is high, and enhancing the storm tide when approaching low tide. In demonstrating this feature, storm surges were simulated using the observed meteorological forcing of Hurricane Rita but doubling the tidal amplitude with a low-tide landfall. For low- and high-tide landfalls, the

nonlinear effect is constructive and destructive to the total storm tide, respectively. Nonlinearity is significant, reaching up to about 70% of the tidal amplitude.

For landfalls at mid-ebb or mid-flood the main nonlinear effect is to oppose the tide before and after peak storm tides, generating storm tide curves with moderately different shapes but having the same peak height as the linear superposition. For landfalls at high- and low-tide the nonlinear effect opposes the tide, i.e. peak heights are lower and higher, respectively, than a linear superposition of surge and tide. Nonlinearity effects reach up to 80% of the tidal amplitude on a wide shelf under a semi-diurnal tide. Under diurnal tides, nonlinearity effects reach up to 47% for a wide shelf, 41% for a wide shelf 4 m deeper, and 26% for a narrow shelf.

This demonstrates the effect of amplification of nonlinearity over a wide shelf. The reason that the semi-diurnal tide has larger nonlinear effect compared to the diurnal tide is because the former has shorter wave length and thus "sensed" the shelf as being wider when the same geometry is used. The nonlinear effect is the greatest for landfalls at low tide, followed by landfalls at high tide and then by landfalls at mid-ebb or mid-flood. Not accounting for such tide-surge interaction may result in a significant overestimation of peak storm tide heights for a landfall at high tide and in a significant underestimation for a landfall at low tide.

The change in the storm tide was found to be appreciable in shallow water and was produced by changes in non-linear bottom friction and momentum advection due to the presence of the tide. A detailed examination of these residuals showed that the nonlinear residuals of advection dominate in the realistic simulations, while the nonlinear residuals of the quadratic bottom friction dominate in idealized simulations (see also Li et al., 2008).

6.4. The Importance of Barrier Islands

The exceptional surge data collected by the USGS during Hurricane Ike (for which coastal surge heights of up to 5.2 m were measured) allowed for the validation of the model and the simulation

of the storm surge by a powerful hurricane traveling next to and to the left of a medium-sized, semi-enclosed bay. Storm surge depends to a large extent on the path of the storm and on the geometric properties of a waterbody, and thus we focus on how the surge wave propagates into and within Galveston Bay and on the importance of its barrier system to surge development.

Hurricane Ike's coastal surge propagated eastward alongshore, in a direction almost perpendicular to the direction of the hurricane track, towards Louisiana. Bolivar Peninsula contributed to this deflection and had a significant role in protecting the bay (although landfall was on Galveston Island). The west-east "sloshing" that occurred as the hurricane traveled northward bordering the western side of this semi-enclosed bay was analyzed. These sharp, alternating surface gradients (of about 0.08 m/km) occurred in just 5 hours and had not been described before.

Insight into how this system's major barrier impacts surge propagation into and within Galveston Bay was gained by running different scenarios in which only Bolivar Peninsula's bathymetry was varied (representing increasing degrees of coastal erosion). Compared to the original bathymetry, the scenarios tested yielded 20-60% greater total peak flooded volumes than the original situation. It is shown that at the time of peak inundation, a realistic erosion scenario to this barrier (elevations reduced to about half, with two breaches) exposes the interior bay to dangerously high water levels almost as much as a peninsula that is leveled to just 0.05 m above MSL (one of the extreme scenarios tested), underlining the nonlinear nature of this bay-barrier system.

6.5. Directions for Further Research

The single most important factor in surge modeling (along with bathymetry information, for all kinds of hydrodynamic modeling) is probably a good representation of the wind forcing at the water surface. Several factors will help reduce the present-day uncertainty in this term.

Continuing work to improve hurricane wind speed observations and its quality control and dissemination, e.g. by NOAA's Hurricane Research Division, is sure to produce better surge forecasting results. Further improvements to conventional synthetic hurricane wind models (e.g. Holland, 1980) can be another significant contribution since it will allow one to be able to interpolate for small time-steps or simulate idealized scenarios (see Sections 2.4 and 5.4). A major uncertainty source is the relation between wind speeds and wind stress fields. Unfortunately the currently used formulations still vary considerably and there is a lack of consensus among researchers (see end of Section 1.3). Lastly, the air pressure gradient term, though relatively minor compared to the wind stress component, should also be included in future simulations of this kind. This term was not included in the parallel-capable version of FVCOM that we used throughout this work, as argued earlier.

There is also the issue of 2-D versus 3-D surge simulations. Weisberg and Zheng (2008) give the example of ADCIRC hindcast analyses for Hurricane Katrina's inundation recently performed by the USACE Intergovernmental Performance Evaluation Taskforce, which produced excellent results when compared quantitatively against available data. The surface stress parameterization in that application allows the drag coefficient (C_d) to increase unboundedly with increasing wind speeds, which can compensate for increased bottom stress and allows the calibrated model to match the observations for reasons that may not be correct. Our (barotropic) applications of FVCOM had two vertical layers, so we only partially accounted for this issue. Additional studies are necessary to improve the description of both the surface and the bottom stresses.

Because bottom friction is probably the most important nonlinear term (see Sections 1.5 and 2.11), it would be physically more correct to have a spatially variable drag coefficient and a comparison against simulations having spatially-varying values should be of interest. While there

are applications where lower values are used “offshore” and higher values for shallower waters (e.g. Retana, 2008), our study produced very good validations with constant “high” values (probably because our focus was on nearshore areas).

A study like Chapter 3’s would benefit from the inclusion of a term representing evaporation losses. Unlike for conventional “incoming surge” simulations, the water volume lost to the atmosphere from the vast areas of very shallow water over the marshes during the receding stage (8-12 days) may not be negligible. Evaporation would be even more important if future simulations include salinity variations in the water density (unlike the current study, which was fully barotropic). Adding baroclinicity is a natural step forward, if one is to evaluate post-hurricane ecological impacts to the marshes. Another improvement would be the added effort to improve mesh resolution in areas where one initially did not expect such a need. This is because the existing mesh was designed to better resolve hydrodynamics in major coastal passes, without an *a priori* knowledge of circulation under widespread coastal inundation; to further complicate matters, given the contrasting dynamics between surge build-up and set-down, different areas were relevant in later stages.

To improve on the work of Chapter 4, more simulations under different shelves and tides would be a good addition. The author suggests simulating other observed hurricanes on the Atlantic coast of Florida, where the continental shelf is much narrower than Louisiana’s and the tidal range about three times as large.

The kind of simulations illustrated in Chapter 5 would greatly benefit from improvements in the post-landfall wind field description. Inaccurate winds blowing from land, after the hurricane center is “off the map”, were probably the cause for the minor validation errors we had on the upper bay stations.

REFERENCES

AGU (American Geophysical Union), 2006. Hurricanes and the U.S. Gulf Coast: Science and Sustainable Rebuilding. [Available online at http://www.agu.org/report/hurricanes/].

Allen, J.S., 1980. Models of wind-driven currents on the continental shelf. *Annual Review of Fluid Mechanics* 12, 389-433, doi:10.1146/annurev.fl.12.010180.002133.

Allison, M.A., Sheremet, A. Goñi, M.A., and Stone, G.W., 2005. Storm layer deposition on the Mississippi-Atchafalaya subaqueous delta generated by Hurricane Lili in 2002. *Cont. Shelf Res.* 25, 2213-2232.

Aoki, A., and Isobe, A., 2007. Application of Finite Volume Coastal Ocean Model to hindcasting the wind-induced sea-level variation in Fukuoka Bay. *J. Oceanogr.* 63 (2), 333-339.

As-Salek, J.A., 1997. Negative Surges in the Meghna Estuary in Bangladesh. *Mon. Wea. Rev.* 125, 1638–1648.

As-Salek, J.A., 1998. Coastal trapping and funneling effects on storm surges in the Meghna estuary in relation to cyclones hitting Noakhali-Cox's Bazar coast of Bangladesh. *J. Phys. Oceanogr.* 28, 227-249.

As-Salek, J.A., and Yasuda, T., 2001. Tide-surge interaction in the Meghna Estuary: Most severe conditions. *J. Phys. Oceanogr.* 31, 3059-3072.

Berenbrock, C., Mason Jr., R.R., and Blanchard S.F., 2009. Mapping Hurricane Rita inland storm tide. *J. Flood Risk Manage.* 2, 76-82.

Berg, R., 2009. Tropical Cyclone Report: Hurricane Ike (AL092008) 1-14 September 2008. National Hurricane Center, Miami, Florida, 55 pp.

Beven, J., 2008. Hurricane Gustav Advisory Number 32. National Hurricane Center. [Available online at http://www.nhc.noaa.gov/archive/2008/al07/].

Blain, C.A., Westerink, J.J., and Luettich, R.A., 1994. The influence of domain size on the response characteristics of a hurricane storm surge model. *J. Geophys. Res.* 99 (C9), 18467-18479.

Blake, E.S., Rappaport, E.N., Jarrell, J.D., and Landsea, C.W., 2006. The deadliest, costliest, and most intense United States tropical cyclones from 1851 to 2005 (and other frequently requested hurricane facts). NOAA Tech. Memo NWS TPC-4, 48pp.

Blumberg, A.F., and Mellor, G.L., 1987. A description of a three-dimensional coastal ocean circulation model. In N. Heaps (ed.), Three-dimensional Coastal Ocean Models, Coastal and Estuarine Series 4, 1-16. AGU, Washington, DC.

Brier, G.W., and Simpson, R.H., 1967. Stormfury cumulus seeding experiments 1965: Statistical analysis and main results. *J. Atmos. Sci.* 24, 508-521.

Casulli, V., and Walters, R.A., 2000. An unstructured grid, three-dimensional model based on the shallow water equations. *Int. J. Numer. Methods Fluids* 32, 331-348.

Chen, C, Liu, H., and Beardsley, R.C., 2003. An unstructured grid, finite-volume, three-dimensional, primitive equation ocean model: application to coastal ocean and estuaries. *J. Atmos. Ocean. Technol.* 20, 159-186.

Chen, C., Cowles, G., and Beardsley, R.C., 2006. An unstructured grid, finite-volume coastal ocean model: FVCOM user manual, 2nd ed. SMAST/UMASSD Tech. Rep. 06-0602, 315 pp., School for Marine Science and Technology, University of Massachusetts-Dartmouth, New Bedford, MA.

Chen, C., Huang, H., Beardsley, R.C., Liu, H., Xu, Q., and Cowles, G., 2007. A finite-volume numerical approach for coastal ocean circulation studies: comparisons with finite difference models. *J. Geophys. Res.* 112, C03018, doi:10.1029/2006JC003485.

Chen, C., Qi, J., Li, C., Beardsley, R.C., Lin, H., Walker, R., and Gates, K., 2008. Complexity of the flooding/drying process in an estuarine tidal-creek salt-marsh system: an application of FVCOM. *J. Geophys. Res.* 113, C07052, doi:10.1029/2007jc004328.

Chu, P. C., Veneziano, J.M., Fan, C., Carron, M.J., and Liu, W.T., 2000. Response of the South China Sea to Tropical Cyclone Ernie 1996. *J. Geophys. Res.*, 105(C6), 13991-14009.

Church, J. A., Gregory, J.M., Huybrechts, P., Kuhn, M., Lambeck, K., Nhuan, M.T., Qin, D. and Woodworth, P.L. 2001. Changes in sea level, in Climate Change 2001: The Scientific Basis. Eds. J.T. Houghton et al., 639-694, Cambridge Univ. Press, New York.

Conner, W.C., Kraft, K.H., and Harris, D.L., 1957. Empirical methods for forecasting the maximum storm tide due to hurricanes and other tropical storms. *Mon. Wea. Rev*. 85 (4), 113-116.

Constantin, A., 2001. Edge waves along a sloping beach. *J. Phys. A: Math. Gen.* 34, 9723-9731.

DeMaria, M., Knaff, J.A., and Kaplan, J., 2006. On the decay of tropical cyclone winds crossing narrow landmasses. *J. Appl. Meteor. Climatol.* 45, 491-499.

Dietsche, D., Hagen, S.C., and Bacopoulos, P., 2007. Storm Surge Simulations for Hurricane Hugo (1989): On the Significance of Inundation Areas. *J. Wtrwy. Port Coast. and Oc. Engrg.* 133 (3), 183-191.

Doodson, A.T., 1956. Tides and storm-surges in a long uniform gulf. *Proc. Roy. Soc. A*, 237 (1210), 325-343.

Dube S.K., Chittibabu, P., Rao, A.D., Sinha, P.C., and Murty, T.S., 2000. Extreme sea levels associated with severe tropical cyclones hitting Orissa coast of India. *Marine Geodesy* 23 (2), 75-90.

Dube, S.K., Sinha, P.C., Rao, A.D., Jain, I., Agnihotri, N., 2005. Effect of the Mahanadi River on the development of storm surge along the Orissa coast of India: A numerical study. *Pure and Applied Geophysics* 162(9), 1673-1688.

East, J.W., Turco, M.J., Mason, R.R., 2008. Monitoring inland storm surge and flooding from Hurricane Ike in Texas and Louisiana, September 2008. U.S. Geological Survey, Open-File Report 2008-1365 [Available online at http://pubs.usgs.gov/of/2008/1365/].

Emanuel, K. A., 2005. Increasing destructiveness of tropical cyclones over the past 30 years. *Nature* 436, 686-688.

Emanuel, K., 2007. Putting the brakes on the hurricane heat engine. *Physics Today* 60 (7), 13.

FEMA (Federal Emergency Management Agency), 2008. Hurricane Rita Flood Recovery Maps (Louisiana); Surge Elevation Contours. [Available online at http://www.fema.gov/hazard/flood/recoverydata/].

Flather, R.A., 1994. A storm surge prediction model for the Northern Bay of Bengal with application to the cyclone disaster in April 1991. *J. Phys. Oceanogr.* 24, 172-190.

Flather, R.A., 2001. Storm surges. In: J.H. Steele, S.A. Thorpe, and K.K. Turekian (Editors), Encyclopedia of Ocean Sciences. Academic Press, San Diego, 2882-2892.

Galperin, B., Kantha, L.H., Hassid, S., and Rosati, A., 1988. A quasi-equilibrium turbulent energy model for geophysical flows. Journal of Atmospheric Science 45, 55-62.

Garvine, R.W., 1985. A simple model of estuarine subtidal fluctuations forced by local and remote wind stress. *J. Geophys. Res.* 90 (C6), 11945-11948.

Gill, A.E., 1982. Atmosphere-Ocean Dynamics. Academic Press, 661pp.

Gong, W., Shen, J., and Reay, W.G., 2007. The hydrodynamic response of the York River estuary to Tropical Cyclone Isabel, 2003. *Estuarine, Coastal and Shelf Science* 73, 695-710.

Gornitz, V., 2005. Storm Surge. In: M.L. Schwartz (ed.), Encyclopedia of Coastal Science. Springer, 912-914.

Graber, H.C., Cardone, V.J., Jensen, R.E., Slinn, D.N., Hagen, S.C., Cox, A.T., Powell, M.D., and Grassl, C., 2006. Coastal Forecasts and Storm Surge Predictions for Tropical Cyclones: A Timely Partnership Program. *Oceanography* 19 (1), 130-141.

Graumann, A., Houston, T., Lawrimore, J., Levinson, D., Lott, N., McCown, S., Stephens, S., and Wuertz, D., 2006. Hurricane Katrina: A climatological perspective. NOAA's National Climatic Data Center, Asville, NC [Available online at http://www.ncdc.noaa.gov/oa/reports/tech-report-200501z.pdf].

Guidroz, W.S., Stone, G.W., and Dartez, D., 2006. Hurricane Rita, 2005: Assessment of a storm-induced geological event along the southwestern Louisiana coast and adjacent interior marsh. *Gulf Coast Association of Geological Societies Transactions* 56, 229-239.

Haidvogel, D.B., and Beckmann, A., 1999. Numerical Ocean Circulation Modeling. World Scientific Publishing Company, 300pp.

Harris, L.D., 1959. An interim hurricane storm surge forecasting guide. National Hurricane Research Project 32, U.S. Weather Bureau, Washington, DC, 23 pp.

Harris, L.D., 1963. Characteristics of the hurricane storm surge. Technical Paper No. 48. U.S. Dept. of Commerce, Weather Bureau, Washington, D.C., 135 pp.

Harris, D.L., and Jelesnianski, C.P., 1964. Some problems involved in the numerical solutions of tidal hydraulics equations. *Mon. Wea. Rev*. 92 (9), 409-422.

Heaps, N.S., 1965. Storm Surges on a Continental Shelf. *Phil. Trans. R. Soc. Lond. A, Mathematical and Physical Sciences* 257 (1082), 351-383.

Heaps, N.S., 1983. Storm surges, 1967–1982. *Geophys. J. R. Astron. Soc.* 74, 331-376.

Holland, G.J., 1980. An analytic model of the wind and pressure profiles in hurricanes. *Mon. Wea. Rev.* 108, 1212-1218.

Horsburgh, K.J., and Wilson, C., 2007. Tide-surge interaction and its role in the distribution of surge residuals in the North Sea. *J. Geophys. Res.* 112, C08003, doi:10.1029/2006JC004033.

Houston, S.H., Shaffer, W.A., Powell, M.D., and Chen, J., 1999. Comparison of HRD and SLOSH surface wind fields in hurricanes: Implications for storm surge modeling. *Weather and Forecasting* 14, 671-686.

Hsu, S.A., and Yan, Z., 1998. A Note on the Radius of Maximum Wind for Hurricanes. *J. of Coastal Research* 14(2), 667-668.

Hsu, S.A., 2006. Measurements of overwater gust factor from NDBC buoys during hurricanes. National Weather Association Electronic Journal. [Available online at http://www.nwas.org/ej/pdf/2006-EJ2.pdf].

Hsu, S.A., Braud, D., and Blanchard, B., 2006. Rapid Estimation of Maximum Storm Surges Induced by Hurricanes Katrina and Rita in 2005. NWA Electronic Journal of Operational Meteorology EJ9.

Huang, H, Chen, C., Cowles, G.W., Winant, C.D., Beardsley, R.C., Hedstrom, K.S., and Haidvogel, D.B., 2008. FVCOM validation experiments: comparisons with ROMS for three idealized barotropic test problems. *J. Geophys. Res.* 113, C07042, doi:10.1029/2007JC004557.

Hubbert G.D., and McInnes K.L. 1999. A storm surge inundation model for coastal planning and impact studies. *J. of Coastal Research* 15, 168-185.

Hughes, L.A., 1952. On the low level wind structure of tropical cyclones. *Journal of Meteorology* 9, 422-428.

Hurricane Research Division, 2009. Surface Wind Analysis dataset. Atlantic Oceanographic and Meteorological Laboratory (AOML) at NOAA [Available online at http://www.aoml.noaa.gov/hrd/data_sub/wind.html].

Irish, J.L., Resio, D.T., and Ratcliff, J.J., 2008. The influence of storm size on hurricane surge. *J. Phys. Oceanogr.* 38, 2003-2013.

Jain, I., Chittibabu, P., Agnihotri, N., Dube, S.K., Sinha, P.C., and Rao, A.D., 2007. Numerical storm surge model for India and Pakistan. *Natural Hazards* 42, 67-73.

Jarosz, E., Mitchell, D.A., Wang, D.W., and Teague, W.J., 2007. Bottom-up determination of air-sea momentum exchange under a major tropical cyclone. *Science* 315 (5819), 1707-1709.

Jelesnianski, C.P., 1966. Numerical computations of storm surges without bottom stress. *Mon. Wea. Rev.* 94 (6), 379-394.

Jelesnianski, C.P., 1967. Numerical computations of storms surges with bottom stress. *Mon. Wea. Rev.* 95, 740–756.

Jelesnianski, C.P., 1972. SPLASH (Special Program To List Amplitudes of Surges From Hurricanes): 1. Landfall Storms. NOAA Technical Memorandum NWS TDL-46. NWS Systems Development Office, Silver Spring, MD, 56 pp.

Jelesnianski, C.P., Chen, J., and Shaffer, W.A., 1992. SLOSH: Sea, Lake, and Overland Surges from Hurricane. National Weather Service, Silver Springs, MD, 71pp.

Johns, B., Rao, A.D., Dube, S.K., and Sinha, P.C., 1985. Numerical modelling of tide surge interaction in the Bay of Bengal. *Philos. Trans. Roy. Soc. London A* 313, 507-535.

Jones, J.E., and Davies, A.M., 2004. On the sensitivity of computed surges to open-boundary formulation. *Ocean Dynamics* 54 (2), 142-162.

Jones, J.E., and Davies, A.M., 2007. Influence of non-linear effects upon surge elevations along the west coast of Britain. *Ocean Dynamics* 57 (4-5), 401-416. doi:10.1007/s10236-007-0119-0.

Jones, J.E., and Davies, A.M., 2008. On the modification of tides in shallow water regions by wind effects. *J. Geophys. Res.* 113, C05014, doi:10.1029/2007JC004310.

Keim, B.D., Muller, R.A., and Stone, G.W., 2007. Spatiotemporal Patterns and Return Periods of Tropical Storm and Hurricane Strikes from Texas to Maine. *J. Climate* 20, 3498-3509.

Kim, S.Y., Yasuda, T., and Mase, H., 2008. Numerical analysis of effects of tidal variations on storm surges and waves. *Applied Ocean Research* 40 (4), 311-322, doi:10.1016/j.apor.2009.02.003.

Kliem, N., Nielsen, J.W., and Huess, V., 2006. Evaluation of a shallow water unstructured mesh model for the North Sea–Baltic Sea. *Ocean Modelling* 15, 124-136.

Knabb, R.D., Brown, D.P., and Rhome, J.R., 2006. Tropical cyclone report: Hurricane Rita, 18-26 September 2005. National Hurricane Center, Miami, Florida, 33 p.

Kohno, N., Kamakura, K., Minematsu, H., Yorioka, Y., Hisashige, K., Shinizu, E., Sato, Y., Fukunaga, A., Taniwaki, Y., and Tanijo, S., 2007. The Mechanism of the Storm Surges in the Seto Inland Sea Caused by Typhoon Chaba (0416). Technical Review No.9, RSMC Tokyo-Typhoon Center.

Kowalik, Z., and Murty, T.S., 1993. Numerical Modeling of Ocean Dynamics. Advanced Series on Ocean Engineering 5, World Scientific Publishing Company, 481pp.

Large, W., and Pond, S., 1981. Open Ocean Momentum Flux Measurements in Moderate to Strong Winds. *J. Phys. Oceanogr.* 11, 324-336.

Li, C., 1988. Theoretical research on nonlinear interaction of free tide wave and forced surge. *Marine Forecasts* 5(1), 1-7. (in Chinese; abstract in English)

Li, C., 2006. Modeling of bathymetry locked residual eddies in well-mixed tidal channels with arbitrary depth variations. *J. Phys. Oceanogr.* 36, 1974-1993.

Li, M., Zhong, L., Boicourt, W.C., Zhang, S., and Zhang, D.-L. 2006. Hurricane-induced storm surges, currents and destratification in a semi-enclosed bay. *Geophys. Res. Lett.* 33, L02604, doi:10.1029/2005GL024992.

Li, C., Chen, C., Guadagnoli, G., and Georgiou, I.Y., 2008. Geometry induced residual eddies in estuaries with curved channel-observations and modeling studies. *J. Geophys. Res*. 113, C01005, doi: 10.1029/2006JC004031.

Li, C., Weeks, E., and Blanchard, B.W., 2009. Storm surge induced flux through multiple tidal passes of Lake Pontchartrain estuary during Hurricanes Gustav and Ike. *Estuarine Coastal Shelf Sci*. (under review).

Madsen, H., and Jakobsen, F., 2004. Cyclone induced storm surge and flood forecasting in the northern Bay of Bengal. *Coastal Engineering* 51 (4), 277-296.

McGee, B.D., Goree, B.B., Tollett, R.W., Woodward, B.K., and Kress, W.H., 2006. Hurricane Rita surge data, Southwestern Louisiana and Southeastern Texas, September to November 2005. U.S. Geological Survey Data Series 220.

McInnes, K.L., Hubbert, G.D., Abbs, D.J., and Oliver, S.E., 2002. A numerical modelling study of coastal flooding. *Meteorology and Atmospheric Physics* 80, 217-233.

McInnes, K.L., and Hubbert, G.D., 2003. A numerical modelling study of storm surges in Bass Strait. *Aust. Meteorol. Mag*. 52, 143-156.

McInnes, K.L., O'Grady, J.G., and Hubbert, G.D., 2009. Modelling sea level extremes from storm surges and wave setup for climate change assessments in Southern Australia. *J. Coastal Res.* 56 (2), 1005-1009.

Mellor, G.L., and Yamada, T., 1982. Development of a turbulence closure model for geophysical fluid problem. *Rev. Geophys. Space Phys.* 20, 851-875.

Mercer, D., Sheng, J., Greatbatch, R.J., and Bobanović, J., 2002. Barotropic waves generated by storms moving rapidly over shallow water. *J. Geophys. Res.* 107(C10), 3152, doi:10.1029/2001JC001140.

Moon, I.J., Ginis, I., Hara, T., and Thomas, B., 2007. A Physics-based parameterization of air-sea momentum flux at high wind speeds and its impact on hurricane intensity predictions. *Mon. Wea. Rev.* 135, 2869-2878.

Moon, I.J., Kwon, J.I., Lee, J.C., Shim, J.S., Kang, S.K., Oh, I.S., and Kwon, S.J., 2009. Effect of the surface wind stress parameterization on the storm surge modeling. *Ocean Modelling* 29 (2), 115-127, doi:10.1016/j.ocemod.2009.03.006.

Morey, S.L., Baig, S., Bourassa, M.A., Dukhovskoy, D.S., and O'Brien, J.J., 2006. Remote forcing contribution to storm-induced sea level rise during Hurricane Dennis. *Geophys. Res. Lett.* 33, L19603, doi:10.1029/2006GL027021.

Mukai A.Y., Westerink, J.J., Luettich Jr., R.A., and Mark, D., 2002. Eastcoast 2001: a tidal constituent database for the western North Atlantic, Gulf of Mexico and Caribbean Sea, U.S. Army Engineer Research and Development Center, Coastal and Hydraulics Laboratory; Technical Report, ERDC/CHL TR-02-24, 201pp.

Munk, W., Snodgrass, F., and Carrier, G., 1956. Edge Waves on the Continental Shelf. *Science* 123 (3187), 127-132.

Murty, T.S., 1984. Storm Surges: Meteorological Ocean Tide. Department of Fisheries and Oceans, Ottawa, Canada, 897pp.

National Geodetic Survey, 2009. CO-OPS/NGS Elevation Data [Available online at http://www.ngs.noaa.gov/newsys-cgi-bin/ngs_opsd.prl].

National Hurricane Center, 2007. SLOSH model. [Available online at http://www.nhc.noaa.gov/HAW2/english/surge/slosh.shtml].

National Oceanic and Atmospheric Administration, 2005. Storm surge: a "rising" concern among coastal residents. NOAA Magazine, Commerce Department. [Available at http://www.magazine.noaa.gov/stories/mag178.htm].

National Weather Service, 2009. Hurricane Ike: storm surge inundation maps. The National Weather Service Forecast Office in Lake Charles, Louisiana [Available online at http://www.srh.noaa.gov/lch/ike/ikesurge.php].

Nichols, M.M., 1994. Response of estuaries to storms in the Chesapeake Bay region: summary. In: Dyer, K.R., Orth, R.J. (Eds.), Changes in Fluxes in Estuaries: Implications From Science to Management. Olsen and Olsen, Fredensberg, Denmark, 67-70.

Otvos, E.G., and Carter, G.A., 2008. Hurricane degradation – Barrier development cycles, Northeastern Gulf of Mexico: Landform evolution and island chain history. *J. Coastal Res.* 24 (2), 463-478.

Pain, C.C., Piggott, M.D., Goddard, A.J., Fang, F., Gorman, G.J., Marshall, D.P., Eaton, M.D., Power, P.W., and de Oliveira, C.R.E., 2005. Three-dimensional unstructured mesh ocean modelling. *Ocean Modelling* 10 (1), 5-33, doi:10.1016/j.ocemod.2004.07.005.

Peng M., Xie L., and Pietrafesa L.J., 2004. A numerical study of storm surge and inundation in the Croatan-Albemarle-Pamlico Estuary System. *Estuarine, Coastal and Shelf Science* 59(1), 121-137.

Peng, M., Xie, L., and Pietrafesa, J., 2006a. A numerical study on hurricane induced storm surge and inundation in Charleston, South Carolina. *J. of Geophysical Research* 111, C08017, doi:10.1029/2004JC002755.

Peng, M., Xie, L., and Pietrafesa, L.J., 2006b. Tropical cyclone induced asymmetry of sea level surge and fall and its presentation in a storm surge model with parametric wind fields. *Ocean Modelling* 14, 81-101.

Phadke, A.C., Martino, C.D., Cheung, K.F., and Houston, S.H., 2003. Modeling of tropical cyclone winds and waves for emergency management. *Ocean Engineering* 30, 553-578.

Platzman, G.W., 1963. The dynamical prediction of wind tides on Lake Erie. *Meteorological Monographs* 4 (26), 44 pp.

Powell, M.D., Houston, S.H., and Reinhold, T.A., 1996. Hurricane Andrew's landfall in South Florida Part I: Standardizing measurements for documentation of surface wind fields. *Wea. Forecast*. 11, 304-328.

Powell, M.D., Vickery, P.J., and Reinhold, T.A., 2003. Reduced drag coefficient for high wind speeds in tropical cyclones. *Nature* 422, 278-283.

Powell, M.D., and Reinhold, T.A., 2007. Tropical cyclone destructive potential by Integrated Kinetic Energy. *Bull. Amer. Meteor. Soc.* 88, 513-526.

Prandle, D. 1975. Storm surges in the southern North Sea and River Thames. *Proc. R. Soc. Lond. A* 344, 509-539.

Prandle, D., and Wolf, J., 1978. The interaction of surge and tide in the North Sea and River Thames. *Geophys. J. R. Astron. Soc*. 55, 203-216.

Proudman, J., 1953. Dynamical Oceanography, John Wiley, New York, 409 pp.

Proudman, J., 1954. Note on the dynamics of storm-surges. *Mon. Not. R.A.S., Geophys. Supp*. 7, 44-48.

Proudman, J., 1955. The propagation of tide and surge in an estuary. *Proc. R. Soc. London* A 231, 8-24.

Proudman, J., 1957. Oscillations of tide and surge in an estuary of finite length. *J. Fluid Mech*. 2, 371-382.

Pugh, D.T., 1987. Tides, Surges and Mean Sea-Level: A Handbook for Engineers and Scientists. John Wiley, Hoboken, N. J., 472 pp.

Pugh, D.T., and Vassie, J.M., 1980. Applications of the joint probability method for extreme sea level computations. *Proc.-Inst. Civ. Eng*. 69, 959- 975.

Qin, Z., Duan, Y., Wang, Y., Shen, Z., and Xu, K., 1994. Numerical simulation and prediction of storm surges and water levels in Shanghai harbour and its vicinity. *Natural Hazards* 9, 167-188, doi: 10.1007/BF00662597.

Rappaport, E.N., and Fernandez-Partagas, J., 1995. The Deadliest Atlantic Tropical Cyclones, 1492-1996. NOAA Technical Memorandum NWS NHC 47 [Available online at http://www.nhc.noaa.gov/pastdeadly.shtml].

Rego, J.L., Li, C., 2009a. On the receding of storm surge along Louisiana's low-lying coast. *J. Coastal Res.* SI56 (2), 1045-1049.

Rego, J.L., Li, C., 2009b. On the importance of the forward speed of hurricanes in storm surge forecasting: A numerical study. *Geophys. Res. Lett*. 36, L07609, doi:10.1029/2008GL036953.

Resio, D.T., Westerink, J.J., 2008. Modeling the physics of storm surges. *Physics Today* 61 (9), 33-38.

Retana, A.G., 2008. Salinity transport in a finite-volume sigma-layer three-dimensional model. New Orleans, Louisiana: University of New Orleans, Doctoral Thesis, 706pp.

Rossiter, J.R., 1961. Interaction between tide and surge in the Thames. *Geophys. J. R. Astron. Soc.* 6, 29-53.

Russo, E.P., 1998. Estimating hurricane storm surge amplitudes for the Gulf of Mexico and Atlantic coastlines of the United States. OCEANS '98 Conference Proceedings 3, 1301-1305.

Shen, J., Gong, W., and Wang, H.V., 2006. Water level response to 1999 hurricane Floyd in the Chesapeake Bay. *Cont. Self Res.* 26, 2484-2502.

Shen, J., and Gong, W., 2009. Influence of model domain size, wind directions and Ekman transport on storm surge development inside the Chesapeake Bay: a case study of extratropical cyclone Ernesto. *J. Mar. Sys.* 75, 198-215.

Signorini, S.R., Wei, J.S., and Miller, C.D., 1992. Hurricane-induced surge and currents on the Texas-Louisiana shelf. *J. Geophys. Res.* 97 (C2), 2229-2242.

Simpson, R.H., and Simpson, J., 1966. Why experiment on tropical hurricanes? *Trans. N.Y. Acad. Sci*. 28, 1045–1062.

Simpson, J., 1979. Field experimentation in weather modification: Comment. *Journal of the American Statistical Association* 74 (365), 95-97.

Simpson, R.H., and Riehl, H., 1981. The Hurricane and Its Impact. Louisiana State University Press, Baton Rouge, LA, 398pp.

Smagorinsky, J., 1963. General circulation experiments with the primitive equations, I: The basic experiment. *Mon. Wea. Rev.* 91, 99-164.

Stone, G.W., Liu, B., Pepper, D.A., and Wang, P., 2004. The importance of extratropical and tropical cyclones on the short-term evolution of barrier islands along the northern Gulf of Mexico, USA. *Marine Geology* 210, 63-78.

Tang, Y.M., Grimshaw, R., Sanderson, B., and Holland, G., 1996. A Numerical Study of Storm Surges and Tides, with Application to the North Queensland Coast. *J. Phys. Oceanogr.* 26, 2700-2711.

Tang, Y.M., Holloway, P., and Grimshaw, R., 1997. A numerical study of the storm surge generated by Tropical Cyclone Jane. *J. Phys. Oceanogr.* 27, 963-976.

USGS Hurricanes and Extreme Storms Group, 2009. Hurricane Ike: Pre-Storm and Post-Storm 3D Lidar Topography for Bolivar Peninsula, TX. U.S. Geological Survey [Available online at http://coastal.er.usgs.gov/hurricanes/ike/].

URS Group, Inc., 2006. Hurricane Rita rapid response: Louisiana coastal & riverine high water mark collection: Federal Emergency Management Agency, Hazard Mitigation Technical Assistance Program, Contract No. EMW-2000-CO-0247, Task Orders 445 & 450, Gaithersburg, Maryland, 42 pp.

Valle-Levinson, A., Wong, K., and Bosley, K.T., 2002. Response of the lower Chesapeake Bay to forcing from Hurricane Floyd. *Cont. Shelf Res.* 22, 1715-1729.

Verboom, G.K., De Rond, J.G. and Van Dijk, R.P., 1992. A fine grid tidal flow and storm surge model of the North Sea. *Cont. Shelf Res.* 12, 213-233.

Webster, P. J., Holland, G.J., Curry, J.A., and Chang, H.R., 2005. Changes in tropical cyclone number, duration, and intensity in a warming environment. *Science* 309, 1844-1846.

Webster, P.J., 2008. Myanmar's deadly daffodil. *Nat. Geosci*. 1, 488- 490, doi:10.1038/ngeo257.

Weisberg, R.H., and Zheng, L.Y., 2006a. Hurricane storm surge simulation for Tampa Bay. *Estuaries and Coasts* 29(6), 899-913.

Weisberg, R.H., and Zheng, L., 2006b. A simulation of the hurricane Charley storm surge and its breach of North Captiva Island. *Florida Scientist* 69, 152-165.

Weisberg, R. H., and Zheng, L., 2008. Hurricane storm surge simulations comparing three-dimensional with two-dimensional formulations based on an Ivan-like storm over the Tampa Bay, Florida region. *J. Geophys. Res.* 113, C12001, doi:10.1029/2008JC005115.

Welander, P., 1961. Numerical predictions of storm surges. *Advances in Geophysics* 8, Academic Press, 315-379.

Westerink, J.J., Luettich, R.A., Feyen, J.C., Atkinson, J.H., Dawson, C., Roberts, H.J., Powell, M.D., Dunion, J.P., Kubatko, E.J., and Pourtaheri, H., 2008. A Basin- to Channel-Scale Unstructured Grid Hurricane Storm Surge Model Applied to Southern Louisiana. *Mon. Wea. Rev*. 136, 833–864.

Wolf, J., 1978. Interaction of tide and surge in a semi-infinite uniform channel, with application to surge propagation down the east coast of Britain. *Appl. math. Modelling* 2, 245-253.

Wolf, J., 1981. Surge-tide interaction in the North Sea and River Thames. In D.H. Peregrine (ed.), Floods due to high winds and tides, 75-94. Academic Press, London, UK.

Wolf, J., 2008. Coastal flooding: impacts of coupled wave–surge–tide models. *Nat. Hazards* 49, (2). 241-260. 10.1007/s11069-008-9316-5.

Xie, L., Pietrafesa, L.J., and Wu, K., 2003. A numerical study of wave-current interaction through surface and bottom stresses: Coastal ocean response to Hurricane Fran of 1996. *J. Geophys. Res.* 108(C2), 3049, doi:10.1029/2001JC001078.

Xie, L., Pietrafesa, L., and Peng, M., 2004. Incorporation of a mass-conserving inundation scheme into a three dimensional storm surge model. *J. Coastal Res.* 20 (4), 1209-1223.

Xie, L., Bao, S., Pietrafesa, L., Foley, K., and Fuentes, M., 2006. A real-time hurricane surface wind forecasting model: Formulation and verification. *Mon. Wea. Rev.* 134, 1355-1370.

Xue, P., Chen, C., Ding, P., Beardsley, R.C., Lin, H., Ge, J., and Kong, Y., 2009. Saltwater intrusion into the Changjiang River: A model-guided mechanism study. *J. Geophys. Res.* 114, C02006, doi:10.1029/2008JC004831.

Zampato, L., Umgiesser, G., and Zecchetto, S., 2006. Storm surge in the Adriatic Sea: observational and numerical diagnosis of an extreme event. *Advances in Geosciences* 7, 371-378.

Zedler, S.E., Niiler, P.P., Stammer, D., Terrill, E., and Morzel, J., 2009. Ocean's response to Hurricane Frances and its implications for drag coefficient parameterization at high wind speeds. *J. Geophys. Res.* 114, C04016, doi:10.1029/2008JC005205.

Zhang, Y., Zhao, Y., and Wang, Y., 1993. Analysis of disaster caused by typhoon surges and study of the numerical prediction methods for the disastrous sea level. In Tropical Cyclone Disasters, edited by J. Lighthill, Z. Zhemin, G.J. Holland, and K.A. Emanuel, Peking University Press, Beijing, 452-459.

Zhang, Z., Xiao, C., and Shen, J. 2008. Comparison of the CEST and SLOSH Models for Storm Surge Flooding. *J. Coastal Res.* 24 (2), 489-499.

APPENDIX A: THREE DIMENSIONAL GOVERNING EQUATIONS IN SIGMA COORDINATES

After the Boussinesq and hydrostatic approximations the primitive equations for momentum and mass conservation used in FVCOM are (Chen et al., 2007; Weisberg and Zheng, 2008):

$$\frac{\partial uD}{\partial t}+\frac{\partial u^2 D}{\partial x}+\frac{\partial uvD}{\partial y}+\frac{\partial u\omega}{\partial \sigma}-fvD=$$
$$=-gD\frac{\partial(\eta-\eta_a)}{\partial x}-\frac{gD}{\rho_0}\left[\frac{\partial}{\partial x}\left(D\int_{\sigma}^{0}\rho' d\sigma'\right)+\sigma\rho'\frac{\partial D}{\partial x}\right]+\frac{1}{D}\frac{\partial}{\partial \sigma}\left(K_m\frac{\partial u}{\partial \sigma}\right)+DF_u \qquad \text{(A.1)}$$

$$\frac{\partial vD}{\partial t}+\frac{\partial uvD}{\partial x}+\frac{\partial v^2 D}{\partial y}+\frac{\partial v\omega}{\partial \sigma}+fuD=$$
$$=-gD\frac{\partial(\eta-\eta_a)}{\partial y}-\frac{gD}{\rho_0}\left[\frac{\partial}{\partial y}\left(D\int_{\sigma}^{0}\rho' d\sigma'\right)+\sigma\rho'\frac{\partial D}{\partial y}\right]+\frac{1}{D}\frac{\partial}{\partial \sigma}\left(K_m\frac{\partial v}{\partial \sigma}\right)+DF_v \qquad \text{(A.2)}$$

$$\frac{\partial \eta}{\partial t}+\frac{\partial uD}{\partial x}+\frac{\partial vD}{\partial y}+\frac{\partial \omega}{\partial \sigma}=0 \qquad \text{(A.3)}$$

where u, v and ω are the x, y and σ velocity components, respectively; f is the Coriolis parameter; $D=h+\eta$ is the total water depth, where η and h are the surface elevation and reference depth below mean sea level, respectively; η_a is the sea level displacement induced by the "inverse barometer effect"; g is the gravitational acceleration; ρ_0 and ρ' are the reference and perturbation water densities, respectively; K_m is the vertical eddy viscosity coefficient; F_u and F_v represent the horizontal momentum diffusion terms in the x and y directions, respectively.

The 2nd term on the right-hand side of Equations A.1, A.2 represents baroclinicity and did not enter the (barotropic) simulations used in this work. The surface and bottom boundary conditions for u, v and ω are specified as

$$\left(\frac{\partial u}{\partial \sigma}, \frac{\partial v}{\partial \sigma}\right) = \frac{D}{\rho_0 K_m}\left(\tau_{sx}, \tau_{sy}\right),\ \omega = 0 \text{ at } \sigma = 0 \tag{A.4}$$

$$\left(\frac{\partial u}{\partial \sigma}, \frac{\partial v}{\partial \sigma}\right) = \frac{D}{\rho_0 K_m}\left(\tau_{bx}, \tau_{by}\right),\ \omega = 0 \text{ at } \sigma = -1 \tag{A.5}$$

where $\left(\tau_{sx}, \tau_{sy}\right)$ and $\left(\tau_{bx}, \tau_{by}\right)$ are the *x* and *y* components of surface wind and bottom roughness stresses, respectively.

APPENDIX B.1: COVER PAGE OF JOURNAL OF COASTAL RESEARCH PAPER

Journal of Coastal Research	SI 56	1045 - 1049	ICS2009 (Proceedings)	Portugal	ISSN 0749-0258

On the receding of storm surge along Louisiana's low-lying coast

J. L. Rego† and C. Li‡
Coastal Studies Institute, Dept. of Oceanography and Coastal Sciences
Louisiana State University, Baton Rouge, LA 70803
United States of America
† jrego1@lsu.edu, ‡ cli@lsu.edu

ABSTRACT

REGO, J.L. and LI, C., 2009. On the receding of storm surge along Louisiana's low-lying coast. Journal of Coastal Research, SI 56 (Proceedings of the 10th International Coastal Symposium), 1045 – 1049. Lisbon, Portugal, ISSN 0749-0258.

Severe damage from storm surge often occurs over low-lying, small slope land subject to inundation. The extent of the environmental damage depends on the flooding as well as how long the flood water remains – or how long the receding of the surge takes. An investigation of storm surge impact to the coast of Louisiana is conducted using the state-of-the-art finite-volume coastal ocean model, FVCOM (CHEN *et al.*, 2003). All nonlinear terms are included in FVCOM's governing 2D equations, and hurricane simulations in this paper are forced by tides and wind stress. An application of the model to Hurricane Rita's storm surge event is described, and data along the Louisiana-Texas coast in September 2005 used for model validation. We combine USGS surge data covering Hurricane Rita, our own data covering Hurricane Gustav (September 2008) and our modeling results to study the receding stage of surge waters. We quantify typical longer term hurricane-induced inundation patterns, for different locations affected by the surge. We show that the surge outflow, which peaks at about 24 hours after landfall, takes much longer than the initial flooding due to different dynamics over coastal passes and floodplain near the shoreline. Whereas flooding occurs along large parts of the shoreline (decreased bottom friction results in a brief, vast landward transport of water), the surge flows back to the Gulf constrained by the existing channels, and surge waters flow out of the region's major coastal passes in a plume-like pattern.

ADITIONAL INDEX WORDS: *Flooding, Hurricane, FVCOM*

INTRODUCTION

A storm surge is a long gravity wave with a length scale similar to the size of the generating tropical cyclone, which lasts for several hours depending on the cyclone size and speed of movement. The surge usually consists of a single passing wave that elevates or depresses the sea surface height (FLATHER, 2001). Storm surges can cause severe damage to property and loss of lives. Hurricane Katrina's storm surge in August 2005 exceeded 10 meters in several locations along the Mississippi coastline and became the costliest hurricane to ever strike the USA, resulting in the death of over 1000 people in Louisiana and 200 in Mississippi (FRITZ *et al.*, 2007).

Major destructive storm surges tend to occur when extreme storm winds act over extensive regions of shallow water, because in the governing equations the wind stress term is divided by the total depth whereas the surface pressure gradient force is not (*e.g.*, FLATHER, 2001). Coastal peak surges created by a given standard hurricane over wide continental shelves can be up to three times greater than those created by the same hurricane over narrower shelves (JELESNIANSKI, 1972).

Since it is the initial surge impact that causes the largest part of human deaths and destruction, most surge hydrodynamics studies focus on peak coastal surge timing, elevations and currents, and the return to sea of storm waters is often overlooked. However, this receding surge is reportedly important from an ecological standpoint (e.g., NICHOLS, 1994) in that the longer surge inundation lasts, the more environmental damage will take place (endangering animals, fish and plants by keeping excessive amounts of saltwater in marshes). NICHOLS (1994) studied the response of Chesapeake Bay estuaries to storms and concluded that the "recovery" stage extends from 7 to 26 days. GONG *et al.*'s (2007) model results for the York River estuary suggest that the influence of Tropical Cyclone Isabel's (September 2003) storm surge itself on estuary transport mainly occurs within the first 48 h, whereas the recovery of the estuary to its natural state required about 20 days. The study by GONG *et al.* (2007), however, focused on salt flux mechanisms during storm surge and subsequent high river pulse event, and did not attempt to explain the surge hydrodynamics.

Hurricane Rita attained Category-5 status and peak sustained winds of 280 km/h within 24 hours after entering the Gulf of Mexico (GoM). The barometric pressure reached 895 mbar, the third-lowest ever recorded for a tropical system in the Atlantic Basin at that time. Rita moved ashore as a Cat-3 hurricane about 10 km east of the Louisiana-Texas state border (Figure 1), at 08h UTC, 09/24/2005 with sustained winds of 195 km/h. Hurricane Rita generated a substantial storm surge east of its landfall that reached 5-6 m, then weakened rapidly as it continued northward (KNABB *et al.*, 2006). Hurricane Gustav occurred three years later. After devastating large parts of Cuba, Gustav reached its maximum strength with maximum sustained winds of 240 km/h and a minimum pressure of 941 mbar (becoming the second major hurricane of the 2008 Atlantic hurricane). On 09/01/2008 at 15h UTC the center of Gustav made landfall in the United States along the Louisiana coast near Cocodrie (Figure 1) as a very strong Category 2 hurricane, with winds of 175 km/h (BEVEN, 2008).

APPENDIX B.2: REQUEST FOR PERMISSION TO REPRINT; JOURNAL OF COASTAL RESEARCH

Joao Rego <jrego1@tigers.lsu.edu>

permission to reprint in PhD dissertation

Joao Rego <jrego1@tigers.lsu.edu> **Wed, May 13, 2009 at 1:49 PM**
To: Carlos Pereira da Silva <ics2009@fcsh.unl.pt>

Dear Sir

I am completing a doctoral dissertation at the Louisiana State University entitled "Storm surge dynamics over wide shelves: Numerical experiments using the Finite-Volume Coastal Ocean Model." I would like permission from the Journal of Coastal Research to reprint in my dissertation excerpts from the following:

Rego, J.L., and Li, C. (2009). On the receding of storm surge along Louisiana's low-lying coast. Journal of Coastal Research SI 56(2), 1045-1049.

Of which I am the first and corresponding author; my PhD adviser is second and last author. The excerpts to be reproduced are the "Discussion", "Concluding Remarks", and Figures 1 through 4.

If this meets with your approval, please reply favorably to this email.

Thank you so much

Sincerely,

Joao Rego

APPENDIX B.3: LETTER OF PERMISSION; JOURNAL OF COASTAL RESEARCH

Joao Rego <jrego1@tigers.lsu.edu>

permission to reprint in PhD dissertation

ICS 2009 <ics2009@fcsh.unl.pt> **Thu, May 14, 2009 at 9:35 AM**
To: Joao Rego <jrego1@tigers.lsu.edu>

Dear Colleague

As you know you didn't sign any "Copyright Assignment & Author Disclosure Form". Therefore you are free to reprint excepts of the article, but I strongly adivise you to include the SI article in the Bibliography to self protection.

Sincerely yours

Carlos Pereira da Silva

APPENDIX C.1: COVER PAGE OF GEOPHYSICAL RESEARCH LETTERS PAPER

GEOPHYSICAL RESEARCH LETTERS, VOL. 36, L07609, doi:10.1029/2008GL036953, 2009

On the importance of the forward speed of hurricanes in storm surge forecasting: A numerical study

João Lima Rego[1] and Chunyan Li[1]

Received 9 December 2008; revised 26 February 2009; accepted 17 March 2009; published 15 April 2009.

[1] A systematic investigation of storm surge along the coast of Louisiana was conducted by using the fully nonlinear Finite-Volume Coastal Ocean Model. FVCOM was first applied to Hurricane Rita and validated by in situ measurements. Experiments were conducted with different parameters to evaluate the impacts of each factor on inundation over a wide and shallow shelf. Results show that a hurricane's forward speed is a significant parameter which has been overlooked in previous studies. Resonance may occur for certain hurricane forward motion speeds: increasing this speed increases peak surge heights while decreasing inland volume of flood. The effects of wind intensity, Radius of Maximum Winds, tidal timing, amplitude, and wind inflow angle were also examined. It was concluded that varying a storm's forward motion may account for variations in flooded volumes equivalent to an upgrade or downgrade of about 1 category on the Saffir-Simpson scale. **Citation:** Rego, J. L., and C. Li (2009), On the importance of the forward speed of hurricanes in storm surge forecasting: A numerical study, *Geophys. Res. Lett.*, *36*, L07609, doi:10.1029/2008GL036953.

1. Introduction

[2] A storm surge is an abnormal variation in the sea surface height caused by atmospheric forcing associated with extra-tropical cyclones or tropical storms such as hurricanes and typhoons [*Flather*, 2001]. Storm surges can cause severe damage to property and loss of lives. In the Gulf of Mexico (GoM), a hurricane flooded Galveston Island, Texas in 1900 with the loss of over 6000 lives [*Blake et al.*, 2006]. Hurricane Katrina's storm surge in August 2005 exceeded 10 m in several locations along the Mississippi coast and became the costliest hurricane to ever strike the USA, resulting in the death of over 1000 people in Louisiana and 200 in Mississippi [*Blake et al.*, 2006].

[3] Major destructive storm surges tend to occur when extreme storm winds act over extensive regions of shallow water. This is because in the governing equations the wind stress term is divided by the total depth, whereas the surface pressure gradient force is not – wind forcing thus increases in importance over shallower water [e.g., *Flather*, 2001]. Since it is the wind stress that generates most of the total hurricane-induced storm surge in coastal seas [e.g., *Kohno et al.*, 2007], many numerical studies do not include the atmospheric pressure term at all [*Chu et al.*, 2000; *Dube et al.*, 2005]. We are only investigating the effects of the conventional long wave storm surge, and do not include short surface waves. Whereas faster surface flows reduce the air-sea momentum transfer rate (thereby reducing surge), bottom-layer return currents produce a shoreward bottom stress that adds to the wind stress (enhancing surge). These complex opposing effects due to waves depend strongly on local bathymetry [*Resio and Westerink*, 2008].

[4] Linear theory predicts that the ocean's response to an atmospheric traveling disturbance is proportional to $(1\text{-}U^2/gh)^{-1}$, *i.e.* when the speed of the traveling disturbance, U, is very close to that of the propagation of a long wave, there is resonance and the elevation becomes very large [*Proudman*, 1953]. *Jelesnianski*'s [1972] numerical experiments with a standard hurricane over representative shelves suggested that a "critical speed" exists, greater than 30 mph (13.4 m/s), which gives the highest possible surge. *Peng et al.*'s [2004] numerical experiments on a North Carolina estuary suggested that both storm surge heights and inundation areas decreased as hurricane translation speed increased (for 1.74–13.88 m/s). *Peng et al.* [2006a], using a modified inundation scheme, concluded for Charleston Harbor in South Carolina that while slower hurricanes invariably induce greater inundation areas, whether or not they induce higher storm surges depends on their track and speed (only 5.07 and 10.14 m/s were tested). *Irish et al.* [2008] created an idealized, straight coastline basin representing the northern GoM with different slopes to investigate the effect of varying storm sizes on coastal peak surges. They also varied the storm motion (2.6–10.3 m/s) and concluded that for moderate bottom slopes a 50% increase in forward speed translates to a 15–20% increase in peak surge.

[5] Hurricane Rita attained Category-5 status and peak sustained winds of 280 km/h within 24 hours after entering the GoM. The barometric pressure reached 895 mbar, the third-lowest ever recorded for a tropical system in the Atlantic Basin at that time. It moved ashore as a Cat-3 hurricane near the Louisiana-Texas border at about 8am UTC, September 24, 2005 with sustained winds of 195 km/h. Hurricane Rita generated a substantial storm surge east of its landfall that reached 5–6 m, then weakened rapidly as it continued northward [*Knabb et al.*, 2006].

[6] This paper applies the FVCOM to Hurricane Rita's storm tide (the total height of the surge plus the astronomical tide) over the Louisiana-Texas shelf with a successful validation. Hurricane Rita was chosen for two reasons: the relatively simple coastline and shelf geometry of the landfall area (allowing for a simplified, quasi-idealized look into surge results) and the unique dataset from the USGS, which recorded flooding along the southwest Louisiana coast (permitting the report of differences to a "base case" that is fully validated against observations). Our conclusions are thus representative of powerful hurricanes over mild slopes, impacting low-lying coasts consisting of marshes and inland

[1]Department of Oceanography and Coastal Sciences, Coastal Studies Institute, Louisiana State University, Baton Rouge, Louisiana, USA.

0094-8276/09/2008GL036953$05.00

APPENDIX C.2: REQUEST FOR PERMISSION TO REPRINT; GEOPHYSICAL RESEARCH LETTERS

Gmail by Google BETA

joao rego <jlimarego@gmail.com>

2008GL036953R: Permission to reprint

joao rego <jlimarego@gmail.com> **Mon, May 4, 2009 at 8:05 PM**
To: grlonline@agu.org

To whom this may concern

I am completing a doctoral dissertation at the Louisiana State University entitled "Storm surge dynamics over wide shelves: Numerical experiments using the Finite-Volume Coastal Ocean Model." I would like permission from Geophysical Research Letters to reprint in my dissertation excerpts from the following:

Rego, J.L., and Li, C. (2009). "On the importance of the forward speed of hurricanes in storm surge forecasting: a numerical study." Geophysical Research Letters 36, L07609, doi:10.1029/2008GL036953.

Of which I am the first and corresponding author; my PhD adviser is second and last author. The excerpts to be reproduced are the the "Discussion", "Concluding Remarks", and Figures 1 and 2.

If this meets with your approval, please reply favorably to this email.

Sincerely,

Joao Rego

APPENDIX C.3: LETTER OF PERMISSION; GEOPHYSICAL RESEARCH LETTERS

Gmail by Google BETA

joao rego <jlimarego@gmail.com>

permission

1 message

Michael Connolly <MConnolly@agu.org> **Tue, May 5, 2009 at 7:50 AM**
To: joao rego <jlimarego@gmail.com>

We are pleased to grant permission for the use of the material requested for inclusion in your thesis. The following non-exclusive rights are granted to AGU authors:

- All proprietary rights other than copyright (such as patent rights).
- The right to present the material orally.
- The right to reproduce figures, tables, and extracts, appropriately cited.
- The right to make hard paper copies of all or part of the paper for classroom use.
- The right to deny subsequent commercial use of the paper.

Further reproduction or distribution is not permitted beyond that stipulated. The copyright credit line should appear on the first page of the article or book chapter. The following must also be included, "Reproduced by permission of American Geophysical Union." To ensure that credit is given to the original source(s) and that authors receive full credit through appropriate citation to their papers,
we recommend that the full bibliographic reference be cited in the reference list. The standard credit line for journal articles is: "Author(s), title of work, publication title, volume number, issue number, citation number (or page number(s) prior to 2002), year. Copyright [year] American Geophysical Union."

If an article was placed in the public domain, in which case the words "Not subject to U.S. copyright" appear on the bottom of the first page or screen of the article, please substitute "published" for the word "copyright" in the credit line mentioned above.

Copyright information is provided on the inside cover of our journals. For permission for any other use, please contact the AGU Publications Office at AGU, 2000 Florida Ave., N.W., Washington, DC 20009.

Michael Connolly
Journals Publications Specialist

VITA

João Ramalho de Lima Rego was born in Lisbon, Portugal, in April 1978. He entered the Faculty of Sciences of the University of Lisbon in September 1999 and received his *Licenciado* degree in geophysics (majors in meteorology and physical oceanography) in December 2004.

In January 2005, João started the master's program in civil and environmental engineering at the University of Louisiana at Lafayette, which he completed in July 2006. His thesis work under Prof. Ehab Meselhe focused on the sediment transport and fate of the Mississippi and Atchafalaya rivers' plumes.

In August 2006, João started the doctoral program with Prof. Chunyan Li at the Louisiana State University, in Baton Rouge. He has been studying the physics of hurricane-induced storm surge over wide and shallow continental shelves, surge dynamics over low-lying coasts and surge propagation in semi-enclosed bays for the past three years.